2009

Functionalized mesoporous silica nanoparticles for stimuli-responsive and targeted drug delivery

Nikola Knezevic
Iowa State University

Functionalized mesoporous silica nanoparticles for stimuli-responsive and targeted drug delivery

by

Nikola Knežević

A dissertation submitted to the graduate faculty

in partial fulfillment of the requirements for the degree of

DOCTOR OF PHILOSOPHY

Major: Chemistry

Program of Study Committee:
Victor S. Y. Lin, Major Professor
Keith L. Woo
Srdija Jeftinija
Aaron D. Sadow
Marek Pruski

Iowa State University

Ames, Iowa

2009

TABLE OF CONTENTS

LIST OF ABBREVIATIONS

9AA = 9-aminoacridine
Ams = amsacrine
AP = aminopropyl
BET = Brunauer-Emmett-Teller
BJH = Barrett-Joyner-Halenda
bpy = 2,2'-bipyridine
CdS-NMBAl-CPT@MMSN = CPT loaded MMSN-h, capped by NMBAl functionalized CdS nanoparticles
CdS-NMBAl-MMSN = MMSN-h capped by NMBAl functionalized CdS nanoparticles
GABA = γ-aminobutyric acid
CHO = Chinese hamster ovarian
CPP = critical packing parameter
CPT = camptothecin
CTAB = cetyltrimethylammonium bromide
DDS = drug delivery system
DMEM = Dubelcco's modified eagle medium
Dox = doxorubicin
DTA = differential thermal analysis
EDS = energy dispersive X-ray spectroscopy
EPR = enhanced permeability and retention effect
IUPAC = International Union of Pure and Applied Chemistry
MMSN = magnetic mesoporous silica nanoparticles
MMSN-h = hexagonal mesoporous silica nanoparticles
MMSN-r = radial magnetic mesoporous silica nanoparticles
MP = mercaptopropyl
MSN = mesoporous silica nanoparticles
NMBAl = 2-nitro-5-mercaptobenzyl alcohol
NV = nitroveratryl
NVCAP = nitroveratryl-carbamate protected aminopropyl
PEI = polyethyleneimine
PPh_3 = triphenylphosphine
SEM = scanning electron microscopy

Sr101 = sulforhodamine 101
TEM = transmission electron miscroscopy
TEOS = tetraethoxysilane
TES = triethoxysilane
TGA = thermogravimetric analysis
TMS = trimethoxysilane
UV = ultraviolet
XRD = X-ray diffraction

ABSTRACT

Construction of functional supramolecular nanoassemblies has attracted great deal of attention in recent years for their wide spectrum of practical applications. Mesoporous silica nanoparticles (MSN) in particular were shown to be effective scaffolds for the construction of drug carriers, sensors and catalysts. Herein, we describe the synthesis and characterization of stimuli-responsive, controlled release MSN-based assemblies for drug delivery.

First we report on devising a functional UV light responsive delivery system for doxorubicin, a widely used anticancer drug. A positively charged drug molecule is adsorbed on the surface of the MSN through charge interaction and hydrogen bonding with surface silanols. The surface of MSN contained nitroveratryl carbamate protected aminopropyl moieties which undergo deprotection upon irradiation with UV light. The drug delivery principle is based on charge repulsion between UV light-generated, positively charged propylammonium ions and positively charged doxorubicin molecules. Release of the drug also increases by lowering the pH from 7.4 to 6.4. This result is beneficial for selective drug delivery to tumor tissues, as most tumor tissues have low extracellular pH value.

We then set forth to develop magnetic analogues of mesoporous silica nanoparticles in order investigate possibilities for magnetic field induced targeted drug delivery. A series of new materials was obtained with radial and hexagonal packing of the mesopores, containing magnetic nanoparticles inside the core of the mesoporous silicate framework. We monitored the ability of the magnetic materials to adsorb and deliver anticancer drugs, 9-aminoacridine and camptothecin, and an interesting result was obtained. If 9-aminoacridine was adsorbed on the magnetic materials, its release from the surface in PBS buffer was promoted if the silica surface was not functionalized with organic moieties. If camptothecin was adsorbed on the same materials, the presence of phenylethyl functional groups inside the mesopores

promoted the loading and delivery of the drug. The results were confirmed by *in vitro* drug delivery studies on Chinese hamster ovarian cells (CHO).

We further applied the magnetic mesoporous silica nanomaterial to develop a magnetically active nanocarrier for photosensitive delivery of camptothecin to cancer cells. The mesopores were loaded with the drug and the pore entrances were blocked by functionalized cadmium-sulfide nanoparticles through an o-nitrobenzyl-based photolabile linker. Upon irradiation with UV light the photolabile linker was cleaved which induced release of the anticancer drug. The cooperative anticancer effect of capping CdS nanoparticles and loaded camptothecin was demonstrated by *in vitro* viability studies on CHO cells, upon exposure of the cell cultures to low power UV light**.**

Finally, we constructed a mesoporous silica nanoparticle-based nanocarrier which was capable of delivering the mesopore-loaded molecules upon irradiation with visible light or upon the treatment with nitrogen-monoxide, histidine or imidazole, which are known intracellular molecules. Sulforhodamine 101 was used as a cargo molecule and it was entrapped inside the mercaptopropyl functionalized mesopores of MSN by mercapto-coordinated $Ru(bpy)_2(PPh_3)$-moieties (bpy = 2,2'-bipyridine, PPh_3 = triphenylphosphine). Upon exposure to visible light the Ru-S coordination bond is cleaved which allows release of the mesopore-loaded dye. Ligand substitution of the Ru-S coordination bond by nitrogen monoxide, imidazole and histidine was also shown to induce the release of cargo molecules, although with lower efficiency than with visible light.

CHAPTER 1. GENERAL INTRODUCTION

Dissertation Organization

This dissertation is divided into 6 chapters. The first chapter contains the general introduction of mesoporous silica nanoparticles, including the synthesis, mechanisms, modification methods and potential applications. Some of the recent reports on mesoporous silica nanoparticle-based functional supramolecular assemblies for targeted drug delivery are also included. Chapters 2 to 5 present journal papers on my research accomplishments for the past 6 years of my graduate studies, in chronological order.

Chapter 2 describes functional UV light responsive delivery system for doxorubicin, a widely used anticancer drug. A positively charged drug molecules are adsorbed on organically modified surface of the MSN and the drug delivery principle is based on charge repulsion between UV light-generated, positively charged moieties on MSN surface and doxorubicin molecules. Release of the drug was also responsive to increase in acidity. My personal contribution represents 90 % of the presented research.

Chapter 3 describes the development of magnetic analogues of mesoporous silica nanoparticles. A series of new materials was obtained with radial and hexagonal packing of the mesopores, containing magnetic nanoparticles inside the core of mesoporous silica framework. Loading and delivery capabilities of 9-aminoacridine (9AA) and camptothecin (CPT) from magnetic mesoporous silica nanoparticles (MMSN) are shown to be dependent on porous structure and presence of phenylethyl moiety inside the mesopores. Characterization of the magnetic drug delivery systems and *in vitro* viability studies on Chinese hamster ovarian (CHO) cells are presented. My personal contribution represents 80 % of the presented research.

Chapter 4 presents the application of magnetic mesoporous silica nanoparticles for the construction of functional UV light sensitive drug carrier. Anticancer drug camptothecin was loaded inside the mesopores of the magnetic material and it was entrapped by functionalized cadmium-sulfide nanoparticles though a photolabile MSN-bonded linker. Release of the drug was triggered upon irradiation with UV light. Cooperative cytotoxic activity of capping CdS nanoparticles and loaded drug was observed upon the treatment of CHO cells and exposure to low power UV irradiation. My personal contribution represents 80 % of the presented research.

Chapter 5 describes encapsulation of sulforhodamine 101 as a cargo molecule inside the mercaptopropyl functionalized mesopores of MSN by mercapto-coordinated $Ru(bpy)_2(PPh_3)$-moieties (bpy = 2,2'-bipyridine, PPh_3 = triphenylphosphine). Thus constructed nanocarrier was capable of delivering the mesopore-loaded molecules upon irradiation with visible light or upon the treatment with nitrogen-monoxide, histidine or imidazole. My personal contribution represents 90 % of the presented research.

Chapter 6 is a general conclusion.

Literature Overview

Nanoscience, nanotechnology, nanomaterials and similar "nano"-words are word compounds developed only a few decades ago but the terms are very frequently used in recent years in and outside of scientific community. Among the nanoscopic materials, mesoporous silica nanoparticles (MSN) have attracted much attention [1-5] owing to their large surface area (up to 1000 m^2/g), tunable pore diameter (2-30 nm), narrow pore size distribution, and high thermal stability. MSN material have been demonstrated as applicable for selective catalysis,[6-10] drug delivery,[2-5] sensing,[11-14] and separation techniques.[15-17]

Mesoporous materials are classified as having a pore diameter between 2 and 50 nm,[18] based on International Union of Pure and Applied Chemistry (IUPAC) nomenclature. Microporous materials have pore diameter smaller then 2 nm while macroporous materials have pore diameter larger then 50 nm. MSN material is usually synthesized by hydrolysis and condensation of silica precursors (typically tetraethoxysilane) in alkaline or acidic environment in the presence of structure directing agents. These structure templating molecules are usually surfactants with hydrophilic headgroups and long hydrophobic organic tails (like cetyltrimethylammoniumbromide (CTAB)), which typically self-assemble in water into more complex structures.[19] The tails of these amphiphilic molecules aggregate into hydrophobic domains while headgroups arrange on the phase separation interface, in contact with water molecules. Surfactants can adopt different structures in water environment (Figure 1), which mostly depends on their molecular structure, solution composition and concentration of the surfactant.

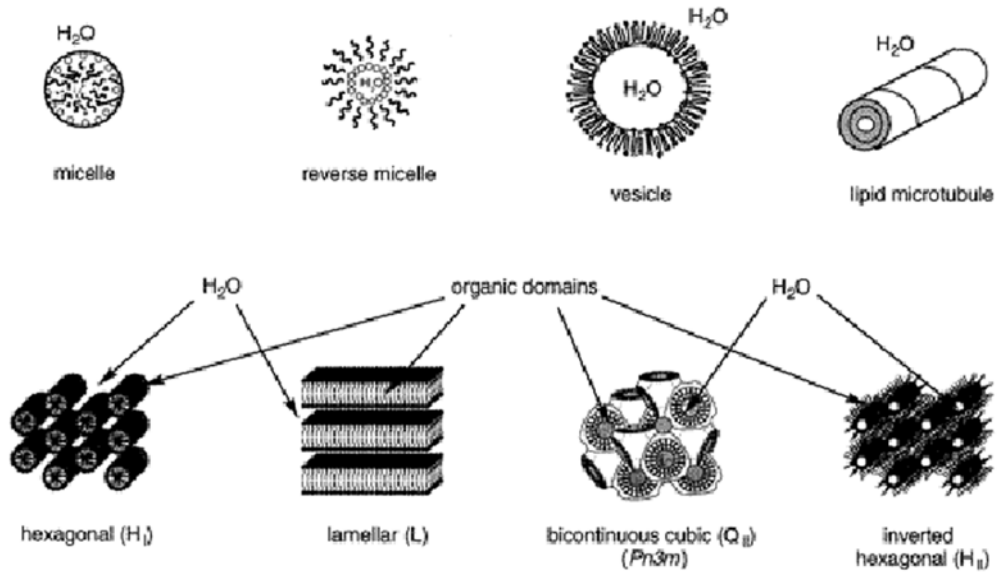

Figure 1. Common aggregate structures (top row) and liquid crystalline phases (bottom row) of amphiphiles in water.[19]

Critical packing parameter (CPP) is a quantity which helps in predicting the expected structures of amphiphiles in water.[20,21] The expression is CPP = v/a_0l_c, where l_c is the length and v is the volume of space occupied by the hydrophobic tail of the amphiphile while a_0 is the area of the headgroup. Small CPP (< 1/3) favors formation of structures with high surface curvature (for example micelles) while CPP in the range 1/3-1/2 favors tubular structures which are necessary for the formation of MSN type materials. Lamellar structure is favored if CPP value is around 1 while inverted hexagonal packing is achieved for CPP values higher then 1.

All the surfactant self-assemble structures exist in solution and cannot be isolated without destroying the structure. However, addition of silica precursors affords formation of a layer of SiO_2 polymer around micelle interfaces which stabilizes the assemblies.

Mesoporous silica material with hexagonal porous structure was developed in 1992 by scientists at Mobil corporation.[1] The authors reported on a series of silicate and aluminosilicate mesoporous molecular sieves, designated as M41S. One member of that series was MCM-41 material which contained hexagonal arrangement of mesopores. The authors also speculated on formation mechanisms of the material and two possible pathways are represented in Figure 2. Pathway (1) represents the scenario where surfactant first self-assembles into hexagonal array of micellar rods, after which the silicate precursors serve to solidify the structure. In the pathway (2), silicate precursors play an active role in every step of assembly formation and help in achieving the final structure

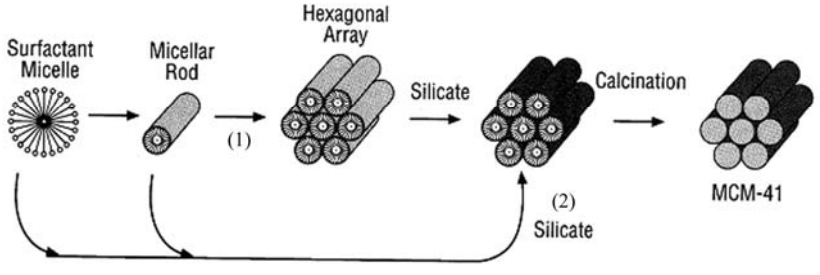

Figure 2. Possible mechanistic pathways for the formation of MCM-41: (1) liquid crystal phase initiated and (2) silicate anion initiated.

However, the as prepared MCM-41 material typically had non-uniform particle morphology as various shapes and particle diameters were obtained by the procedure. Subsequent modification of the preparation steps allowed construction of uniform, monodispersed nanoparticles. Particle morphology may be also influenced by addition of different organosilanes during the process of co-condensation of silica precursors (Figure 3).[22] This co-condensation process allows direct functionalization of silica surface during the synthesis of the material, which was shown to be preferential for internal surface of the mesopores. Typically, organosilanes (R-TMS or R-TES, where R is organic functional group while TMS is trimethoxysilane and TES is triethoxysilane) is added into the reaction solution together with TEOS or immediately after the addition of TEOS, which affords incorporation of organosilanes in the final material.

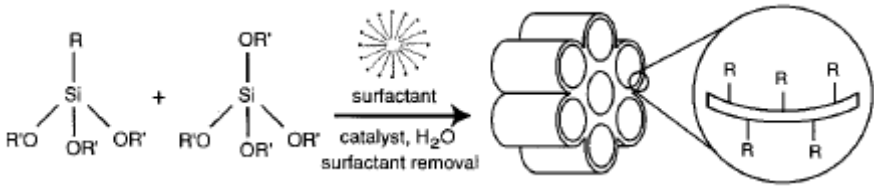

Figure 3. Organic functionalization of MSN by co-condensation

Another technique for organic functionalization of silica surface is post-synthesis grafting. In this procedure non-functional MSN is first isolated and then condensed with added organosilane. Typically the grafting is done at elevated temperature (120 ºC) in water-free solvents (toluene, DMF etc.). If MSN used for grafting still contains surfactant inside the mesopores, preferential functionalization of only external surface of MSN can be accomplished.

After the preparation of MSN, surfactant molecules from the mesopores can be removed either by washing with acidified methanol solution or by calcination. The difference between materials isolated by the two procedures is that after washing procedure the material still contains most of its surface silanol groups. Calcination at high temperature (usually

550 ºC) removes those silanol moieties along with any present organic molecules. However, silanol groups of the calcined material can be recovered by boiling in water.

In terms of drug delivery application, MSN offers many beneficial characteristics for the construction of an efficient drug delivery system (DDS). We have shown *in vitro* that MSN is biocompatible material up to a concentration of 100 μmol/g.[23] Recent report also showed that non-functionalized MSN was biocompatible in mice for internalization by intraperitoneal injection up to a concentration of 1 mg/ml and if subcutaneous injection was used up to ~ 30 mg/ml.[24]

Diameter of MSN nanoparticles is typically 100-200 nm which allows them to penetrate the cell membrane and enter the cell cytoplasm by the process of endocytosis.[25] In addition, the size of MSN enables selective accumulation of a MSN based DDS in the extracellular medium of tumor tissue due to enhanced permeability and retention effect (EPR) of cancerous tissue.[26] This effect in cancer tissue occurs due to formation of additional vasculature system through angiogenesis because of increased need for nutrients. Namely, once the cluster of tumor cells reaches the size of about 2 mm the angiogenesis must be activated in order to sustain the growth of the tumor tissue. These newly formed blood vessels are typically highly permeable and do not have functional lymphatic drainage system which enables the selective accumulation of macromolecules.

Additional DDS-beneficial characteristic of MSN is its high surface area, which is typically around 1000 m^2/g. This feature allows high loading of the therapeutic agents on the surface of MSN. The drug can be adsorbed on the silica surface typically through electrostatic interactions, van der Waals forces or/and through forming hydrogen bonds with the surface silanols. In addition, surface of MSN can be easily functionalized by condensation reaction with desired organosilanes, which allows construction of more complex drug delivery systems.

Hence, MSN offers the possibility of construction of functional supramolecular assemblies. Drug molecules can be filled inside the mesopores of MSN and entrapped by capping the pore entrances with suitable blockers. Up to now there have been reports on application of CdS,[27] Au,[28] Fe_3O_4 nanoparticles,[29] rotaxanes,[30] dendrimers,[31] polymers[11] and proteins[32] as capping moieties while triggering the release of entrapped molecules was accomplished by chemical agents,[27,30] enzymes,[32] temperature change,[33] light irradiation[34] or change in pH value.[35] For example, we demonstrated encapsulation of molecules inside the mesopores of MSN by covalently bonded CdS nanoparticles (Figure 4).[27]

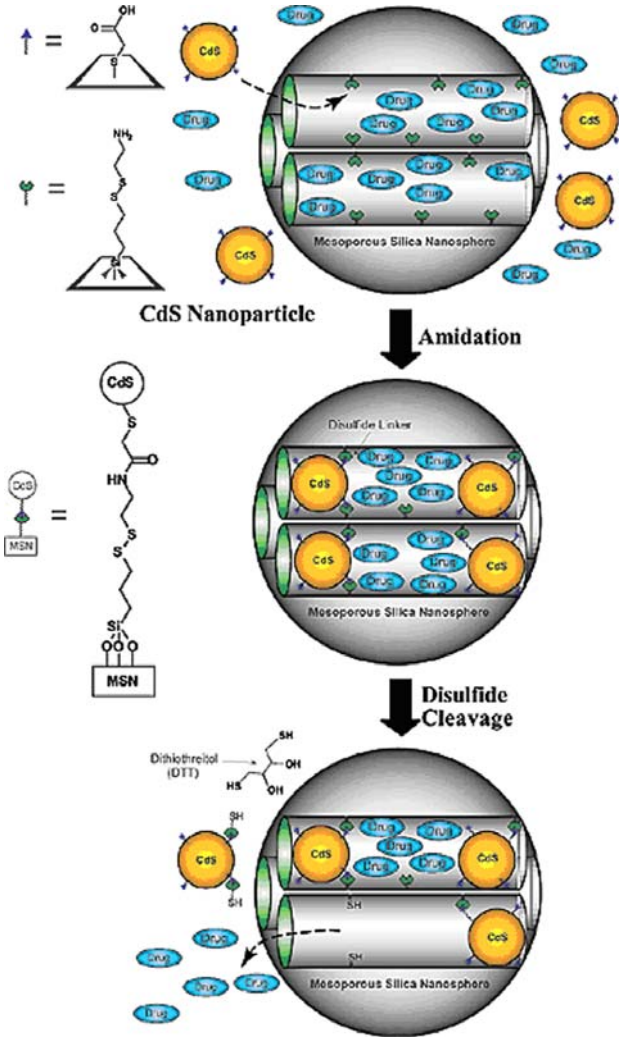

Figure 4. Schematic representation of the CdS nanoparticle-capped MSN-based drug delivery system.[27]

The controlled-release of the drug molecules was achieved upon chemical reduction of the disulfide linkage between the CdS nanoparticles and the MSN. In the case of using magnetite nanoparticles as caps for the MSN mesopores,[29] the whole system was shown to be magnetically active, which showcased the possibility of controlling the location of drug release with external magnetic field, i.e., magnetically targeted drug delivery. Another recent report from our group demonstrated the use of MSN based DDS for the stimuli responsive delivery of both bioactive caps and cargo molecules.[36] Namely, saccharide responsive, insulin capped MSN was used to deliver gluconic acid-modified insulin (G-Ins) and the encapsulated drug (cyclic adenosine monophosphate (cAMP)), both of which can be used in diabetes treatment (Figure 5).

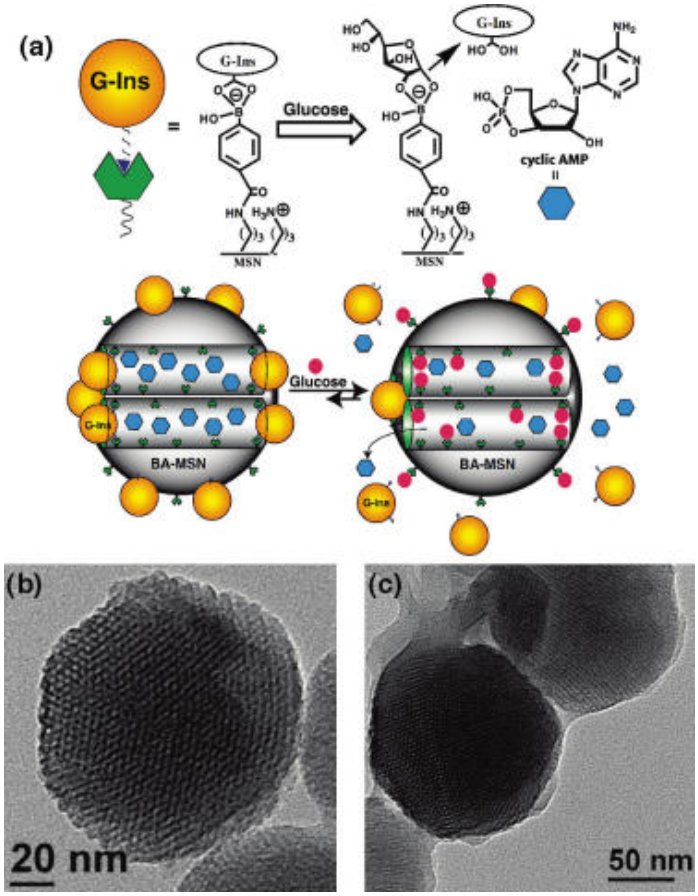

Figure 5. (a) Schematic representation of the glucose-responsive MSN based delivery system for controlled release of bioactive G-Ins and cAMP. Transmission electron micrographs of (b) boronic acid-functionalized MSN and (c) FITC-G-Ins-capped MSN.[36]

MSN based molecular valve for the entrapment and delivery of cargo molecules was also devised by a combined effort from Stoddart and Zink research groups.[30,37] The authors reported on a rotaxane functionalized MSN which reversible entraps and releases small molecules from the mesopores (Figure 6).

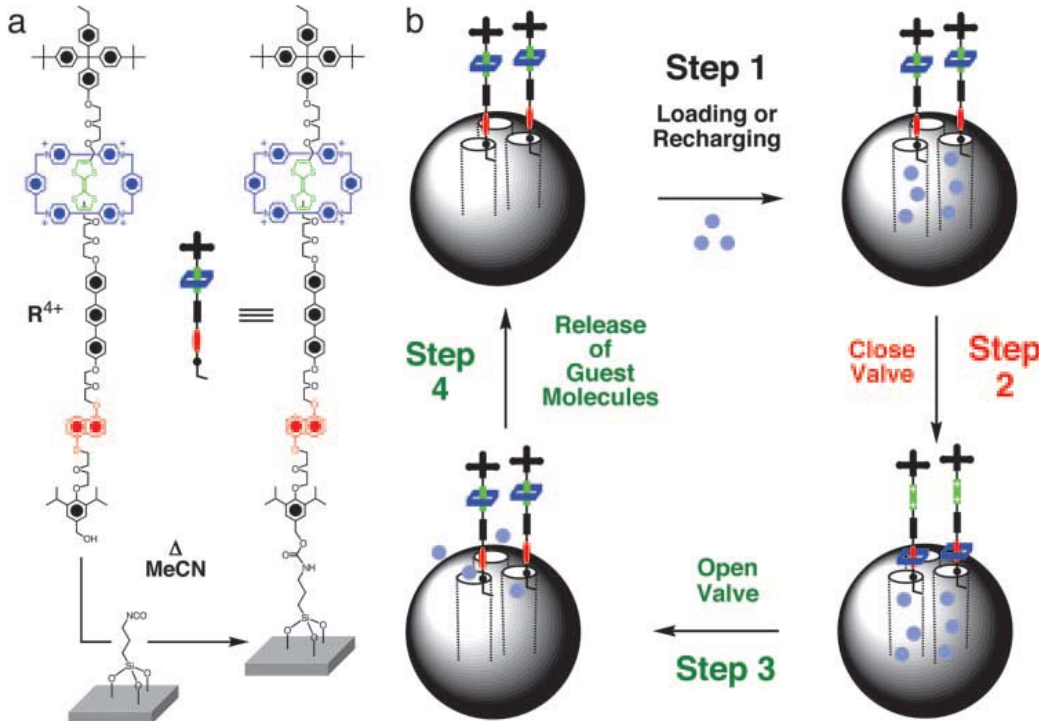

Figure 6. Graphical representations of the surface attachment of bistable rotaxanes to silica particles along with a cycle for loading and release of guest molecules. (*a*) The structural formula of the bistable [2]rotaxane R^{4+} and the procedure used for tethering R^{4+} to the surface of mesoporous silica particles. (*b*) The proposed mechanism for the operation of the nanovalve. The moving part of the molecular valve is a $CBPQT^{4+}$ ring (blue), which shuttles between a TTF station (green) and a DNP station (red) under redox control. The openings of the cylindrical pores on the silica are blocked by the $CBPQT^{4+}$ ring when the valve is closed. Guest molecules (turquoise spheres) are loaded in Step 1 by diffusion into the open pores when the $CBPQT^{4+}$ ring is located on the TTF station. The valve is closed in Step 2 by oxidation of the TTF unit to its dication, causing the $CBPQT^{4+}$ ring to move to the DNP station, which is much closer to the openings of the pores. The valve can be opened (Step 3) by adding ascorbic acid to reduce the TTF dication back to its neutral state, whereupon the $CBPQT^{4+}$ ring moves back from the DNP station to be relocated around the much more π electron-rich TTF station, releasing the guest molecules in Step 4. The valve is ready for recharging (i.e., returning to Step 1). Thus, the valve can be closed and opened reversibly. The silica particles are not drawn to scale, and only a few of the ordered pores are shown. [30]

Schlossbauer et al. recently demonstrated utilization of nature's host-guest chemistry for capping the mesopores of MSN.[32] Namely, tetrameric protein avidin was used as a cap for entrapping molecules inside the mesopores of biotin functionalized MSN. Furthermore, release of the cargo molecules was achieved by exposure to a solution of proteolytic enzyme which disintegrates the protein cap.

Targeting specific cells and organs within the body can also be accomplished by modification of a surface of DDS with antibodies or appropriate ligands.[38] For example, Rosenholm et al recently reported targeting of cancer cells by folic acid (FA) functionalized MSN.[39] The authors first functionalized the surface of MSN with a layer of polyethyleneimine (PEI) onto which they attached folic acid molecules. PEI layer in this case had a role in multiplying possible FA attachment sites as well as in increasing the suspension stability of the DDS and improving its cell uptake ability.[40] The results showed that the cancer cells internalized an order of magnitude more of FA functionalized MSN compared to the healthy cells. In addition, endocytosis of the DDS was successfully inhibited by the addition of free folic acid. This cancer targeting effect was possible due to overexpression of folate receptors on the surface of cancer cells.[41]

Other possible pathways exist for the development of cancer homing nanodevices. For example it has been shown that if anticancer drug doxorubicin was attached to a tripeptide sequence Arg-Gly-Asp (RGD), α_v integrins are selectively targeted, which are overexpressed on the angiogenic vessels of solid tumors.[42] This type of cancer targeting which is based on interaction with specific receptors of tumor tissue or based on its EPR effect can be considered as passive cancer targeting. That is, drug-carrier system is intravenously introduced into the organism and its spontaneous accumulation at the cancer site is expected. However, even with the higher affinity for tumor tissue, much of the cytotoxic drugs still end up in healthy cells.

Alternatively (or in addition to some forms of passive targeting), the site of drug delivery can be actively targeted by an external stimulus, which is a topic of this dissertation. For example, the drug carriers can be magnetically active which would open the possibility to control the location of a DDS by an externally applied magnetic force.[43] Additionally, release of the drug from DDS can be actively controlled by an external stimulus, for instance by light irradiation.

This dissertation will cover design and development of novel nanodevices for UV light (chapters 2 and 4) and visible light (chapter 5) responsive drug delivery. In addition, development of magnetic analogues of mesoporous silica nanoparticles (MMSN) for drug delivery is described in chapter 3. We envision that these results can be used to improve the efficacy of cancer treatment and reduce the harmful effects of anticancer drugs on healthy tissue.

References

(1) Kresge, C. T.; Leonowicz, M. E.; Roth, W. J.; Vartuli, J. C.; Beck, J. S. *Nature (London)* **1992**, 359, 710-12.
(2) Vallet-Regi, M.; Balas, F.; Arcos, D. *Angew. Chem., Int. Ed.* **2007**, 46, 7548-7558.
(3) Trewyn, B. G.; Slowing, I. I.; Giri, S.; Chen, H.-T.; Lin, V. S. Y. *Acc. Chem. Res.* **2007**, 40, 846-853.
(4) Trewyn, B. G.; Giri, S.; Slowing, I. I.; Lin, V. S. Y. *Chem. Commun. (Cambridge, U. K.)* **2007**, 3236-3245.
(5) Angelos, S.; Liong, M.; Choi, E.; Zink, J. I. *Chem. Eng. J. (Amsterdam, Neth.)* **2008**, 137, 4-13.
(6) Huh, S.; Chen, H.-T.; Wiench, J. W.; Pruski, M.; Lin, V. S. Y. *Angew. Chem., Int. Ed.* **2005**, 44, 1826-1830.
(7) Inumaru, K.; Ishihara, T.; Kamiya, Y.; Okuhara, T.; Yamanaka, S. *Angew. Chem., Int. Ed.* **2007**, 46, 7625-7628.
(8) Mori, K.; Kondo, Y.; Morimoto, S.; Yamashita, H. *Chem. Lett.* **2007**, 36, 1068-1069.
(9) Fukuoka, A.; Kimura, J. I.; Oshio, T.; Sakamoto, Y.; Ichikawa, M. *J. Am. Chem. Soc.* **2007**, 129, 10120-10125.
(10) Li, C.; Zhang, H. D.; Jiang, D. M.; Yang, Q. H. *Chem. Commun.* **2007**, 547-558.
(11) Radu, D. R.; Lai, C.-Y.; Wiench, J. W.; Pruski, M.; Lin, V. S. Y. *J. Am. Chem. Soc.* **2004**, 126, 1640-1641.
(12) Descalzo, A. B.; Marcos, M. D.; Monte, C.; Martinez-Manez, R.; Rurack, K. *J. Mat. Chem.* **2007**, 17, 4716-4723.

(13) Lei, B. F.; Li, B.; Zhang, H.; Zhang, L. M.; Li, W. L. *J. Phys. Chem. C* **2007**, 111, 11291-11301.
(14) Basabe-Desmonts, L.; Reinhoudt, D. N.; Crego-Calama, M. *Chm. Soc. Rev.* **2007**, 36, 993-1017.
(15) Kim, S.; Ida, J.; Guliants, V. V.; Lin, J. Y. S. *J. Phys. Chem. B* **2005**, 109, 6287-6293.
(16) Oh, S.; Kang, T.; Kim, H.; Moon, J.; Hong, S.; Yi, J. *J. Membr. Sci.* **2007**, 301, 118-125.
(17) Brady, R.; Woonton, B.; Gee, M. L.; O'Connor, A. J. *Innovat. Food Sci. Emerg.Technol.* **2008**, 9, 243-248.
(18) Sing, K. S. W.; Everett, D. H.; Haul, R. A. W.; Moscou, L.; Pierotti, R. A.; Rouquerol, J.; Siemieniewska, T. *Pure Appl. Chem.* **1985**, 57, 603-619.
(19) Gin, D. L.; Gu, W.; Pindzola, B. A.; Zhou, W. J. *Acc. Chem. Res.* **2001**, 34, 973-80.
(20) Israelachvili, J. N. *Intermolecular and surface forces : with applications to colloidal and biological systems*; Academic Press: London ; Orlando, [Fla]. 1985.
(21) Huo, Q. S.; Margolese, D. I.; Stucky, G. D. *Chem. Mater.* **1996**, 8, 1147-1160.
(22) Huh, S.; Wiench, J. W.; Trewyn, B. G.; Song, S.; Pruski, M.; Lin, V. S. Y. *Chem. Commun. (Cambridge, U. K.)* **2003**, 2364-2365.
(23) Slowing, I.; Trewyn, B. G.; Lin, V. S. Y. *J. Am. Chem. Soc.* **2006**, 128, 14792-14793.
(24) Hudson, S. P.; Padera, R. F.; Langer, R.; Kohane, D. S. *Biomaterials* **2008**, 29, 4045-55.
(25) Sun, W.; Fang, N.; Trewyn, B. G.; Tsunoda, M.; Slowing, I. I.; Lin, V. S. Y.; Yeung, E. S. *Anal. Bioanal. Chem.* **2008**, 391, 2119-2125.
(26) Greish, K. *J. Drug Target.* **2007**, 15, 457-64.
(27) Lai, C.-Y.; Trewyn, B. G.; Jeftinija, D. M.; Jeftinija, K.; Xu, S.; Jeftinija, S.; Lin, V. S. Y. *J. Am. Chem. Soc.* **2003**, 125, 4451-4459.
(28) Vivero-Escoto, J. L.; Slowing, I. I.; Wu, C.-W.; Lin, V. S. Y. *J. Am. Chem. Soc.* **2009**, 131, 3462-3463.
(29) Giri, S.; Trewyn, B. G.; Stellmaker, M. P.; Lin, V. S. Y. *Angew. Chem., Int. Ed.* **2005**, 44, 5038-5044.
(30) Nguyen, T. D.; Tseng, H. R.; Celestre, P. C.; Flood, A. H.; Liu, Y.; Stoddart, J. F.; Zink, J. I. *Proc. Natl. Acad. Sci. U. S. A.* **2005**, 102, 10029-10034.
(31) Radu, D. R.; Lai, C.-Y.; Jeftinija, K.; Rowe, E. W.; Jeftinija, S.; Lin, V. S. Y. *J. Am. Chem. Soc.* **2004**, 126, 13216-13217.
(32) Schlossbauer, A.; Kecht, J.; Bein, T. *Angew. Chem. Int. Ed.* **2009**, 48, 3092-5.
(33) You, Y.-Z.; Kalebaila, K. K.; Brock, S. L.; Oupicky, D. *Chem. Mater.* **2008**, 20, 3354-3359.
(34) Mal, N. K.; Fujiwara, M.; Tanaka, Y. *Nature* **2003**, 421, 350-3.
(35) Hong, C. Y.; Li, X.; Pan, C. Y. *J. Mater. Chem.* **2009**, 19, 5155-5160.
(36) Zhao, Y.; Trewyn, B. G.; Slowing, II; Lin, V. S. *J. Am. Chem. Soc.* **2009**, 131, 8398-400.
(37) Nguyen, T. D.; Liu, Y.; Saha, S.; Leung, K. C. F.; Stoddart, J. F.; Zink, J. I. *J. Am. Chem. Soc.* **2007**, 129, 626-634.
(38) Brannon-Peppas, L.; Blanchette, J. O. *Adv. Drug Deliv. Rev.* **2004**, 56, 1649-59.
(39) Rosenholm, J. M.; Meinander, A.; Peuhu, E.; Niemi, R.; Eriksson, J. E.; Sahlgren, C.; Linden, M. *ACS Nano* **2009**, 3, 197-206.
(40) Godbey, W. T.; Wu, K. K.; Mikos, A. G. *J. Control. Release* **1999**, 60, 149-60.
(41) Sudimack, J.; Lee, R. J. *Adv. Drug. Deliv. Rev.* **2000**, 41, 147-62.
(42) Arap, W.; Pasqualini, R.; Ruoslahti, E. *Science* **1998**, 279, 377-380.
(43) Jurgons, R.; Seliger, C.; Hilpert, A.; Trahms, L.; Odenbach, S.; Alexiou, C. *J. Phys.: Condens. Matter* **2006**, 18, S2893-S2902.

CHAPTER 2. LIGHT AND pH SENSITIVE RELEASE OF DOXORUBICIN FROM MESOPOROUS SILICA NANOPARTICLE-BASED DRUG CARRIER

Manuscript submitted for publication to *Chemistry-a European Journal*

Nikola Ž. Knežević and Victor S.-Y. Lin*

Department of chemistry, Iowa State University, Ames, Iowa, 50011

Abstract

Anticancer drug doxorubicin (Dox) was adsorbed on nitroveratryl carbamate-protected aminopropyl-functionalized mesoporous silica nanoparticles (MSN). Upon exposure to UV light positively charged propylammonium moieties were formed on MSN surface which caused expulsion of positively charged doxorubicin molecules from the surface of nanoparticles. Light induced release of the drug was a faster process then its photodegradation which yielded a net effect of photosensitive Dox release. The drug release was also increased with lowering pH value from 7.4 to 6.4. We believe that these results may be beneficial for targeting the doxorubicin delivery selectively to tumor cell clusters by externally applied light irradiation, which would work in cooperation with targeting weakly acidic extracellular matrix of tumor tissues.

Introduction

Ever since its discovery and first antitumor tests in 1969,[1] Doxorubicin (Dox) has been one of the most used anticancer drugs in chemotherapy. Even though it was shown effective against wide range of tumors,[2] the severe adverse effects that Dox induces on

healthy tissue are still problems that are preventing its more effective use.[3] The same issue exists with implementation of other cytotoxic drugs and it brought a need for development of targeting drug delivery systems (DDS), which would account for administration of cytotoxic drugs specifically to the cancer cells.[4]

Much of the efforts have been concentrated on devising the DDS based on mesoporous silica nanoparticles (MSN).[5] Their solid silica framework ensures the structural integrity of DDS but at the same time allows easy manipulation of its chemical characteristics by condensation reaction with various organosilanes to form a surface layer of organic functional groups. In addition, MSN offers high surface area, isostructural mesoporosity and a particle diameter (100 - 200 nm) which is in range to enhance the targeting ability of a DDS due to enhanced permeability and retention (EPR) effect of cancerous tissue.[6]

Light responsive DDS have been recently investigated and it was shown to be a promising route toward establishing functional targeted drug delivery.[7] However, light responsive Dox delivery is a challenge because the drug have been found to undergo degradation upon exposure to light.[8] The process is manifested by decrease in drug fluorescence due to destruction of the chromophore. First order kinetics was determined for the process, it is inversely proportional to Dox concentration and the degradation increases with pH value of the solution. Additionally, release of drugs upon lowering pH value is a desirable feature of drug delivery systems because most solid tumors have lower extracellular pH compared to the surrounding healthy tissue.[9] Hence, we set a goal to construct a doxorubicin delivery system responsive to both a decrease in pH value and light irradiation.

For that function we devised a MSN functionalized with propyl-carbamic acid 4,5-dimethoxy-2-nitrobenzyl ester (or nitroveratryl-carbamate protected aminopropyl functionalized mesoporous silica nanoparticles = NVCAP-MSN). Nitroveratryl (NV) moiety have been known for several decades as an effective photoresponsive protection group.[11]

Scheme 1a depicts the organic functional groups attached on the silica surface and their photochemically induced degradation pathway. Irradiation of the suspension of the material in PBS buffer with UV light (350 nm) triggers the degradation of carbamate linkage, followed by the release of 4,5-dimethoxy-2-nitroso-benzaldehyde, CO_2 and free amine groups. We propose that if doxorubicin (Scheme 1b) was adsorbed on the silica surface of NVCAP-MSN, its delivery to the surrounding medium upon irradiation of the material would be induced by electrostatic repulsion between freed surface-bound propylammonium moieties and positively charged amine group from doxorubicin.

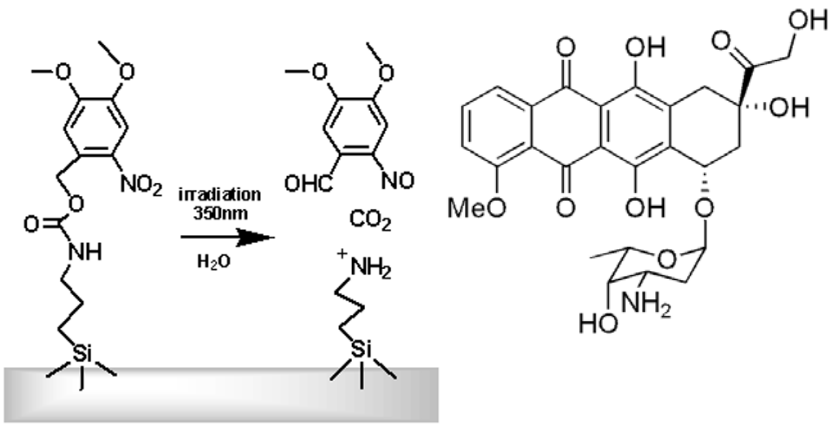

Scheme 1. a) Structural representation of NVCAP-MSN and UV light triggered deprotection of amine groups; b) molecular structure of doxorubicin.

Experimental Section

Tetraethoxyorthosilicate (TEOS), *n*-Cetyltrimethylammoniumbromide (CTAB), 3-aminopropyltrimethoxysilane (AP-TMS), 1,1'-carbonyldiimidazole and 4,5-dimethoxy-2-nitrobenzyl alcohol were commercially available (Aldrich) and were used as received.

Instrumental Methods, Conditions and Parameters for Structural Characterization:

Powder XRD diffraction data were collected on a Scintag XRD 2000 X-ray diffractometer using Cu (Kα) radiation. Nitrogen adsorption and desorption isotherms, surface areas, and median pore diameters were measured using a Micromeritics Tristar 3000 surface area and porosity analyzer. Sample preparation included degassing at 100 °C for 5 h. Specific surface areas and pore size distributions were calculated using the Brunauer-Emmett-Teller (BET) and Barrett-Joyner-Halenda (BJH) method, respectively. Particle morphology of the material was determined by scanning electron microscopy (SEM) using a JEOL 840A scanning electron microscope. IR spectra were recorded by using Nicolet Nexus 470 FT-IR. Solid-state ^{29}Si and ^{13}C CP-MAS NMR spectra were obtained on Bruker AVANCE-600 NMR spectrometer. Fluorescence measurements were performed on Horiba group Fluoromax-2 fluorometer.

Synthesis of double-functionalized aminopropyl-MSN material (AP^2-MSN):

n-Cetyltrimethylammoniumbromide (CTAB, 1.00 g, 2.74 x 10^{-3} mol) was first dissolved in 480 mL of Nanopure water. NaOH(aq) (2.00 M, 3.50 mL) was added to CTAB solution, followed by adjusting the solution temperature to 353 K. TEOS (5.00 mL, 2.57 x 10^{-2} mol) was first introduced dropwise to the surfactant solution, followed by the dropwise addition of a freshly prepared solution of APTMS (0.9 mL, 5.13 x 10^{-3} mol) in 9.1 ml of water. The mixture was allowed to stir for 2 h to give rise to white precipitate (as synthesized AP-MSN). The solid product was filtered, washed with deionized water and methanol, and dried for 12 h under high vacuum and 353 K in order to stabilize the mesoporous structure. Additional grafting of APTMS on the external surface of AP-MSN was performed by refluxing APTMS (353 µl, 2 x 10^{-3} mol) with the suspension of as synthesized AP-MSN (1 g) in dry toluene (50 ml). After filtering and washing with toluene, 2-propanol and methanol, the as synthesized AP^2-MSN was again dried under high vacuum at 353 K. Final

double-functionalized aminopropyl-MSN material was obtained upon removal of the CTAB surfactant template by Soxhlet extraction with a solution of HCl in methanol (1%, v:v). After 24 h of extraction the material was additionally washed with deionized water and methanol, and it was again placed under high vacuum at 353 K to remove the remaining solvent from the mesopores.

Preparation of 2-nitroveratrylcarbamate-aminopropyl-MSN (NVCAP-MSN):

The following procedure was done under nitrogen atmosphere. Solution of 1,1'-carbonyldiimidazole (324.4 mg, 2 x 10-3 mol) in 4 ml of dry dichloromethane was cooled in an ice-water bath to 273 K. Solution of 4,5-dimethoxy-2-nitrobenzyl alcohol (426.4 mg, 2 x 10-3 mol) in 23 ml of dry dichloromethane was separately prepared and added drop-wise to the stirred solution of 1,1'-carbonyldiimidazole. The solution was protected from light and then stirred for additional 1 h at room temperature after which 500 mg of dry AP2-TMS was added. The suspension was stirred for additional 48 h in order to form the carbamate linkage. Prepared NVCAP-MSN material was filtered, washed with plenty of dichloromethane, methanol, water and finally again with methanol and dried in a lyophilizer. In order to determine the amount of nitroveratryl groups on the surface of MSN, the filtrate was collected and solvents evaporated. The residue was dissolved in PBS buffer (10 mM, pH = 7.4, I = 154 mM) which now contained free 2-nitroveratryl alcohol, imidazole and carbonates, due to degradation of any intermediate imidazolide derivative in water environment. UV-VIS spectrum of the solution was taken and the amount of nitroveratryl groups on the surface of MSN (1.2 mmol of NV groups/g AP^2-MSN) was determined from the difference between the starting amount of nitroveratryl alcohol and the amount determined by measuring absorbance of nitroveratryl alcohol from the filtrate at 350 nm, quantified from a standard curve.

Adsorption of doxorubicin on the surface of NVCAP-MSN (Dox@NVCAP-MSN):

Doxorubicin hydrochloride (5.8 mg, 1 x 10^{-5} mol) was dissolved in 3 ml of methanol and neutralized with NaOH solution in methanol. NVCAP-MSN (100 mg) was added to the solution and the suspension was protected from light and stirred at room temperature for 24 h. The as prepared Dox@NVCAP-MSN was filtered and washed with plenty of methanol. The amount of adsorbed drug (80 mg of Dox/g of NVCAP-MSN) was determined from the difference between the starting amount of doxorubicin and the amount determined by measuring absorbance of the drug from the filtrate at 490 nm in PBS solution, quantified from a standard curve.

Irradiation of the samples was performed on Rayonet RPR-100 photoreactor equipped with 16 RPR-3500 lamps. The lamps have an emission maximum at 350 nm. Light intensity of the irradiation source was measured with Spectroline DSE-2000HA/L Radiometer/Photometer. At the center of the photoreactor the measured light intensity was 5.5 mW/cm2. Prepared materials were subjected to irradiation by placing them in the center of the photoreactor as PBS suspensions (1 mg/ml). During irradiation the samples were stirred with magnetic stirrer and light induced heating was prevented by cooling with an integrated fan.

For the first experiment release of the drug was measured in PBS buffer at two pH values (6.4 and 7.4). Suspension of the material (1 mg/ml) was first stirred in dark for 20 h and fluorescence of doxorubicin was measured at 595 nm (exc. 495 nm) from the PBS supernatant after centrifugation at designated times The samples were then placed in a photoreactor and subjected to irradiation for 30 minutes under stirring. After that, fluorescence of the supernatant was again measured as described and the suspensions were returned to stirring in dark as the measurements continued.

Second release experiment was done in PBS buffer at pH = 7.4. Suspension of the material (1 mg/ml) was first stirred in dark for 5 h until no additional release of Dox was

observed. The sample was then placed in photoreactor and subjected to irradiation. At designated times the suspension was centrifuged, fluorescence of doxorubicin was measured and the samples were immediately returned to the photoreactor for additional irradiation. Amount of the released drug was determined from a previously prepared standard curve.

Results and Discussion

Preparation of the material included synthesis of aminopropyl-functionalized MSN by our established co-condensation procedure.[3c,d] In order to increase the surface coverage of organic functionality as synthesized material was additionally grafted with aminopropyl-trimethoxysilane, followed by surfactant extraction with diluted solution of HCl in methanol. Formation of nitroveratryl carbamate was accomplished by following the procedure reported by D'Addona and Bochet.[12] Namely, NV alcohol and 1,1'-carbonyldiimidazole were initially coupled in dry dichloromethane solution, after which the as made imidazolide derivative was reacted with primary amine groups from the MSN surface. The amount of nitroveratryl groups on the surface of MSN was determined after the reaction to be 1.2 mmol/g NVCAP-MSN, by measuring UV-VIS absorbance of NV alcohol from PBS solution of the filtrate residue.

SEM image of NVCAP-MSN (Figure 1a) reveals the spherical morphology of the material with average diameter of 184 ± 44 nm. XRD analysis of NVCAP-MSN (Figure 1b) showed the presence of a single diffraction peak, attributed to [100] reflection from hexagonally packed mesopores. Higher order reflections ([110] and [200]) which are often seen on MSN type materials are missing in this case due to disruption of longer range symmetry after the grafting procedure and carbamate formation.

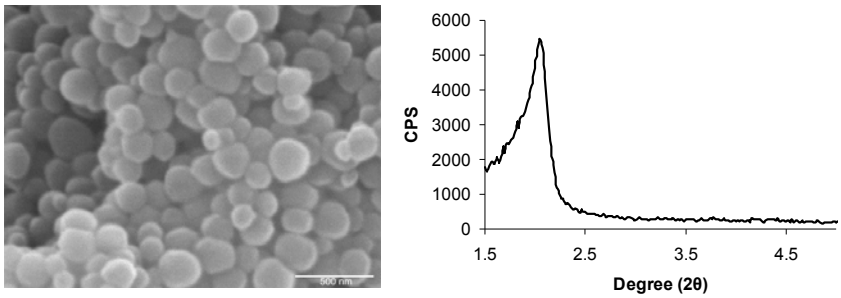

a) b)

Figure 1. a) Scanning electron micrograph (SEM) image and b) small angle powder X-ray diffractogram (XRD) of NVCAP-MSN.

The presence of nitroveratryl carbamate protection groups was confirmed by ^{13}C CPMAS NMR spectrum (Figure 2) and IR spectrum (Table 1, Figures 3 and S1).

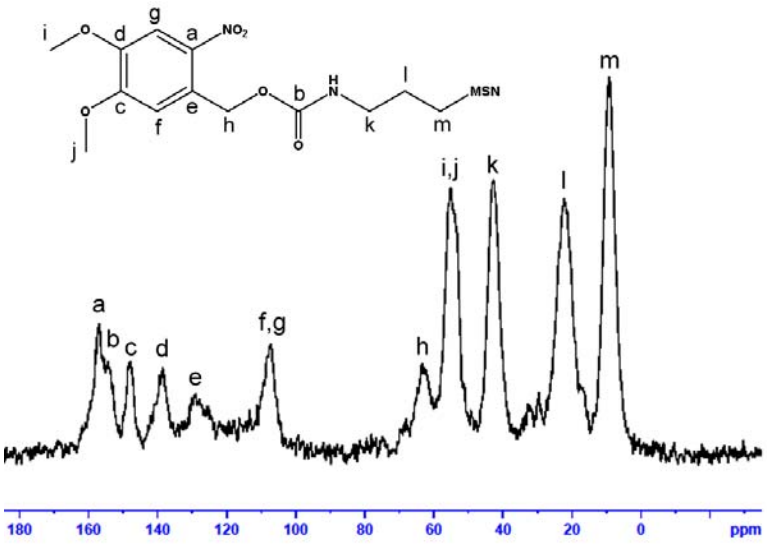

Figure 2. 13C CPMAS NMR spectrum of NVCAP-MSN and peak assignment

In order to test the reactivity of NVCAP-MSN and capability to produce the free amine moieties, material suspension was subjected to UV irradiation for 30 minutes (350 nm, 5.5 mW/cm^2). After extensive washings and drying, IR spectrum of the produced material was taken and the result is shown on Figure 3. As can be seen, the irradiation caused

emergence of a new broad band at 1640 cm-1, which can be assigned to $\delta(NH_3^+)$ of a newly freed aminopropyl moieties. As a comparison, the same vibration band was observed in IR spectrum of aminopropyl-functionalized MSN, before the coupling to nitroveratryl alcohol. In addition, release of 4,5-dimethoxy-2-nitroso-benzaldehyde from the material upon irradiation in PBS was clearly evident by the appearance of intense UV-VIS band, centred at 350 nm (Figure S2).

Zeta potential measurements in PBS buffer at pH = 7.4 revealed that before irradiation NVCAP-MSN showed the value of + 5.7 mV. The value is positive probably because of some free aminopropyl moieties that were left without carbamate protection even after 48 h of coupling reaction. After 5 minutes of irradiation the ζ potential value increased to + 10.3 mV, which is in agreement with the release of positively charged amine moieties.

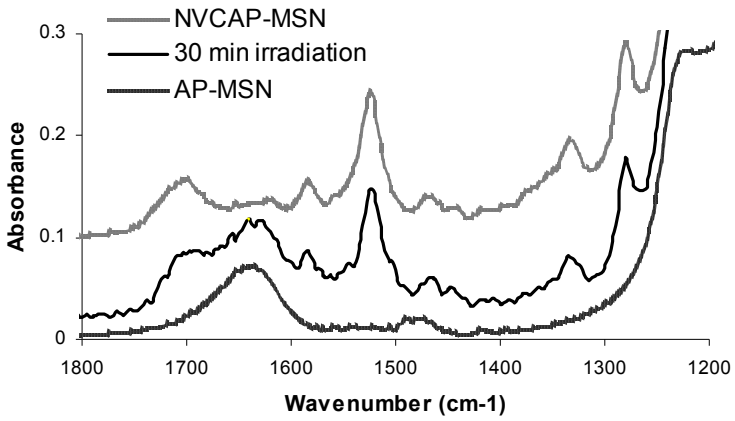

Figure 3. Comparison of IR spectra of NVCAP-MSN (top), NVCAP-MSN after 30 minutes of irradiation (middle) and aminopropyl-functionalized MSN (bottom)

Table 1. Assignment of the bands from IR spectrum of NVCAP-MSN

Wavenumber (cm^{-1})	1700	1584	1524	1333	1280
Assignment	C=O st	N-H δ	NO_2 st as	NO_2 st sy	N-CO-O st as

To study capability of NVCAP-MSN to adsorb and deliver doxorubicin upon exposure to UV light, the material was protected from light and stirred in a methanol solution of the drug. After allowing 24 h for adsorption, doxorubicin loaded material (Dox@NVCAP-MSN) was washed with plenty of methanol and dried. The amount of adsorbed drug was 80 μmol/g NVCAP-MSN, as determined from the UV-VIS absorption of doxorubicin from the filtrate solution. BET surface area (Figure S3) of the resulting Dox@NVCAP-MSN showed the value of 458 m^2/g, which is a decrease from 564 m^2/g as obtained for NVCAP-MSN due to surface adsorption of the drug.

Release of doxorubicin from the material was measured in PBS buffer at two pH values (6.4 and 7.4) and the response upon 30 minutes of irradiation with UV light is represented in Figure 4a. It is evident that the release of doxorubicin is responsive both to pH value and UV irradiation. Solvation of Dox@NVCAP-MSN in PBS induces initial release of the drug as a result of electrostatic repulsion between now positively charged Dox molecules and MSN surface. Higher amount of doxorubicin was released at pH = 6.4 because more of the drug senses electrostatic repulsion from the positively charged solid surface. Namely amine group from doxorubicin is partially deprotonated at pH 7.4 (pKa = 8.22)[13] while fully protonated at pH 6.4. In addition, NCAP-MSN has a higher total positive charge at pH 6.4 because of presence of surface silanol groups (pKa = 6.8) which are deprotonated at pH 7.4, decreasing the total positive charge of the surface. Presence of the silanol groups was confirmed by ^{29}Si NMR DP MAS spectrum of NVCAP-MSN (Figure S4). After irradiation of the sample for 30 minutes doxorubicin fluorescence increased, which indicated successful expulsion of Dox molecules because of repulsion with freed propylammonium ions from the surface. Amount of the drug in solution increased even though employed irradiation conditions cause photodegradation of doxorubicin as well, as tested for the solution of Dox (1 μM) in PBS at pH 7.4 (Figure S5). We can consider that UV irradiation of Dox@NVCAP-MSN has both direct effects: cleavage of carbamate linkage and photodegradation of

doxorubicin. However, the photocleavage of carbamate linkage seems to be a faster process under these conditions, which yields in a net release of the drug from its nanocarrier. As stated above, photodegradation of doxorubicin is known to be inversely proportional to its concentration. Hence, we believe that since doxorubicin molecules are in this case adsorbed on the surface of nanospheres, their photodegradation is reduced due to high local concentration of drug molecules on the surface of nanoparticles. Bandak et. al. already reported that encapsulation of doxorubicin inside polyethyleneglycol-coated liposomes reduced UV-induced degradation of the drug.[10] This result was ascribed to high local concentration of doxorubicin, in addition to low pH value inside the liposomes. Once the drug molecules are released from the surface they are susceptible to faster photodegradation. However, degraded molecules are continuously outnumbered by the newly released molecules from the surface, which effects in net release of the drug.

In order to demonstrate the ability of the DDS to deliver Dox upon prolonged irradiation conditions, we subjected suspension of the drug loaded material to consecutive treatments with UV irradiation (Figure 4b). Continuous release of doxorubicin was successfully achieved which was proportional to the period of UV irradiation.

From the Figure 4a we can also notice that initial increase of doxorubicin concentration was more then 2 times higher at pH 6.4 when compared to the photoresponse at pH 7.4. In addition to better repulsion between the drug and host MSN at lower pH, as discussed above, the reasons for this result can be partially attributed also to slower photodegradation of released Dox molecules and faster deprotection of NV groups at lower pH value.[11c] However, after the initial rise in released drug amount, emission of doxorubicin deteriorates for up to 2 hours after irradiation stopped.

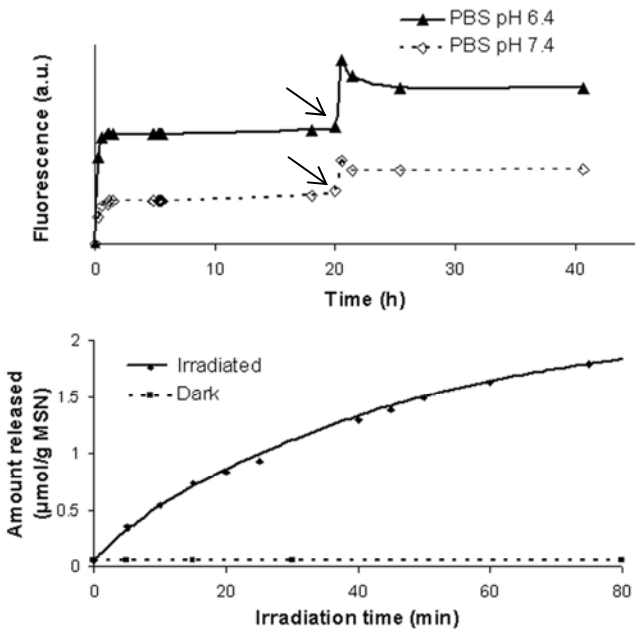

Figure 4. Release of doxorubicin from Dox@NVCAP-MSN: a) in PBS buffer at pH = 6.4 and pH = 7.4. Suspensions were subjected to 30 minutes of irradiation with UV light (350 nm) starting from the points marked by arrows; b) Amount of the released drug as a function of irradiation time in PBS buffer at pH = 7.4 compared to non-irradiated sample (dark). The progress was monitored after the initial solvation induced jump in released drug.

This effect is not due to continued degradation of the drug in dark. We tested if the same effect would be observed on a solution of doxorubicin (2 mg/ml) in PBS buffer for both pH values (6.4 and 7.4). After 30 minutes of irradiation of Dox solution in PBS, the emission intensity decreased when compared to the starting intensity but no further change was noticed after turning off the UV irradiation source. The same reduction of Dox fluorescence was noticed if we did the release experiment in MOPS buffer as well as in water, which indicates that the effect does not happen because of eventual buffering of positive charges of propylammonium ions through specific coupling with anions from buffer solution. We determined that this effect occurs as a result of partial backreaction of photoproducts, i.e. free MSN-attached amines react with 4,5-dimethoxy-2-nitroso-benzaldehyde to form imine derivative (4,5-dimethoxy-2-nitroso-benzylidene)-propylamine-

MSN) on the surface of MSN. Since imine moiety is not charged at the employed conditions, a part of released doxorubicin was able to readsorb on MSN surface. It is possible as well that doxorubicin couples with released benzaldehyde moiety and forms imine derivative in the same manner, which would have similar outcome as imine derivatized Dox would not be charged and would adsorb freely on the surface. This explanation is supported by the fact that doxorubicin concentration decreases more after irradiation at lower pH because imine formation is acid catalyzed process.

The same behavior of photoproducts after deprotection of NV-protected amines is known since 1970, when Patchornik et. al. reported their findings.[11a] The authors were also able to prevent imine formation by addition of semicarbazide and other competing nucleophiles. Hence, we tested the release of doxorubicin in the presence of 5 mM semicarbazide in PBS and as a result no deterioration of Dox fluorescence intensity was noticed after the irradiation stopped (Figure 5).

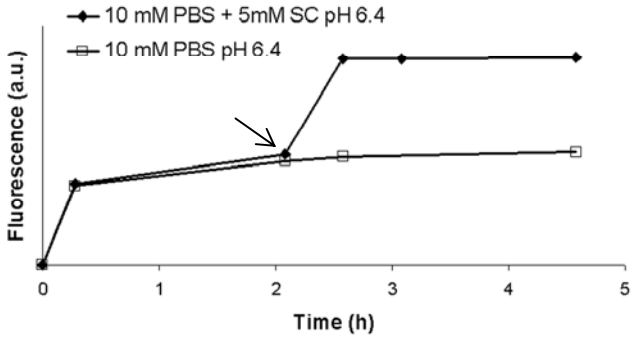

Figure 5. Comparison of the release of doxorubicin monitored as fluorescence emission at 595 nm (exc. 495 nm) of supernatant solution in 10 mM PBS (pH 6.4) and in the 10 mM PBS (pH 6.4) solution containing 5 mM semicarbazide. PBS + SC solution was irradiated with UV light for 30 min starting with the point marked by arrow.

Even though we used continuous UV irradiation to release the drug which also caused its photodegradation, we believe that this DDS can be more effectively applied for targeted doxorubicin delivery if e.g. ultrafast laser pulses are used for triggering the drug release. We

envision that such intense ultrashort laser pulse may effectively target cancerous tissue and induce intracellular release of dox molecules while photodegradation of the drug would be minimized because of its high local concentration on the silica surface. Such implementation is yet to be demonstrated.

Conclusion

We developed a doxorubicin delivery system responsive to UV light irradiation and increase in acidity. The anticancer drug was adsorbed on nitroveratryl carbamate-protected aminopropyl-functionalized mesoporous silica nanoparticles. Upon exposure to UV light positively charged propylammonium moieties were formed on the surface which yielded desorption of positively charged doxorubicin molecules from the surface of nanoparticles. Photosensitive release of the drug was a faster process then its photodegradation, which yielded in a net increase of dox concentration in PBS solution, as a direct response to UV irradiation. The amount of released doxorubicin was proportional to irradiation time and higher amount of the drug was released at weakly acidic conditions when compared to drug release at physiological pH. We believe that these results may open the possibilities for cooperative light and pH responsive selective targeting of doxorubicin delivery to cancerous tissue.

Acknowledgements

The authors thank the financial support for this research from the U.S. National Science Foundation (CHE-0809521).

References

1. a) F. Arcamone, G. Franceschi, S. Penco, A. Selva, *Tetrahedron Lett*. **1969**, 13, 1007-1010; b) A. Di Marco, M. Gaetani, B. M. Scarpinato, *Cancer Chemother. Rep.* **1969**, 53, 33-37
2. a) C. Carvalho, R. X. Santos, S. Cardoso, S. Correia, P. J. Oliveira, M. S. Santos, P. I. Moreira, *Curr. Med. Chem.* **2009**, 16, 3267-3285; b) G. L. Plosker, *Drugs* **2008**, 68, 2535-2551; c) R. Petrioli, A. I. Fiaschi, E. Francini, A. Pascucci, G. Francini, *Cancer. Treat. Rev*. **2008**, 34, 710-718; d) J. M. Connors, *J. Clin. Oncol*. **2005**, 23, 6400-6408.
3. a) P. K. Singal, N. Iliskovic, *N. Engl. J. Med.* **1998**, 339, 900-905; b) Y. Kimura, N. Sawai, H. Okuda, *J. Pharm. Pharmacol.* **2001**, 53, 1373-1378; c) L. Li, G. Takemura, Y. Li, S. Miyata, M. Esaki, H. Okada, H. Kanamori, N. C. Khai, R. Maruyama, A. Ogino, S. Minatoguchi, T. Fujiwara, H. Fujiwara, *Circulation* **2006**, 113, 535-543; d) G. Oktem, A. Bilir, S. Ayla, A. Yavasoglu, G. Goksel, G. Saydam, A. Uysal, Oncol. Res. 2006, 16, 225-233.
4. a) G. B. Sukhorukov, A. L. Rogach, B. Zebli, T. Liedl, A. G. Skirtach, K. Kohler, A. A. Antipov, N. Gaponik, A. S. Susha, M. Winterhalter, W. J. Parak, *Small* **2005**, 1, 194-200; b) A. N. Koo, H. J. Lee, S. E. Kim, J. H. Chang, C. Park, C. Kim, J. H. Park, S. C. Lee, *Chem. Commun.* **2008**, 6570-6572; c) C. Alexiou, W. Arnold, R. J. Klein, F. G. Parak, P. Hulin, C. Bergemann, W. Erhardt, S. Wagenpfeil, A. S. Lubbe, *Cancer Res*. **2000**, 60, 6641-6648; d) W. Arap, R. Pasqualini, E. Ruoslahti, *Science* **1998**, 279, 377-380.
5. a) M. Vallet-Regi, F. Balas, D. Arcos, *Angew. Chem. Int. Ed.* **2007**, 46, 7548-7558; b) S. Angelos, M. Liong, E. Choi, J. I. Zink, *Chem. Eng. J.* **2008**, 137, 4-13; c) S. Giri, B. G. Trewyn, V. S. Lin, *Nanomed.* **2007**, 2, 99-111; d) Y. Zhao, B. G. Trewyn, I. I. Slowing, V. S. Lin, *J. Am. Chem. Soc.* **2009**, 131, 8398-8400
6. K. Greish, *J. Drug Target.* **2007**, 15, 457-464.
7. a) C. Wu, C. Chen, J. Lai, J. Chen, X. Mu, J. Zheng, Y. Zhao, *Chem. Commun.* **2008**, 2662-2664; b) S. Angelos, E. Choi, F. Vogtle, L. De Cola, J. I. Zink, *J. Phys. Chem. C* **2007**, 111, 6589-6592; c) J. L. Vivero-Escoto, I. I. Slowing, C. W. Wu, V. S. Y. Lin, *J. Am. Chem. Soc.* **2009**, 131, 3462-3463.
8. a) N. Tavoloni, A. M. Guarino, P. D. Berk, *J. Pharm. Pharmacol*. **1980**, 32, 860-862; b) M. J. Wood, W. J. Irwin, D.K. Scott, J. *Clin. Pharm. Ther*. **1990**, 15, 291-300.
9. a) M. Stubbs, P. M. McSheehy, J. R. Griffiths, C. L. Bashford, *Mol. Med. Today* **2000**, 6, 15-19; b) I. F. Tannock, D. Rotin, *Cancer Res.* **1989**, 49, 4373-4384.
10. S. Bandak, A. Ramu, Y. Barenholz, A. Gabizon, *Pharm. Res*. **1999**, 16, 841-846.
11. a) A. Patchornik, B. Amit, R. B. Woodward, *J. Am. Chem. Soc.* **1970**, 92, 6333-6335; b) I. Aujard, C. Benbrahim, M. Gouget, O. Ruel, J. B. Baudin, P. Neveu, L. Jullien, *Chem. Eur. J.* **2006**, 12, 6865-6879; c) J. A. McCray, D. R. Trentham, *Annu. Rev. Biophys. Biophys. Chem.* **1989**, 18, 239-270.

12. D. D'Addona, C. G. Bochet, *Tetrahedron Lett.* **2001**, 42, 5227-5229.
13. R. J. Sturgeon, S. G. Schulman, *J. Pharm. Sci.* **1977**, 66, 958-961.

Appendix A

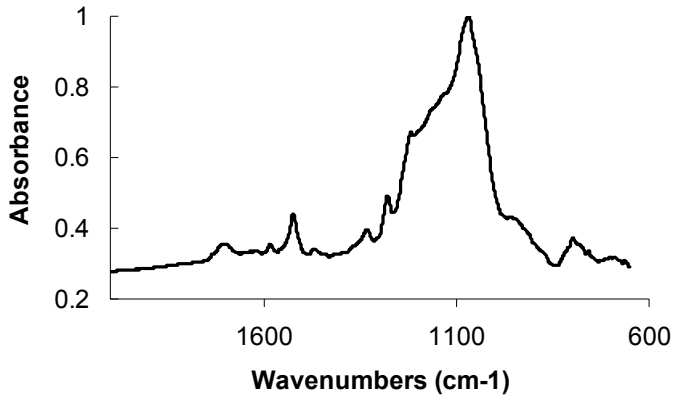

Figure S1. IR spetrum of NVCAP-MSN

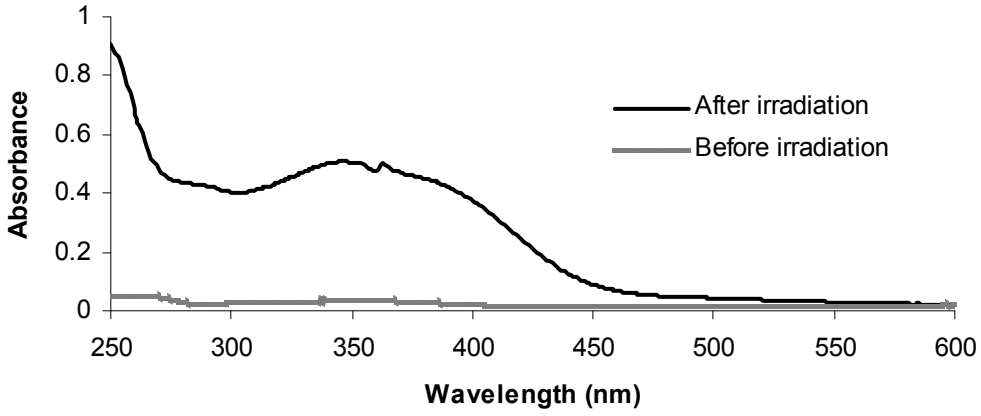

Figure S2. Change in UV-VIS absorbance upon 30 minutes of irradiation with UV light (350 nm) of supernatants obtained after centrifugation of a suspension of NVCAP-MSN in PBS before (bottom curve) and after irradiation (top curve)

Appendix B

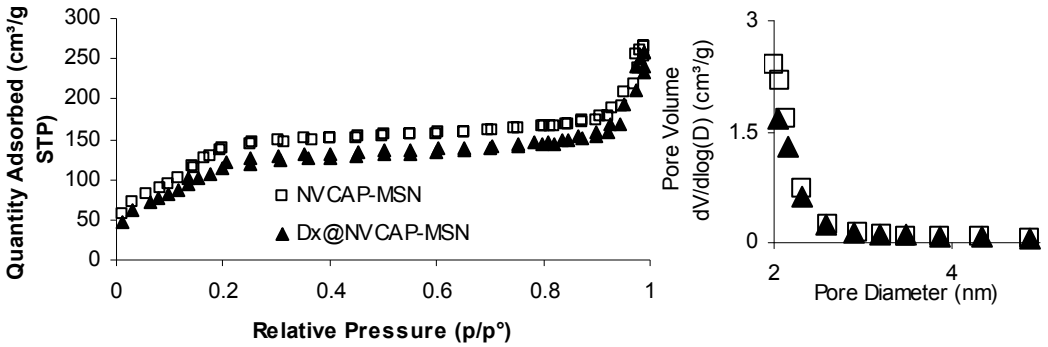

Figure S3. a) BET nitrogen adsorption/desorption isotherms and b) BJH average pore diameter distribution for NVCAP-MSN and Dx@NVCAP-MSN

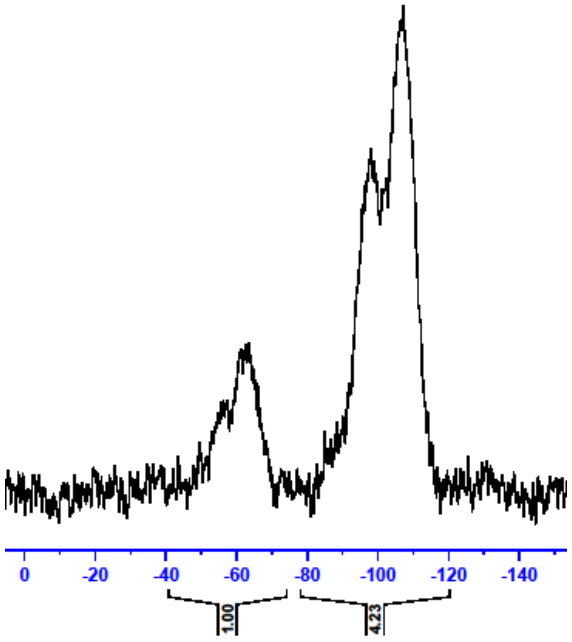

Figure S4. ^{29}Si NMR DP MAS spectrum of NVCAP-MSN

Various Si environments are designated as follows: Q_3=(≡SiO)$_3$SiOH, Q_4=(≡SiO)$_4$Si, T_2=(≡SiO)$_2$Si(OH)R, T_3=(≡SiO)$_3$SiR, where R is an organic functional group.

Appendix C

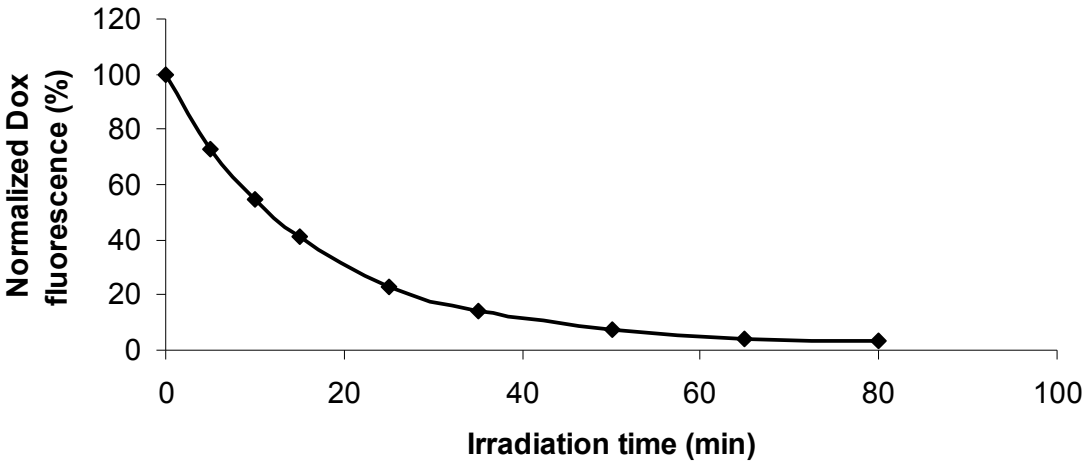

Figure S5. Photodegradation of PBS solution (pH = 7.4) of doxorubicin as a function of irradiation time.

CHAPTER 3. TUNING THE STRUCTURE OF MAGNETIC MESOPOROUS SILICA NANOPARTICLES FOR DRUG DELIVERY

Manuscript submitted for publication to *Journal of Controlled Release*

Nikola Ž. Knežević, Igor I. Slowing, Brian G. Trewyn, Victor S.-Y. Lin*

Department of chemistry, Iowa State University, Ames, Iowa, 50011

Abstract

A series of core-shell, iron-oxide nanoparticle embedded magnetic mesoporous silica nanoparticle materials with radial (MMSN-r) and hexagonal (MMSN-h) porous structures are synthesized via a facile synthetic method. The MMSN materials are loaded with anticancer drugs, 9-aminoacridine (9AA) and camptothecin (CPT) and controlled release profiles of the drugs from these materials are investigated as a function of porous structure and presence of phenylethyl functionality. Completely opposite behavior of the adsorbed drugs is observed in terms of the release from phenylethyl-functionalized pores of MMSN (Ph-MMSN) and non-functionalized material. While large release of 9AA is observed in case of non-functionalized MMSN, the loading and release of camptothecin is promoted by the presence of phenylethyl functionality. Controlled release properties of drug loaded magnetic materials were confirmed by viability studies on Chinese hamster ovarian (CHO) cells, which revealed efficient cytotoxic activity of CPT loaded Ph-MMSN-h and 9AA loaded MMSN-h material. In addition, we demonstrated the ability of externally applied magnetic field induced agitation to promote the release of anticancer drug from magnetic material. We envision that the MMSN materials could serve as a new generation of drug delivery carriers with an externally controlled site-targeting ability and capability to modify the drug release properties of the drug delivery system by the force externally applied magnetic field.

Introduction

The synthesis of structurally ordered mesoporous silica materials with various pore arrangement and particle morphologies have been extensively studied during the recent years.[1-5] Owing to the large surface area (> 700 m^2 g^{-1}), tunable pore diameter (2-30 nm), narrow pore size distribution and high thermal stability, mesoporous silica nanoparticles (MSN) were successfully applied for selective catalysis,[6-10] drug delivery,[2-5] sensing,[11-14] and separation.[15-17] Diameter of MSN spheres is usually in range 100-200 nm which is very suitable for use as drug delivery vehicles in anticancer therapy due to enhanced permeability and retention effect (EPR) of cancerous tissue.[18] This effect enables spontaneous accumulation of drug carriers along with any other macromolecules of suitable size in the extracellular medium of tumor tissue. The nanoparticles are then readily endocytosed by tumor cells as we already reported for mesoporous silica nanoparticles.[19,20] We also demonstrated that *in vitro* biocompatibility of MSN material is fairly high (up to a dosage of 100 μg ml^{-1}) and that hemolysis of red blood cells by MSN is much lower then reported for amorphous silica,[21] which may open the possibilities for pharmacological applications. In other studies we reported that mesopores of MSN could be efficiently loaded with drug molecules and their retention ensured by trapping them inside the pores with different "caps", such as CdS and Fe_3O_4 nanoparticles.[22,23] The caps were covalently bonded to the MSN via chemically cleavable disulfide linkage and triggering of the drug release was achieved by intracellular disulfide reducing agents. In the case of using magnetite nanoparticles as caps, the whole system was shown to be magnetically active, which showcased the possibility of controlling the location of drug release with external magnetic field, i.e., magnetically targeted drug delivery. There has been a growing research interest lately in designing MSN type of mesoporous materials that are intrinsically magnetic, aiming for imaging and delivery

applications.[24-31] For example, magnetic iron oxide nanoparticles were successfully grafted onto the external surface of MCM-41 type of mesoporous silica particles.[24] Also, mesoporous silica frameworks were recently coated on magnetic metal oxide nanoparticles and yielded different core-shell MSN materials.[32-34]

To achieve the goal of using magnetic mesoporous nanomaterials for various drug delivery, separation, catalysis, and sensor applications, an important prerequisite would be to gain the understanding of the release ability of guest molecules from mesoporous framework of the host material. This process can be influenced by the different structural parameters of the mesoporous material.[35] The silica framework can be functionalized with various organic groups and the materials can adopt different porous structure, both of which may have an influence on loading and releasing molecules from the host material.

Herein, we report on the synthesis and characterization of a series of core-shell, iron-oxide nanoparticle embedded, magnetic mesoporous silica nanoparticles (MMSN) with radial (MMSN-r) or hexagonal porous structures (MMSN-h). As detailed below, we developed a facile synthetic method that allows tuning of the pore orientations of MMSN materials. The MMSN materials were loaded with anticancer drugs, 9-aminoacridine (9AA) and camptothecin (CPT) (Scheme 1) and release kinetics of the drugs were monitored while controlling the location of the material by externally applied magnetic field. Release profiles of the drugs were determined as a function of different porous structure as well as presence of phenylethyl functionalization. Controlled release properties of drug loaded materials were also investigated by cell viability study on Chinese hamster ovarian cells (CHO).

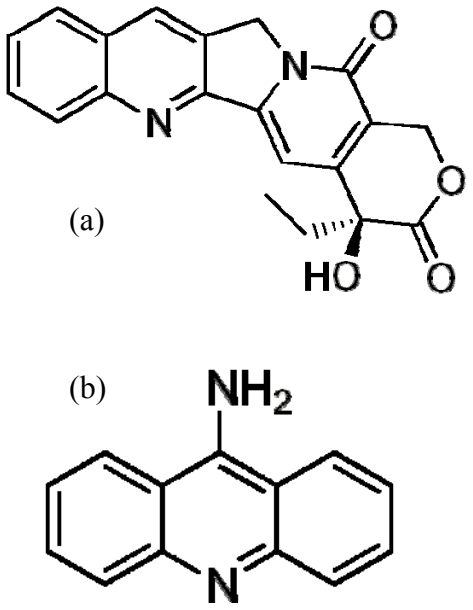

Scheme 1. Molecular structures of camptothecin (a) and 9-aminoacridine (b)

Camptothecin and its derivatives have shown remarkable activity against wide range of cancers[36-40] while 9AA and derivatives are known as mutagens,[41,42] antiseptics and anticancer drugs.[43,44] In addition to cancerous cells, anticancer drugs are known to be very toxic to healthy tissue. This is the reason a method for selective drug delivery to cancer cells is needed. Camptothecin would additionally benefit from an efficient delivery vector due to its hydrophobicity and low solubility in physiological environment. Hence, we focused on developing MMSN into drug delivery vehicles which would then have a possibility of applying external nondestructive force, such as magnetic field, to control the location of the delivery systems and possibly even manipulate the drug release process. Magnetic field-induced control of the location of drug treatment has been shown already to yield a significant improvement in the efficiency and selectivity of the treatment by a drug released from magnetic carriers.[45] For a final study of this report we monitored the release of 9AA from MMSN materials under the influence of agitated magnetic field. This facile method

may be proven an effective tool for manipulation of a drug release from magnetic drug delivery systems.

Experimental Section

Instrumental Methods

Powder XRD diffraction data were collected on a Scintag XRD 2000 X-ray diffractometer using Cu Kα radiation. Nitrogen adsorption and desorption isotherms, surface area and median pore diameter were measured using a Micromeritics ASAP2000 sorptometer. Sample preparation included degassing at 100 °C for 6 h. Specific surface areas and pore size distributions were calculated using the Brunauer-Emmett-Teller (BET) and Barrett-Joyner-Halenda (BJH) method, respectively. Particle morphology of these materials was determined by scanning electron microscopy (SEM) using a JEOL 840A scanning electron microscope. TEM examination with energy dispersive X-ray analysis (EDX) was completed on a Tecnai G2 F20 electron microscope operated at 200 kV. Thermogravimetric measurements, TGA and DTA-TGA were obtained on 2950HR V5.4A (2 deg min^{-1} in air) and 2960 SDT V3.0F (10 deg min^{-1} in air) respectively.

Materials

Tetraethylorthosilicate (TEOS), phenylethyltrimethoxysilane (Ph-TMS) and *n*-cetyltrimethylammonium bromide (CTAB) were purchased (Aldrich) and used as received. Magnetite nanoparticles were prepared by co-precipitation of Fe^{3+} and Fe^{2+} ions with NH_4OH in aqueous solution by already known synthetic procedure.[23,46]

Preparation of MMSN-r

Magnetite nanoparticles (150.0 mg) were sonicated for 12 h in a solution of CTAB (1.0 g, 2.7 mmol) and NaOH (3.5 mL, 2M) in water (480.0 mL). The suspension was then mechanically stirred and heated to 80 ˚C before the dropwise addition of TEOS (5.0 mL, 25.7 mmol). After additional stirring for 2 h at 80 ˚C, the as-synthesized light-brown material was filtrated, washed with water and methanol and air-dried. The resulting MMSNs were isolated by removing the surfactant template (CTAB) via calcination at 550 ˚C for 6 h with a heating rate of 10 ˚C min^{-1}.

Preparation of Ph-MMSN-h and MMSN-h

Magnetite Fe_3O_4 nanoparticles (300.0 mg) were sonicated for 12 h in a solution of CTAB (2.0 g, 5.5 mmol) and NaOH (7.0 mL, 2M) in water (480.0 mL). The suspension was then heated to 80 ˚C under mechanical stirring followed by rapid simultaneous injections of TEOS (10.0 mL, 51.4 mmol) and phenylethyltrimethoxysilane (1.1 mL, 5.7 mmol). After additional 2 hours of stirring, material was filtered, washed with water and methanol and air-dried. Final Ph-MMSN-h was obtained upon removal of CTAB surfactant template by Soxhlet extraction with solution of HCl in methanol (0.1 M) for duration of 48 h. A portion of the as-synthesized Ph-MMSN-h was calcined at 550 ˚C for 6 h with a heating rate of 10 ˚C min^{-1} in order to remove phenylethyl groups and surfactant molecules, which yielded MMSN-h material.

Drug loading and release studies

Camptothecin (2.1 mg, 6 μmol) or 9-Aminoacridine (2.3 mg, 10 μmol) were dissolved in methanol (3.0 mL). MMSN material (MMSN-r, Ph-MMSN-h or MMSN-h, 100 mg) was added and suspension was stirred for 24 h. The resulting drug-loaded MMSNs (9AA@MMSN-r, 9AA@Ph-MMSN-h, 9AA@MMSN-h, CPT@Ph-MMSN-h and

CPT@MMSN-h) were filtered and washed with plenty of MeOH. Camptothecin loaded MMSNs were additionally washed by stirring in PBS buffer (pH=7.4, 5 ml) for 18 hours in order to hydrolyze and remove a part of the loaded drug and thus generate a material which could be easily dispersed in water. Before washing with PBS, CPT@Ph-MMSN-h was extremely hydrophobic and stayed at the surface of PBS solution.

The amount of loaded drugs was calculated from the difference in concentration of drugs in PBS solution before and after the loadings, as determined by fluorescence spectroscopy. Standard curves were prepared and concentration of drugs was determined from the emission of 9-aminoacridine at 430 nm (exc. 343 nm) and camptothecin at 445 nm (exc. 383 nm).

For determination of the drug release from magnetic materials, the drug loaded MMSN (2 mg) was added to a glass vial and the material was fixed to the internal side wall of the vial with a neodymium disk magnet (DA01, K&J Magnetics, Inc, 5/8' x 1/32', surface field: 1110 G, pull force 20.47 lbs), which was taped on the external surface of the vial in a manner which we already reported.[23] PBS buffer (pH = 7.4, 2 ml) was then added to the vials and the samples were kept at room temperature. Aliquots of the solution were taken over time and fluorescence of the released drugs was measured while drug loaded magnetic material remained fixed on the internal side wall of the vials at all times.

Cell cultures

Chinese hamster ovarian (CHO) cells were seeded at a density of 1×10^5 cells mL^{-1} in 6 well plates and allowed to attach for 24 h in D-10 medium (3 mL) at 37 ºC and 5% CO_2. The D-10 medium consists of Dubelcco's Modified Eagle Medium (DMEM) plus 10% equine serum, L-alanyl-L-glutamine, gentamicin, and penicillin/streptomycin. The medium was replaced by suspensions of MMSN materials in fresh D-10 (25 μg mL^{-1} or 50 μg mL^{-1}) and the cells were placed back into the incubator for additional 24 h. Each treatment with

MMSNs or drug loaded MMSNs was done as a triplicate, and a triplicate of cells incubated without any material was prepared as a control. After that time, the material-containing media were removed and the cells were washed with fresh medium and PBS buffer. CHO cells from each well were harvested by trypsinization, centrifuged, resuspended in fresh D-10 medium (1 mL) and the number of viable cells in each sample was measured by flow cytometry using Guava ViaCount assay (Guava Technologies, Inc.; Hayward, CA).

Influence of agitated magnetic field on release kinetic of 9AA

In order to observe the release of 9AA under the influence of magnetic agitation of 9AA loaded MMSNs, axially magnetized neodymium disk magnets (DA01, K&J Magnetics, Inc, 5/8 inch × 1/32 inch, surface field: 1110 gauss) were taped on top of the horizontal orbital shaker, as depicted on Figure S7. Sample vials containing 2 mg of the drug loaded MMSNs were then fixed at 1 mm or 5 mm height directly above the magnet disks. PBS buffer (2.0 mL, 10 mM, pH=7.4, I=154 mmol) was then added into the sample vials and the orbital shaker was immediately set to agitation at 110 rpm rate. To measure the release of 9AA, 1.5 ml of the supernatant was taken periodically; the aliquots were centrifuged at 14000 rpm for 5 min and fluorescence emission of the solution was measured at 430 nm (excitation at 343 nm).

Results and Discussion

Synthesis and Characterization of MMSN Materials

By modifying our previously published procedures for the synthesis of MCM-41 type mesoporous silica nanoparticles,[22,47] we have prepared MMSN materials with different porous structures by a simple direct co-condensation of Fe_3O_4 nanoparticles and silicate precursors. As shown in the scanning and transmission electron micrographs (SEM and

TEM, respectively) (Figure 1), MMSNs with different porous structures were successfully synthesized. Iron oxide-containing mesoporous silica nanoparticles with radial orientation of mesopores (MMSN-r) (Figure 1a-c) were prepared by dropwise addition of tetraethylorthosilicate (TEOS). In contrast, upon rapid injection of TEOS and phenylethyl-TMS, as described in the experimental section, an MCM-41 type of hexagonal channel-like mesoporous structure was observed in the TEM images of phenylethyl-functionalized magnetic MSN (Ph-MMSN-h) (Figure 1e,f).

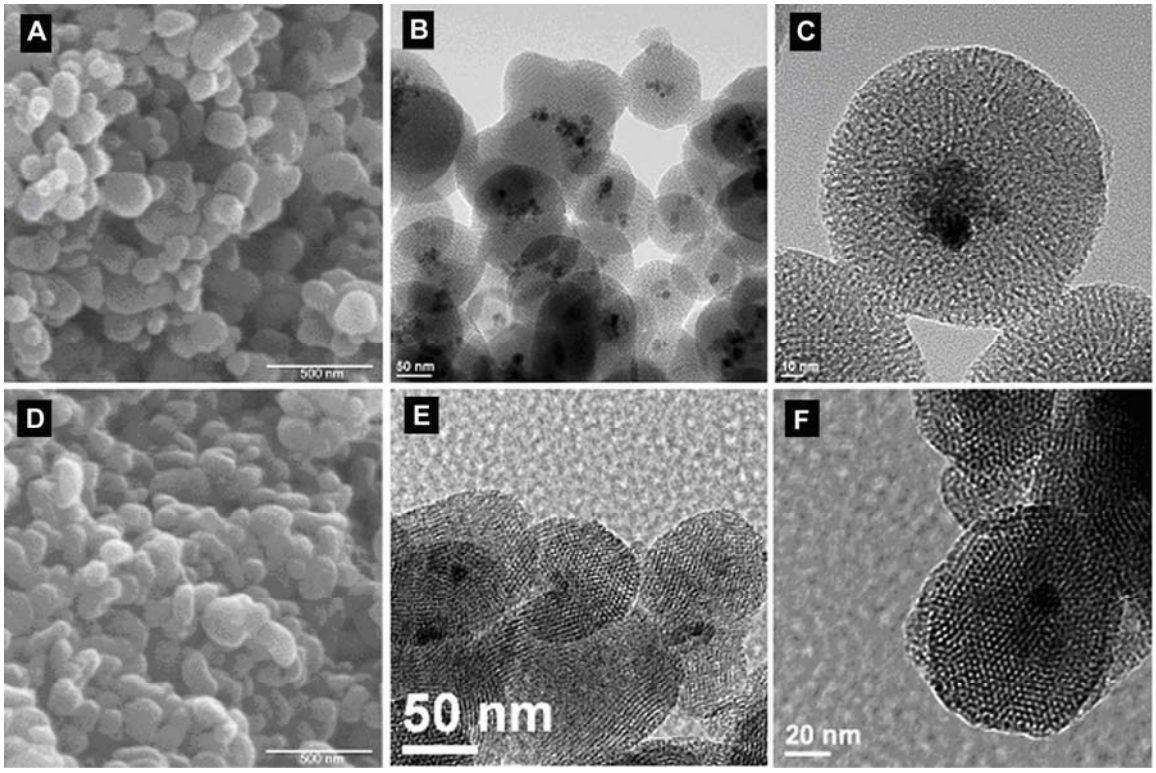

Figure 1. SEM (a,d) and TEM (b,c,e,f) images of MMSN-r (a-c) and Ph-MMSN-h (d-f).

Based on SEM analysis, the average diameter of MMSN-r and Ph-MMSN-h was calculated to be 123 ± 46 nm and 141 ± 34 nm, respectively. The average diameter of magnetite nanoparticles was estimated from TEM images to be 11.9 ± 2.0 nm. CTAB surfactant template was removed from Ph-MMSN-h by Soxhlet extraction with HCl/MeOH solution, which did not hydrolyze the silica-embedded iron oxide nanoparticles. However,

we observed that the usual method of surfactant extraction (stirring in a solution HCl/MeOH at 60 ˚C) resulted in the undesired hydrolysis of iron oxide and consequently led to formation of a non-magnetic material after 3 h of reaction. Evidently Soxhlet extraction method afforded milder conditions for CTAB removal due to slow evaporation of HCl and continuous extraction by methanol. The presence of phenylethyl groups in the material after CTAB-removal was confirmed by FT-IR spectroscopy (Figure S2, Table S1) and TGA analysis (Figure S3). Non-functionalized MMSN-h material was obtained by removing the phenylethyl moieties and CTAB molecules by calcination at 550 ˚C for 6 h.

The N_2 sorption analyses of the materials (Figure S4, Table 1) reported a type-IV BET isotherm characteristic of MCM-41 structure with high surface area for all nanomaterials. The BJH pore size distribution revealed the mesoporous character of the materials with narrow pore size distribution. After calcination of Ph-MMSN-h the XRD reflections (Figure 2) of MMSN-h were shifted to a higher Bragg angle implying a contraction of the mesoporous silica. Since the distance between the [100] planes can be calculated from the Bragg's equation to be 3.62 nm for Ph-MMSN-h and 3.32 nm for MMSN-h, which is a 9% decrease, the average pore diameter in Ph-MMSN-h, as formed by the SiO_2 framework, is expected to be around 2.8 nm, obtained after the 9% correction. However, the BJH analysis of Ph-MMSN-h gave the result of lower then 2 nm for the average pore diameter, due to the presence of phenylethyl moieties.

Table 1. BET and BJH data for MMSN-r, Ph-MMSN-h and MMSN-h materials

	BET surface area [m^2 g^{-1}]	BJH pore Diameter [nm]	Drug loading (9AA or CPT) [μmol g^{-1} MMSN]
MMSN-r	965	2.8	N.A.
Ph-MMSN-h	1089	≤2	N.A.
MMSN-h	1196	2.6	N.A.
9AA@MMSN-r	888	2.8	19.9
9AA@Ph-MMSN-h	972	≤2	25.0
9AA@MMSN-h	1128	2.3	26.7
CPT@Ph-MMSN-h	470	≤2	46.1
CPT@MMSN-h	1024	2.1	13.4

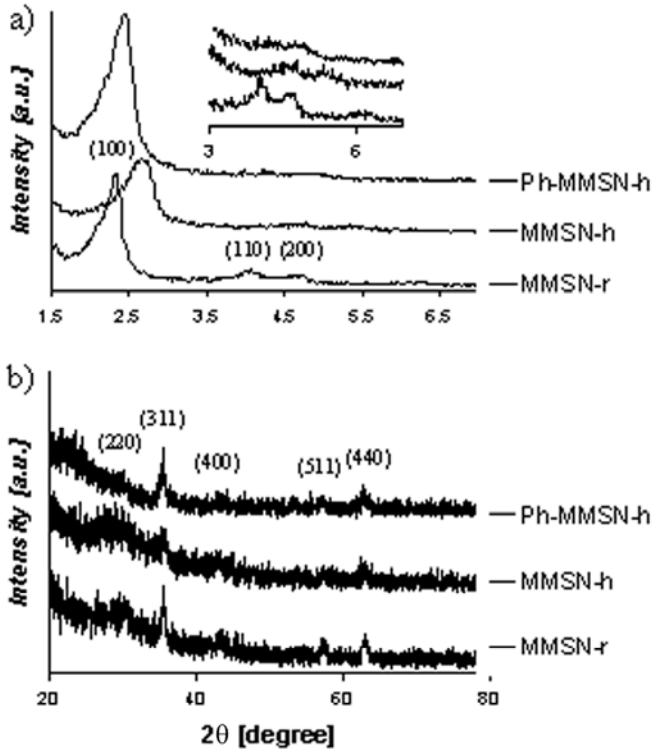

Figure 2. Powder X-ray diffraction patterns of the materials at low angle (a) inset shows the higher order diffraction peaks; and high angle XRD pattern (b).

As depicted in Figure 2, the powder XRDs of the materials revealed that all materials exhibit hexagonal pore packing. In the case of Ph-MMSN-h material higher order reflections ([110] and [200]) have diminished intensity, which is sometimes observed for materials synthesized by our co-condensation method.[47] Mesoporous silica spheres with radial pore structure have been reported to exhibit the hexagonal diffraction patterns.[48-50] This result was attributed to the hexagonal pore packing in the center of the particles. High angle XRD measurements of these MMSN materials showed the typical diffraction patterns of magnetite and maghemite nanoparticles, which are the product of magnetite oxidation upon calcination in air. This is also evidenced by the small positive peak at 374 ˚C in thermogravimetric analysis-differential thermal analysis (TGA-DTA) for Ph-MMSN-h (Figure S3c). The color

change of the Ph-MMSN-h material from light brown to red upon calcination further supports the formation of maghemite.

The chemical compositions of the materials were determined by the energy-dispersive X-ray spectrometry (EDX) and TGA. The amounts of iron were calculated to be 9.7 and 6.1 wt% for MMSN-r and Ph-MMSN-h, respectively. The quantity of the phenylethyl groups in Ph-MMSN-h was calculated to be 14.8 wt%. Field-dependent magnetization curves (Figure 3) show that the materials are superparamagnetic, since there was no hysteresis observed at room temperature. At 5 K, both curves show hysteresis with remnant magnetization of 1.5 emu g^{-1} and 2.8 emu g^{-1} and coercivity field (169 Oe and 188 Oe) for Ph-MMSN-h and MMSN-r, respectively. Saturation magnetizations for Ph-MMSN-h are 4.9 emu g^{-1} and 5.8 emu g^{-1} while for MMSN-r are 8.8 emu g^{-1} and 10.2 emu g^{-1} at 300 K and 5 K, respectively. The values for saturation magnetization are consistent with lower weight ratio of iron-oxide nanoparticles in the core of Ph-MMSN-h compared to MMSN-r.

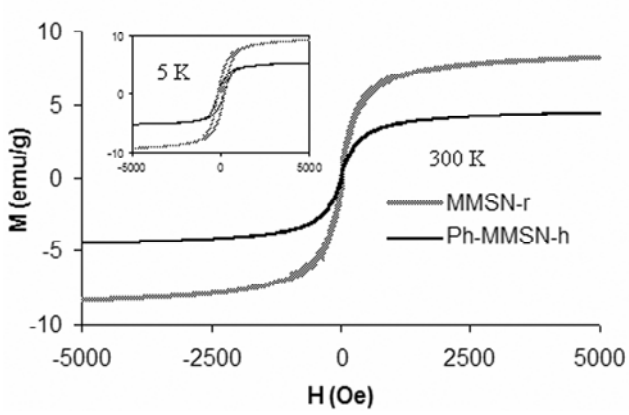

Figure 3. Magnetization curves for MMSN-r and Ph-MMSN-h at 300 K. Inset shows magnetization curves at 5 K.

It is interesting to note that the formation of different mesoporous structures appear to be dependent on the rate of silicate condensation in the presence of well-dispersed iron oxide nanoparticles and CTAB micelles. In the case of MMSN-r, TEOS was added dropwise. The

formation of MMSN-r was first observed when approximately 40% of the TEOS was introduced. Given the fact that the concentration of silicate was low in comparison to iron oxide nanoparticles and CTAB, the condensation would likely take place around or on the surface of the iron oxide nanoparticles serving as nucleation seeds. Subsequent build up and gradual growth of mesoporous silica layers would give rise to the magnetic MSN particles with radial pore orientation. Similar mechanism was already suggested for mesoporous silica spheres with radial pores.[49,50] In contrast, the synthesis of Ph-MMSN-h involved rapid and simultaneous injections of TEOS and Ph-TMS. The formation of Ph-MMSN-h was observed in less then one minute. In this case, the concentration of TEOS was high and the condensation between silicate precursors around CTAB micelles would be preferred over the interaction with Fe_3O_4 surface. Magnetic nanoparticles were thus incorporated into the typical MCM-41 type of mesoporous silica framework.

In addition, we note that absence/presence of phenylethyl functionality was not crucial for yielding radial or hexagonal porous structure respectively. In the case of rapid injection of TEOS without addition of organosilane the porous structure of the obtained material was also hexagonal. However, we observed that the presence of phenylethyl moiety allowed the even distribution of highly dispersed magnetite nanoparticles within the silica framework. When phenylethyl-TMS was not injected along with TEOS, the resulting material was a mixture of different shapes and sizes of MMSN nanoparticles, which also contained large conglomerates of Fe_3O_4, typically seen on the edges of bigger, bean-like particles (Figure S5). Highly dispersed Fe_3O_4 nanoparticles within evenly distributed MMSN nanoparticles were also seen in the case of material synthesized by rapid injection of 3-bromopropyltrimethoxysilane along with TEOS (Figure S6).

Drug Loading and Release Studies

Magnetic materials were further investigated as possible carriers for drug delivery to cancerous cells. Camptothecin and 9-aminoacridine were chosen as loading drugs, which represent a hydrophobic and hydrophilic drug, respectively. Release of the drugs was monitored under simulation of controlling the location of the drug delivery system by an externally applied magnetic field. Inexpensive commercially available neodymium disc magnet, which was taped to the external wall of the sample vial, as described in experimental section, was efficient in keeping the drug delivery system fixed to the internal walls of the vial. We envision that the same straightforward approach may be applicable for *in vivo* tumor site targeting. Hydrophilic 9AA hydrochloride was first adsorbed on the surface of MMSN-r, MMSN-h and Ph-MMSN-h from a methanol solution. The amounts of loaded drugs and BET data for the corresponding materials are specified in Table 1. More 9AA was adsorbed on the MMSN-h materials probably due to the higher surface area. Release of the drug was monitored in PBS solution and is represented in Figure 4a. It was observed that different porous structure did not affect the release kinetics of the drug, as MMSN-r and MMSN-h exhibited similar release profiles. However, a slightly higher percentage of loaded 9AA was released in the case of MMSN-r probably because the radial structure has more mesopore entrances and hence the adsorbed molecules within them are more accessible to the surrounding medium.

Interestingly, the release of 9AA from phenylethyl-functionalized MMSN-h was very low, even though the amount of loaded drug was comparable to the loadings on MMSN-h and MMSN-r. These data suggest that the hydrophobic pore interior, as formed by phenylethyl functionality, hinders the release of 9AA. Most of the drug molecules are probably attached through electrostatic interactions and hydrogen bonds between 9AA molecules and surface silanol groups on MMSN, with a possible contribution from π-π stacking between the drug and phenyl groups inside the mesopores. Hence, in order to release

the drug, water molecules and ions from PBS buffer need a clear access to the site of 9AA adsorption, where the hydrogen bond exchange and ion metathesis would take place. However, this process seems to be hindered in the case of 9AA@Ph-MMSN-h due to hydrophobic environment around adsorbed 9AA molecules. Since the amount of hydrophobic phenylethyl moieties inside the mesopores is very high (14.8 wt%) and the mesopores of Ph-MMSN-h have a small diameter (≤ 2 nm), diffusion of water clusters into the narrow hydrophobic mesopores is probably not a favorable process. In fact, we believe that wetting of those mesopores happens only at the entrance level, which as a consequence yields in low released amount of 9AA.

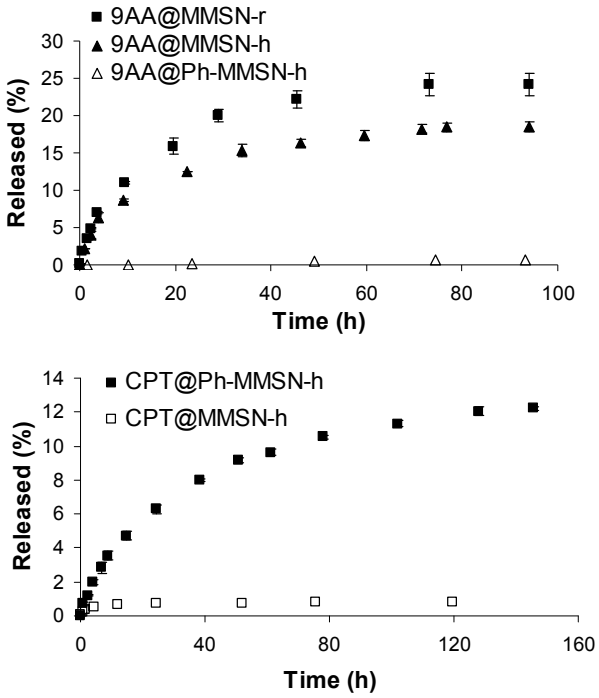

Figure 4. Released portion of the loaded drug from: (a) 9-aminoacridine and (b) camptothecin loaded materials.

In order to further investigate the influence of phenylethyl moiety on drug release, hydrophobic drug camptothecin was adsorbed on Ph-MMSN-h and MMSN-h in a similar manner to 9AA loading and the release kinetics were measured in PBS solution (Figure 4b).

Interestingly, the release of the drug from Ph-MMSN-h was now much larger and there was almost no release from MMSN-h material. In addition, the drug loading was also much larger in the case of CPT@Ph-MMSN-h compared to CPT@MMSN-h and BET measurements (Table 1, Figure S4d) revealed that adsorption of camptothecin on Ph-MMSN-h caused a large decrease in surface area while there was only a minor influence on surface area upon adsorption on MMSN-h. These results suggest that phenylethyl moiety promotes the deposition of CPT probably through π-π stacking and van der Waals interactions. Phenyl moieties were already reported to increase the amount of loaded camptothecin in liposomal delivery vehicles as well as to increase stability of the self-assembled structures.[51] Improved ability of CPT loaded Ph-MMSN-h to release the anticancer drug upon dissolution in PBS can be explained in terms of improved wetting of the mesopores. Even though CPT is a hydrophobic molecule, it is known that it undergoes hydrolysis of its lactone ring in PBS solution.[52] It is a fast process even at pH 7.4 in PBS buffer and it produces negatively charged carboxylate analogue of the drug which is not biologically active. Hence, we believe that gradual hydrolysis of CPT within the mesopores tampers the hydrophobic environment inside the channels and allows better diffusion of PBS solution into the mesopores. Once the wetting was enabled, a large amount of the drug that was relatively weakly attached through π -π stacking interactions with phenyl groups in Ph-MMSN-h was able to diffuse away from the material. Since almost 4 times lower amount of CPT was loaded on MMSN-h and it was attached exclusively on the silica surface, the release kinetics of the drug on Figure 4b showed much lower release. Non-functionalized, non-magnetic mesoporous silica nanoparticles were already used to load camptothecin and also a very small release of the drug in PBS was observed.[53]

Curiously, even though 9AA is a hydrophilic molecule, no promotion of wetting of the mesopores was noted in the case of 9AA@Ph-MMSN-h, as very low drug release was observed. We believe that this result is due to orientation of positively charged amine

moieties of 9AA molecules toward silica walls and ion coupling with surface silanols. If we consider that in addition to that ion pairing 9AA forms peripheral π-π stacking interaction with phenyl moieties inside the mesopores, the channels of 9AA@Ph-MMSN-h may have stayed hydrophobic even with loaded hydrophilic 9AA. Oppositely, hydrolyzed CPT would tend to rotate its negative charge away from silica surface, which means straight toward incoming PBS solution.

Viability Studies on CHO Cells

To test the drug delivery capabilities of our materials *in vitro*, viability studies on CHO cells were done and results are represented in Figure 5. While 9AA loaded Ph-MMSN-h was not cytotoxic at concentration of 50 μg mL^{-1}, number of viable cells decreased to 55% upon treatment with the same concentration of 9AA loaded MMSN-h. Clearly, the greater amount of released drug in case of 9AA@MMSN-h induced the difference in viability. The reverse effect of organic functionalization was confirmed in the case of camptothecin loaded materials. If treated at the concentration of 25 μg mL^{-1}, only CPT@Ph-MMSN-h induced CHO cell death and their final amount decreased to 57.5 % of the total number of cells, as compared to the control sample. We also observed that 9AA loaded materials had lower cytotoxic activity than CPT loaded MMSNs since no influence on viability was noted in the case of treatment with 9AA@MMSN-h at a concentration of 25 μg mL^{-1}. This effect can be attributed to a higher cytotoxicity of camptothecin rather than to the difference in quantities of released drug as similar amounts were released from 9AA@MMSN-h and CPT@Ph-MMSN-h after 24 h in PBS solution (2.9 μmol g^{-1} of CPT and 3.25 μmol g^{-1} of 9AA). Since only non-hydrolyzed camptothecin molecule is cytotoxic, the viability results indicate that plenty of CPT molecules were successfully released from Ph-MMSN-h and delivered to cancerous cells in a native, bioactive form.

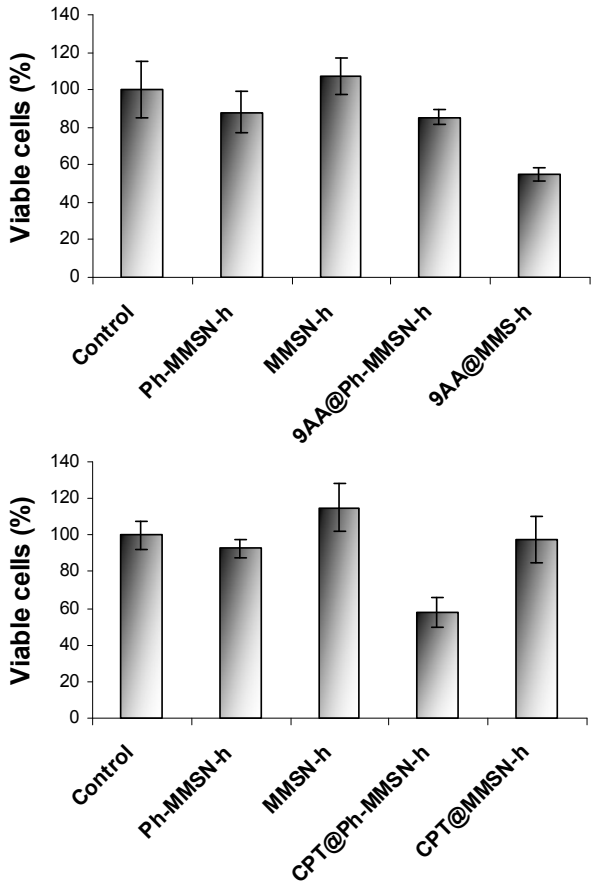

Figure 5. Percentage of live CHO cells upon 24 h incubation with: (a) 50 μg mL^{-1} and (b) 25 μg mL^{-1} dosage of corresponding MMSN materials normalized to the untreated cells (control).

Drug release kinetics as a function of externally applied agitated magnetic field

In order to test the capability of externally applied magnetic field to influence the drug delivery from MMSN based drug carriers, we set the experiment as depicted on Figure S7. Neodymium disk magnets were placed below the vials containing drug loaded MMSN in PBS solution. Position of the vials was fixed to iron stands while motion of disk magnets below the vials caused movement of drug loaded MMSN inside the vials. Circular motion of MMSN materials along the bottom of the vials was very explicit. As can be seen on figure 6, agitation of 9AA loaded MMSN materials, caused by externally applied magnetic field, clearly increased the rate of drug release. This result can be explained by faster mass transfer

of PBS solution into the mesopores as well as faster detachment and transfer of 9AA molecules to the bulk solution, under conditions of agitated versus fixed drug carries. We also tested if magnet induced agitation would improve wetting of 9AA@Ph-MMSN-h mesopores and increase the released drug amount (Figure 6b). Only slight increase in rate of 9AA release from Ph-MMSN-h was noticed and no improvement of release capacity was noted for applied conditions. Finally, we monitored the influence of different strength of magnetic field on the rate of drug release (Figure 6c). If the distance between disk magnets and sample vials was increased by a factor of 5, slower agitation rate of MMSN materials was clearly evident, which resulted in lower rate of 9AA release.

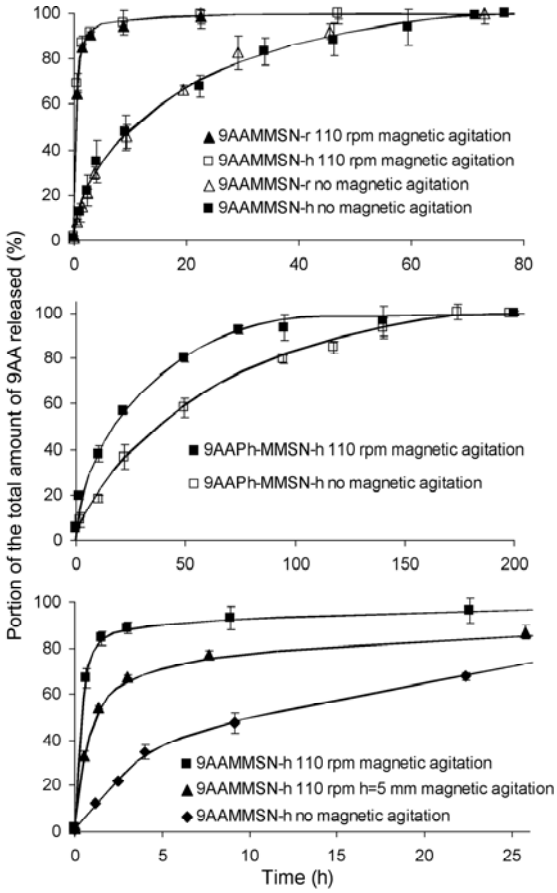

Figure 6. Release curves for: (a) 9AA@MMSN-r and 9AA@MMSN-h and (b) 9AA@Ph-MMSN-h with and without presence of magnetic field agitated at 110 rpm rate. (c) Influence of different magnetic pull on release of 9AA; Comparison of the release under 110 rpm agitation with the sample closely above the magnet (h=1 mm) and the release when sample was at the 5 mm height above the magnet. Release data for all results are normalized to the total released drug amount, which was set to 100 %.

Conclusions

A series of core-shell, iron-oxide nanoparticle embedded superparamagnetic mesoporous silica nanoparticle materials with radial and hexagonal porous structures were successfully prepared via a facile condensation method. We have demonstrated that the loading and release of anticancer drugs, 9-aminoacridine and camptothecin, were influenced by the presence of phenylethyl moiety inside the mesopores of MMSN materials. Release of hydrophilic 9-aminoacridine is hindered and the release of hydrophobic camptothecin was promoted by the organic functionalization. The cell viability assay supported the release kinetic results. Camptothecin loaded phenylethyl functionalized material was cytotoxic while CPT loaded non-functionalized material did not affect the viability of CHO cells at 25 μg ml^{-1} concentration. In case of 9AA loaded materials, feeding the cells with 9AA@MMSN-h at 50 μg ml^{-1} concentration induced a decrease in number of viable cells while addition of 9AA@Ph-MMSN-h did not influence the cell viability. Finally, we demonstrated the ability of externally applied agitated magnetic field to control the rate of drug release from magnetic drug delivery carriers.

Acknowledgments

The authors thank the financial support for this research from the U.S. National Science Foundation (CHE-0809521). We also thank Dr. Sergey L. Bud'ko of the U.S. DOE Ames Laboratory for the SQUID measurements.

References

(1) Kresge, C. T.; Leonowicz, M. E.; Roth, W. J.; Vartuli, J. C.; Beck, J. S. *Nature (London)* **1992**, 359, 710-12.

(2) Vallet-Regi, M.; Balas, F.; Arcos, D. *Angew. Chem., Int. Ed.* **2007**, 46, 7548-7558.
(3) Trewyn, B. G.; Slowing, I. I.; Giri, S.; Chen, H.-T.; Lin, V. S. Y. *Acc. Chem. Res.* **2007**, 40, 846-853.
(4) Trewyn, B. G.; Giri, S.; Slowing, I. I.; Lin, V. S. Y. *Chem. Commun. (Cambridge, U. K.)* **2007**, 3236-3245.
(5) Angelos, S.; Liong, M.; Choi, E.; Zink, J. I. *Chem. Eng. J. (Amsterdam, Neth.)* **2008**, 137, 4-13.
(6) Huh, S.; Chen, H.-T.; Wiench, J. W.; Pruski, M.; Lin, V. S. Y. *Angew. Chem., Int. Ed.* **2005**, 44, 1826-1830.
(7) Inumaru, K.; Ishihara, T.; Kamiya, Y.; Okuhara, T.; Yamanaka, S. *Angew. Chem., Int. Ed.* **2007**, 46, 7625-7628.
(8) Mori, K.; Kondo, Y.; Morimoto, S.; Yamashita, H. *Chem. Lett.* **2007**, 36, 1068-1069.
(9) Fukuoka, A.; Kimura, J. I.; Oshio, T.; Sakamoto, Y.; Ichikawa, M. *J. Am. Chem. Soc.* **2007**, 129, 10120-10125.
(10) Li, C.; Zhang, H. D.; Jiang, D. M.; Yang, Q. H. *Chem. Commun.* **2007**, 547-558.
(11) Radu, D. R.; Lai, C.-Y.; Wiench, J. W.; Pruski, M.; Lin, V. S. Y. *J. Am. Chem. Soc.* **2004**, 126, 1640-1641.
(12) Descalzo, A. B.; Marcos, M. D.; Monte, C.; Martinez-Manez, R.; Rurack, K. *J. Mater. Chem.* **2007**, 17, 4716-4723.
(13) Lei, B. F.; Li, B.; Zhang, H.; Zhang, L. M.; Li, W. L. *J. Phys. Chem. C* **2007**, 111, 11291-11301.
(14) Basabe-Desmonts, L.; Reinhoudt, D. N.; Crego-Calama, M. *Chem. Soc. Rev.* **2007**, 36, 993-1017.
(15) Kim, S.; Ida, J.; Guliants, V. V.; Lin, J. Y. S. *J. Phys. Chem. B* **2005**, 109, 6287-6293.
(16) Oh, S.; Kang, T.; Kim, H.; Moon, J.; Hong, S.; Yi, J. *J. Membr. Sci.* **2007**, 301, 118-125.
(17) Brady, R.; Woonton, B.; Gee, M. L.; O'Connor, A. J. *Innovat. Food Sci. Emerg. Technolog.* **2008**, 9, 243-248.
(18) Greish, K. *J. Drug Target.* **2007**, 15, 457-64.
(19) Slowing, I.; Trewyn, B. G.; Lin, V. S. Y. *J. Am. Chem. Soc.* **2006**, 128, 14792-14793.
(20) Radu, D. R.; Lai, C.-Y.; Jeftinija, K.; Rowe, E. W.; Jeftinija, S.; Lin, V. S. Y. *J. Am. Chem. Soc.***2004**, 126, 13216-13217.
(21) Slowing, I. I.; Wu, C.-W.; Vivero-Escoto, J. L.; Lin, V. S. Y. *Small* **2009**, 5, 57-62.
(22) Lai, C.-Y.; Trewyn, B. G.; Jeftinija, D. M.; Jeftinija, K.; Xu, S.; Jeftinija, S.; Lin, V. S. Y. *J. Am. Chem. Soc.* **2003**, 125, 4451-4459.
(23) Giri, S.; Trewyn, B. G.; Stellmaker, M. P.; Lin, V. S. Y. *Angew. Chem., Int. Ed.* **2005**, 44, 5038-5044.
(24) Bourlinos, A. B.; Simopoulos, A.; Boukos, N.; Petridis, D. *J. Phys. Chem. B* **2001**, 105, 7432-7437.
(25) Zhu, S. M.; Zhou, Z. Y.; Zhang, D.; Jin, C.; Li, Z. Q. *Micropor. Mesopor. Mater.* **2007**, 106, 56-61.
(26) Shokouhimehr, M.; Piao, Y.; Kim, J.; Jang, Y.; Hyeon, T. *Angew. Chem., Int. Ed.* **2007**, 46, 7039-7043.
(27) Kim, J.; Lee, J. E.; Lee, J.; Yu, J. H.; Kim, B. C.; An, K.; Hwang, Y.; Shin, C. H.; Park, J. G.; Kim, J.; Hyeon, T. *J. Am. Chem. Soc.* **2006**, 128, 688-689.
(28) Zhao, W.; Gu, J.; Zhang, L.; Chen, H.; Shi, J. *J. Am. Chem. Soc.* **2005**, 127, 8916-8917.

(29) Zhao, W.; Shi, J.; Chen, H.; Zhang, L. *J. Mater. Res.* **2006**, 21, 3080-3089.
(30) Ruiz-Hernandez, E.; Lopez-Noriega, A.; Arcos, D.; Izquierdo-Barba, I.; Terasaki, O.; Vallet-Regi, M. *Chem. Mater.* **2007**, 19, 3455-3463.
(31) Andersson, N.; Corkery, R. W.; Alberius, P. C. A. *J. Mater. Chem.* **2007**, 17, 2700-2705.
(32) Liong, M.; Lu, J.; Kovochich, M.; Xia, T.; Ruehm, S. G.; Nel, A. E.; Tamanoi, F.; Zink, J. I. *ACS Nano* **2008**, 2, 889-896.
(33) Zhao, W.; Chen, H.; Li, Y.; Li, L.; Lang, M.; Shi, J. *Adv. Funct. Mater.* **2008**, 18, 2780-2788.
(34) Deng, Y.; Qi, D.; Deng, C.; Zhang, X.; Zhao, D. *J. Am. Chem. Soc.* **2008**, 130, 28
(35) Trewyn, B. G.; Whitman, C. M.; Lin, V. S. Y. *Nano Lett.* **2004**, 4, 2139-2143.
(36) Hertzberg, R. P.; Caranfa, M. J.; Holden, K. G.; Jakas, D. R.; Gallagher, G.; Mattern, M. R.; Mong, S. M.; Bartus, J. O.; Johnson, R. K.; Kingsbury, W. D. *J. Med. Chem.* **1989**, 32, 715-720.
(37) Masuda, N.; Fukuoka, M.; Kusunoki, Y.; Matsui, K.; Takifuji, N.; Kudoh, S.; Negoro, S.; Nishioka, M.; Nakagawa, K.; Takada, M. *J. Clin. Oncol.* **1992**, 10, 1225-1229.
(38) Abigerges, D.; Chabot, G. G.; Armand, J. P.; Herait, P.; Gouyette, A.; Gandia, D. *J. Clin. Oncol.* **1995**, 13, 210-221.
(39) Litvak, D. A.; Papaconstantinou, H. T.; Hwang, K. O.; Kim, M.; Evers, B. M.; Townsend, C. M. *Surgery* **1999**, 126, 223-230.
(40) Miller, K. D.; Soule, S. E.; Haney, L. G.; Guiney, P.; Murry, D. J.; Lenaz, L.; Sun, S.-L.; Sledge, G. W., Jr. *Invest. New Drugs* **2004**, 22, 69-73.
(41) Zhu, H. P.; Clark, S. M.; Benson, S. C.; Rye, H. S.; Glazer, A. N.; Mathies, R. A. *Anal. Chem.* **1994**, 66, 1941-1948.
(42) Rehn, C.; Pindur, U. *Monatsh. Chem.* **1996**, 127, 645-658.
(43) Murza, A.; Sanchez-Cortes, S.; Garcia-Ramos, J. V.; Guisan, J. M.; Alfonso, C.; Rivas, G. *Biochemistry* **2000**, 39, 10557-10565.
(44) Sebestik, J.; Hlavacek, J.; Stibor, I. *Curr Protein Pept Sci* **2007**, 8, 471-83.
(45) Jurgons, R.; Seliger, C.; Hilpert, A.; Trahms, L.; Odenbach, S.; Alexiou, C. *J. Phys.: Condens. Matter* **2006**, 18, S2893-S2902.
(46) Vayssieres, L.; Chaneac, C.; Tronc, E.; Jolivet, J. P. *J. colloid interface sci.* **1998**, 205, 205-212.
(47) Huh, S.; Wiench, J. W.; Trewyn, B. G.; Song, S.; Pruski, M.; Lin, V. S. Y. *Chem. Commun. (Cambridge, U. K.)* **2003**, 2364-2365.
(48) Pauwels, B.; Van Tendeloo, G.; Thoelen, C.; Van Rhijn, W.; Jacobs, P. A. *Adv. Mater.* **2001**, 13, 1317-1320.
(49) Lebedev, O. I.; Van Tendeloo, G.; Collart, O.; Cool, P.; Vansant, E. F. *Solid State Sci.* **2004**, 6, 489-498.
(50) Nakamura, T.; Mizutani, M.; Nozaki, H.; Suzuki, N.; Yano, K. *J. Phys. Chem. C* **2007**, 111, 1093-1100.
(51) Maitani, Y.; Katayama, S.; Kawano, K.; Hayama, A.; Toma, K. *Biol. Pharm. Bull.* **2008**, 31, 990-993.
(52) Ziomkowska, B.; Kruszewski, S.; Siuda, R.; Cyrankiewicz, M. *Opt. Appl.* **2006**, 36, 137-146.
(53) Lu, J.; Liong, M.; Zink, J. I.; Tammanoi, F. *Small* **2007**, 3, 1341-1346.

Appendix A

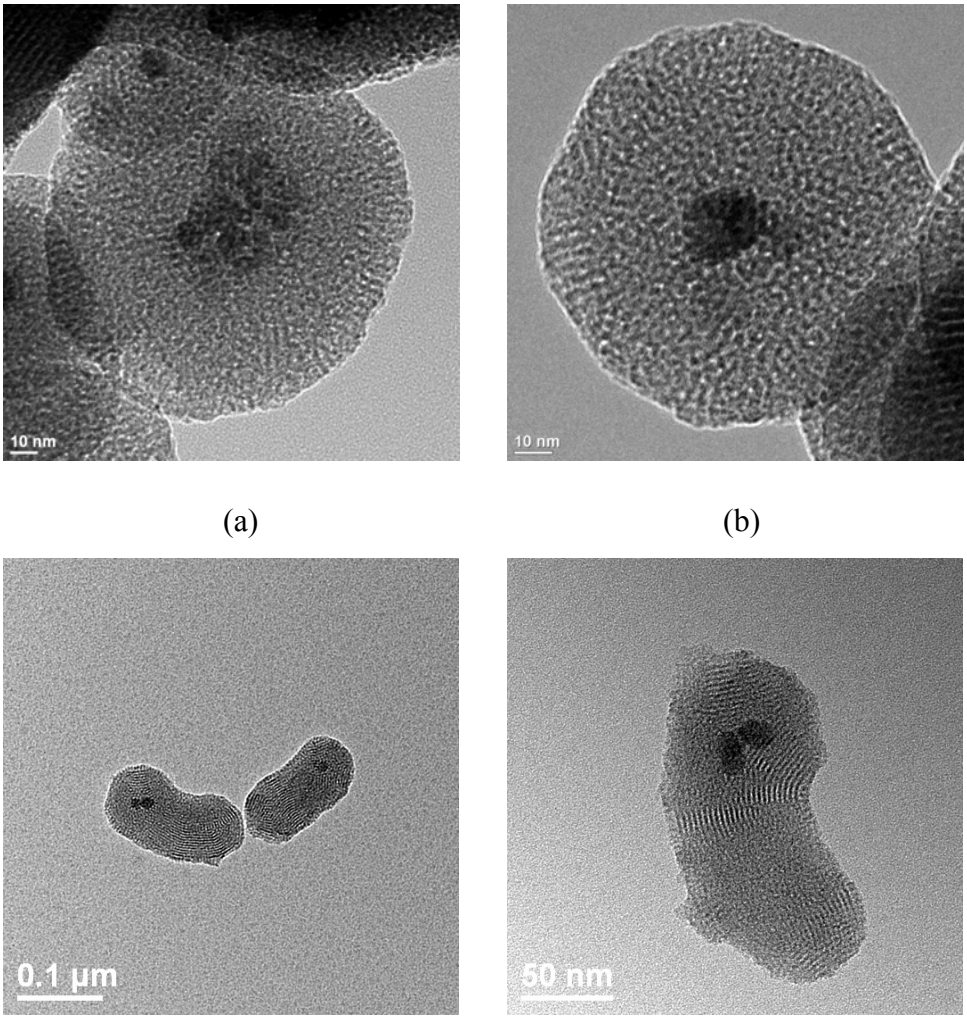

(a) (b)

(c) (d)

Figure S1. Additional TEM images of MMSN-r (a, b) and Ph-MMSN-h (c, d).

Appendix B

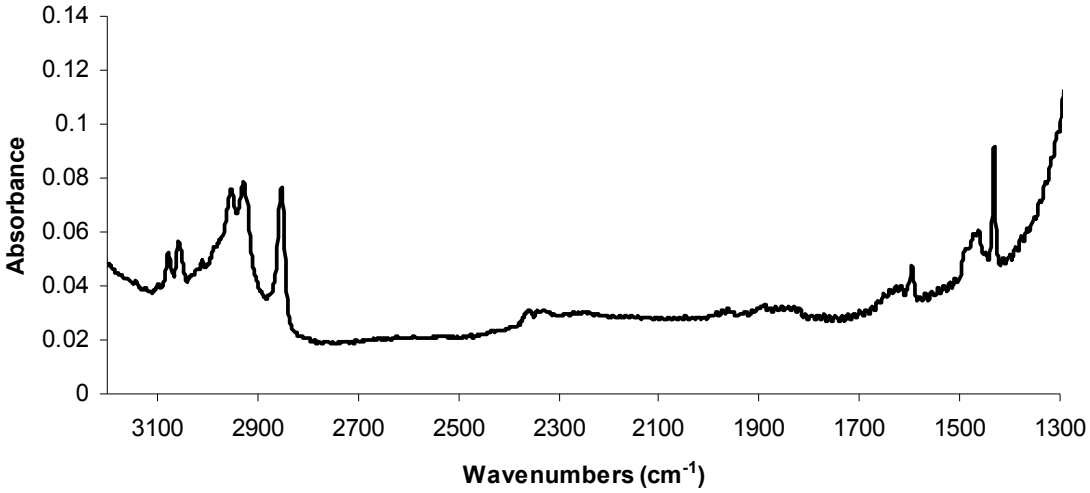

Figure S2. Infrared spectrum of Ph-MMSN-h.

Table S1. Assignment of the bands from IR spectrum of Ph-MMSN-h

Wavenumber (cm^{-1})	3077	3058	2953	2927	2853	1596	1462	1432
Assignment	Phenyl C-H st	Phenyl C-H st	Ethyl C-H st	Ethyl C-H st	Ethyl CH st	Phenyl C-C	Ethyl C-C δ	Phenyl C-C

Appendix C

a)

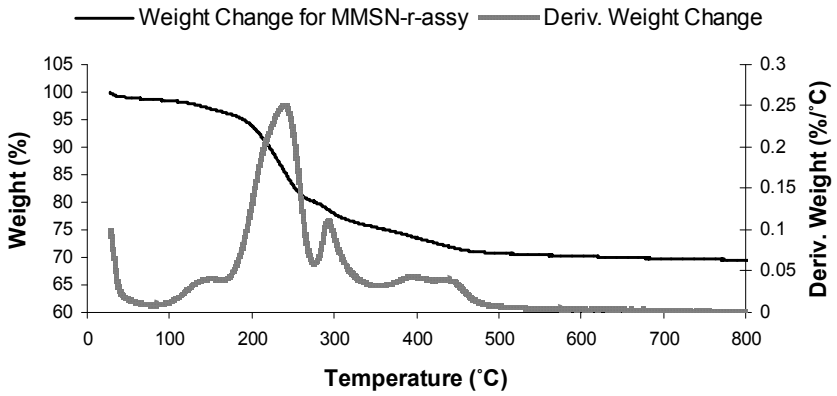

b)

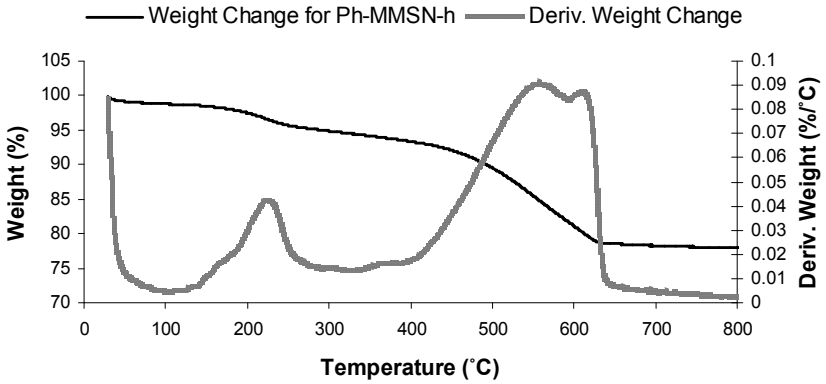

c)

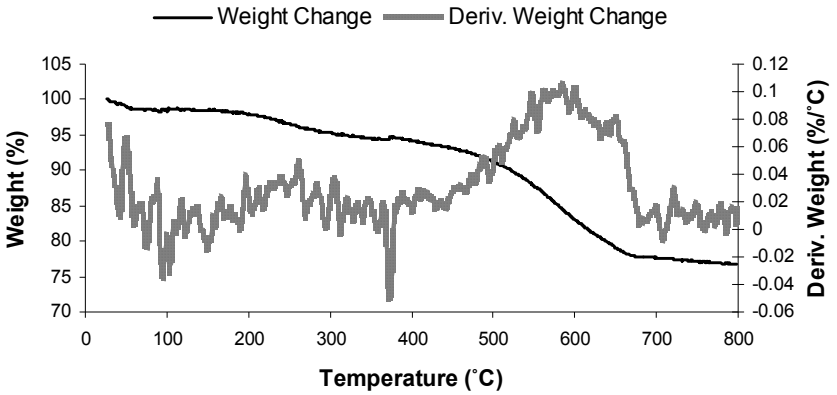

Figure S3. TGA data for (a) MMSN-r-as synthesized, (b) Ph-MMSN-h and (C) DTA-TGA for Ph-MMSN-h.

Appendix D

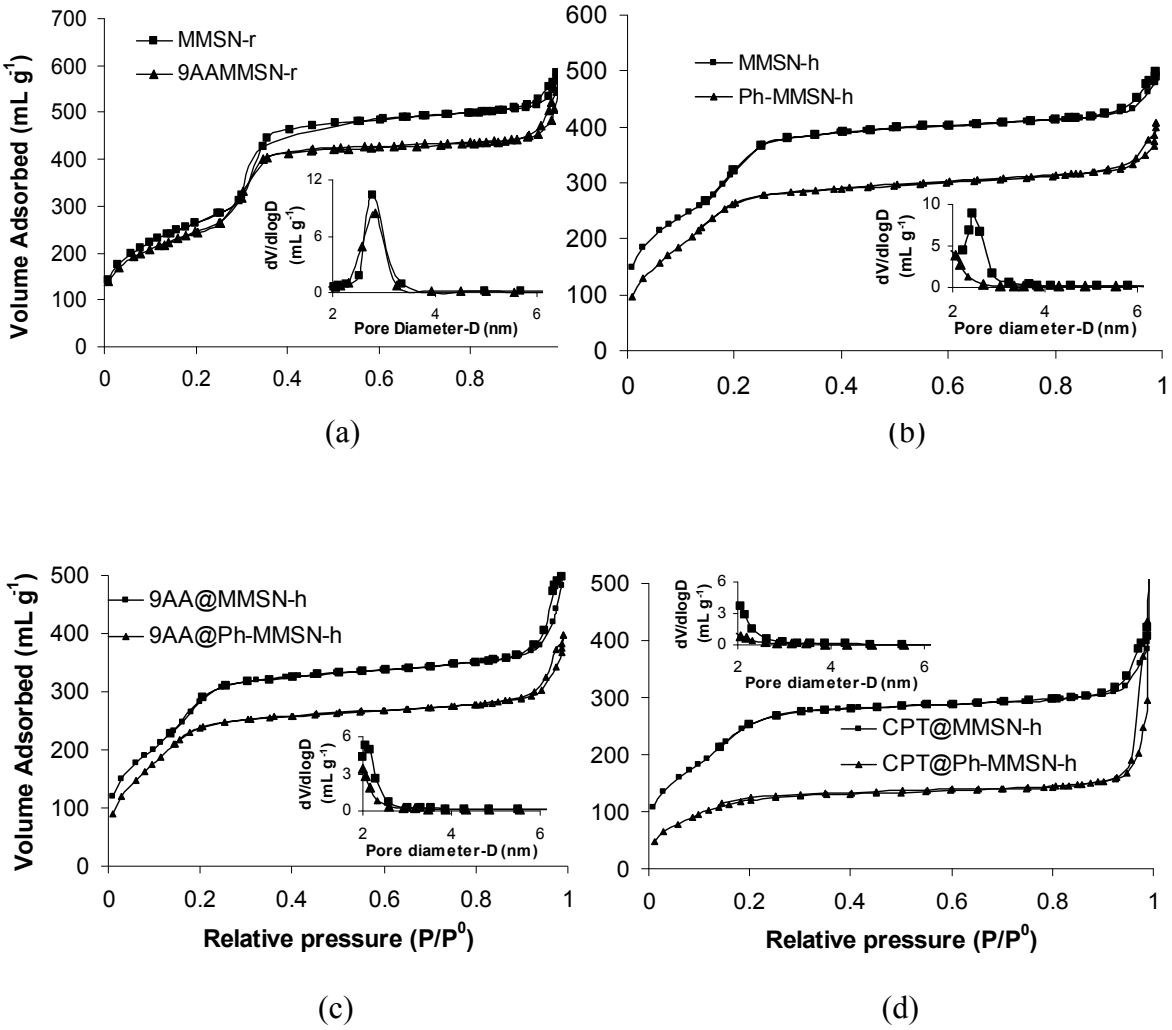

Figure S4. BET nitrogen adsorption/desorption isotherms for: (a) MMSN-r and 9AA@MMSN-r, (b) MMSN-h and Ph-MMSN-h, (c) 9AA@MMSN-h and 9AA@Ph-MMSN-h and (d) CPT@MMSN-h and CPT@Ph-MMSN-h. Insets show BJH average pore diameter distribution.

Appendix E

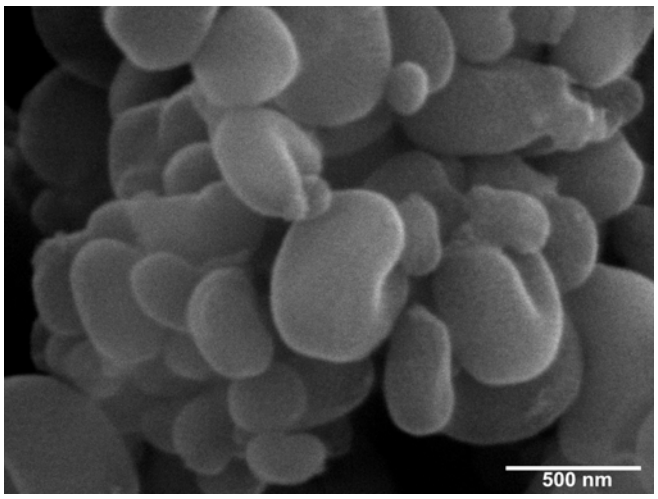

a)

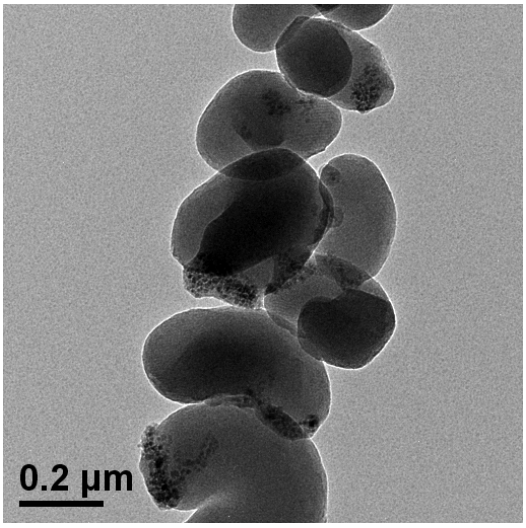

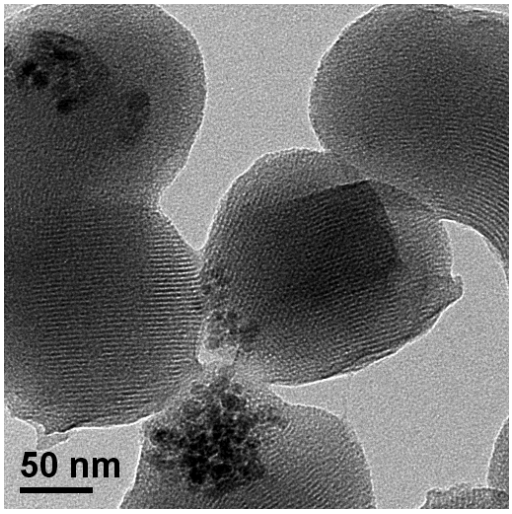

b) c)

Figure S5. SEM (a) and TEM images (b, c) of MMSN material synthesized without addition of Ph-TMS with TEOS.

Appendix F

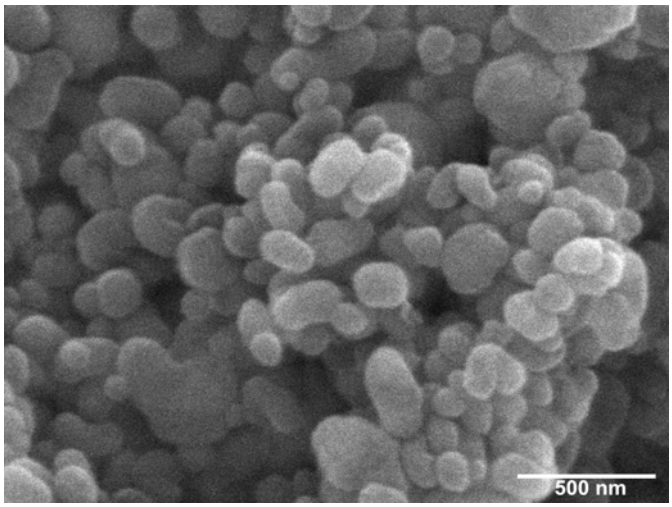

a)

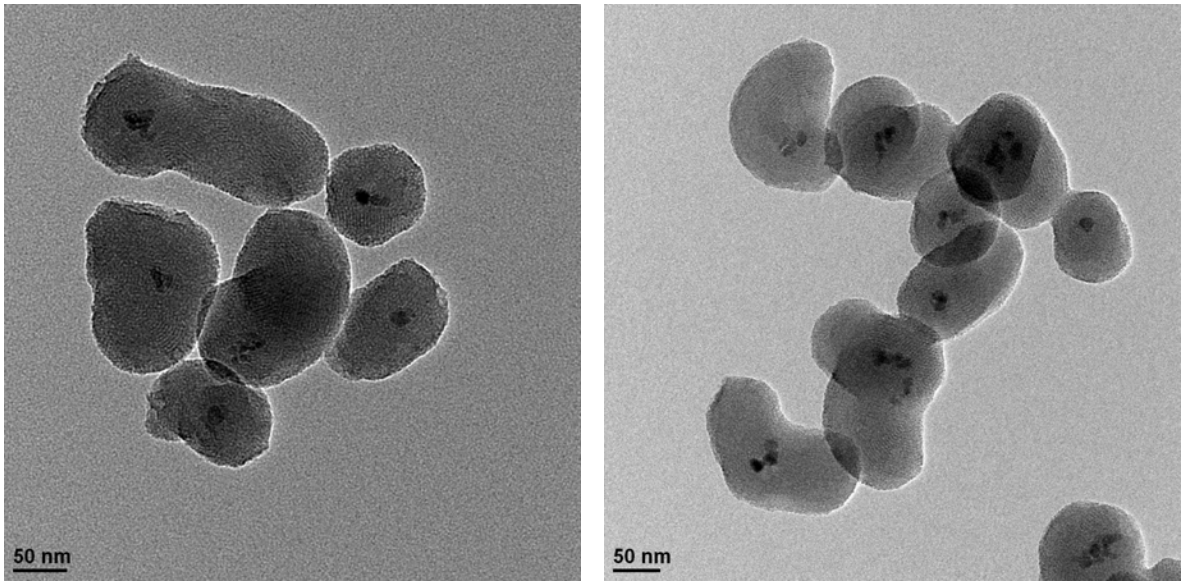

b) c)

Figure S6. SEM (a) and TEM images (b, c) of MMSN material synthesized by addition of 3-bromopropyltrimethoxysilane along with TEOS.

CHAPTER 4. MAGNETIC DRUG DELIVERY SYSTEM FOR PHOTOSENSITIVE TRIGGERING OF CAMPTOTHECIN RELEASE TO CANCER CELLS

Manuscript in preparation for publication

Nikola Ž. Knežević, Igor I. Slowing, Brian G. Trewyn, Victor S.-Y. Lin*

Department of chemistry, Iowa State University, Ames, Iowa, 50011

Abstract

Magnetic mesoporous silica nanoparticles were loaded with the anticancer drug camptothecin and mesopore entrances were blocked with 2-nitro-5-mercaptobenzyl alcohol functionalized CdS nanoparticles through a photocleavable carbamate linkage. Camptothecin release from this magnetic drug delivery system was successfully triggered upon irradiation with UV light. Photosensitive delivery of the anticancer drug was monitored by viability study on Chinese hamster ovarian cells. A cooperative anticancer effect of the capping CdS nanoparticles and loaded camptothecin was observed upon exposure of the cell cultures treated with drug loaded material to low power UV light (365 nm).

Introduction

The development of drug delivery systems (DDS) for cancer therapy has received much attention during the recent years. Due to severe toxic effects that anticancer drugs inflict on healthy tissues, one of the goals for research on DDS has been to devise a system with the ability to target the delivery of drugs to specific regions of the body, i.e. cancerous tissue.[1-4] There are several characteristics of tumor tissues that are currently exploited for

targeted drug delivery. The enhanced permeability and retention (EPR) effect is the first of these properties, which facilitates the spontaneous accumulation of macromolecules in the extracellular medium of tumor tissue.[5] Hence, the primary targeting design is the construction of DDS as nanometric macromolecular assemblies. Additional cancer targeting can be achieved by modification of a surface of DDS with ligands which have a specific interaction with overexpressed receptors on the luminal side of tumor clusters. Folic acid and the Arg-Gly-Asp (RGD) tripeptide were shown as efficient ligands for this purpose.[6] Alternatively (or in addition to other forms of targeting), the site of drug delivery can be actively targeted by an external stimulus. For example, the drug carriers can be magnetically active which would open the possibility to control the location of a DDS by an externally applied magnetic force.[7] Additionally, release of the drug from a DDS can be actively controlled by an external stimulus. That is, the drug carrier would not release its cargo unless triggered by a controlled external incentive, for instance by light irradiation.[8, 9]

We have previously demonstrated the utilization of macromolecules and quantum dots as "caps" for entrapment of various molecules in the pores of mesoporous silica nanoparticles (MSN).[10-12] The molecules are not released from the mesopores unless triggered by chemical reagents. MSN is suitable material for the construction of drug carriers due to its high surface area (> 700 m^2/g), tunable pore diameter (2-30 nm), narrow pore size distribution and particle diameter (typically 100 - 200 nm) which is in range to benefit from EPR effect of tumor tissue. In addition we have shown that these nanospheres can effectively penetrate the cell membrane, usually through clathrin mediated endocytosis.[13] Besides of its applications in drug delivery, MSN has been proven applicable for selective catalysis, sensing and separation techniques.[14-16]

We have also previously reported on magnetic mesoporous silica nanoparticles (MMSN).[17] This is a core-shell type of material with magnetic iron oxide nanoparticles as the core and mesoporous silica framework as the shell of nanospheres. The material still has

all of the drug carrier-beneficial properties of MSN with an added benefit of magnetic activity. We also showed that MMSN is responsive to the action of externally applied magnetic field, exerted by magnetic force of an inexpensive neodymium magnet (1110 G). These results facilitate the devising of a DDS which would contain the possibility of applying an external nondestructive force, such as a magnetic field, to control the location of the drug carriers both *in vitro* and *in vivo*. This method has been shown to yield a significant improvement in the efficiency and selectivity of the drug release.[7]

Hence, in a continuing effort to devise an ultimate targeting DDS, which we imagine would be capable of delivering an exact amount of drug to a precise location; we developed magnetically active DDS with an ability to release anticancer drugs upon UV light irradiation. We report on a CdS nanoparticle-capped magnetic mesoporous silica based DDS for a UV radiation triggered release of anticancer drug camptothecin (CPT). This drug and its derivatives are known to inhibit DNA enzyme topoisomerase I and have been used in chemotherapy for a variety of cancer types.[18, 19] Viability studies confirmed the capability of the DDS to deliver camptothecin to Chinese hamster ovarian (CHO) cells and induce cell death upon irradiation with low power UV lamp.

Experimental Section

Instrumental Methods

Powder XRD diffraction data were collected on a Scintag XRD 2000 X-ray diffractometer using Cu Kα radiation. Nitrogen adsorption and desorption isotherms, surface area and average pore diameter were measured using a Micromeritics ASAP2000 sorptometer. Sample preparation included degassing at 100 °C for 6 h. Specific surface areas and pore size distributions were calculated using the Brunauer-Emmett-Teller (BET) and Barrett-Joyner-Halenda (BJH) methods, respectively. Particle morphology of the materials

was determined by scanning electron microscopy (SEM) using a JEOL 840A scanning electron microscope. Transmission electron microcopy (TEM) examination with energy dispersive X-ray analysis (EDX) was completed on a Tecnai G2 F20 electron microscope operated at 200 kV.

Materials

Tetraethylorthosilicate (TEOS), *n*-cetyltrimethylammonium bromide (CTAB), 3-isocyanatopropyltriethoxysilane (Gelest), 5,5'-dithiobis(2-nitrobenzoic acid) and camptothecin (CPT) were purchased from Aldrich and used as received. Magnetite nanoparticles were prepared by co-precipitation of Fe^{3+} and Fe^{2+} ions with NH_4OH in aqueous solution by a previously reported synthetic procedure.[11, 20] 2-Nitro-5-mercaptobenzyl alcohol (NMBAl) was synthesized by reduction of 5,5'-dithiobis(2-nitrobenzoic acid) (Ellman's reagent) following the reported procedure.[21]

Preparation of magnetic mesoporous silica nanoparticles (MMSN):

Procedure for the preparation of MMSN used in this study was already reported recently.[17] Namely, magnetite Fe_3O_4 nanoparticles (300.0 mg) were sonicated for 12 h in a solution of CTAB (2.0 g, 5.5 mmol) and NaOH (7.0 mL, 2M) in nanopure water (480.0 mL). The suspension was then heated to 80 ˚C under mechanical stirring followed by rapid injection of TEOS (10.0 mL, 51.4 mmol). After additional 2 hours of stirring, the material was filtered, washed with water and methanol and air-dried. Final MMSN was obtained upon removal of surfactant molecules by calcination at 550 ˚C for 6 h with a heating rate of 10 ˚C min^{-1}.

Synthesis of cadmium-sulfide nanoparticles capped with 2-Nitro-5-mercaptobenzyl alcohol (CdS-NMBAl):

CdS nanoparticles were prepared by modification of a published procedure for synthesis of thioglycerol capped CdS nanoparticles.[22] Ethanol solutions (50 ml, 5 mM) of cadmium acetate, sodium sulfide and NMBAl were separately prepared and pH of all three solutions was fixed to 6 by addition of concentrated acetic acid and ethanol solution of sodium acetate. Solutions were degassed by flushing with Ar and were kept under Ar throughout the synthesis. Cadmium acetate and NMBAl were then mixed under vigorous stirring and the solution of Na_2S was added dropwise into the mixture while the whole solution was stirred and protected from light. Addition of sodium sulfide was the dark. Solvent was then evaporated and acetone was added to the oily residue until CdS-NMBAl precipitated. The product was centrifuged, washed with acetone and dried in liophylizer. Yield: 0.1 g. Elemental analysis: found C: 23.085 %, H: 3.0725 %, N: 0.0525 %, S: 1.425 %. Theoretical for: $(CdS)_{13.65}(C_7H_6O_3NS)(CH_3COO)_{321.4}$.

Loading of camptothecin into the mesopores of MMSN and capping with CdS-NMBAl:

The solutions in this procedure were kept constantly under Ar. CdS-NMBAl (120 mg) was dissolved in 4ml of dry DMF after which 3-isocyanatopropyltriethoxysilane (0.1 mmol, 26 µl) was added and the solution was stirred in dark for 24 h. During the same time MMSN (100 mg) and camptothecin (4 mg) were stirred in 2ml of water-free DMF. Then camptothecin (8 mg) was added to the solution containing pre-reacted CdS-NMBAl and 3-isocyanatopropyltriethoxysilane, the solution was stirred for additional 15 minutes and then added to the suspension containing MMSN and CPT. New suspension was then stirred for 20 h under heating at 125 ºC in order to graft CdS-NMBAl on the surface of MMSN and entrap CPT in the process. The new material CdS-NMBAl-CPT@MMSN (CCM) was filtered, washed with DMF, water and methanol and dried in lyophilizer.

Loading of the drug was determined by the absorption of residual CPT from the filtrate solution after evaporation of solvents and redissolving in DMF. Final loaded amount was determined to be 50mg of CPT/g of MMSN, by comparison of the absorption at 364 nm with previously prepared standard curve.

For determination of the drug release from CCM, the drug loaded magnetic material (2 mg) was added to glass vials and the material was fixed to the internal side wall of the vial by the influence of magnetic field of a neodymium disk magnet (DA01, K&J Magnetics, Inc, 5/8' x 1/32', surface field: 1110 G, pull force 20.47 lbs), which was taped on the external surface of the vial in a manner which we already reported.[11] PBS buffer (pH = 7.4, 2 ml) was then added to the vials and samples were kept in dark, at room temperature. Aliquots of the solution were taken over time and the fluorescence of the released drug was measured at 445 nm (exc. 383 nm). After establishing a steady release for the material in dark, one of the samples was subjected to UV irradiation for 30 minutes with a Rayonet RPR-100 photoreactor equipped with 16 RPR-3500 lamps. The lamps have an emission maximum at 350 nm and measured light intensity was 5.5 mW/cm^2 at the center of the photoreactor. Light intensity of the irradiation source was measured with Spectroline DSE-2000HA/L Radiometer/Photometer. After irradiation, the sample was again kept in dark and flurescence measurements continued.

Cell cultures

All experiments were done in triplicate for each of the following designations: CTRL-control cells without any added material; CCM-the cells treated with CPT loaded material. i.e. CdS-NMBAl-CPT@MMSN; CM-the cells treated with empty shell, i.e. CdS-NMBAl-MMSN. All of the samples were also either kept in dark (DARK) at all times or were kept in dark except when subjected to irradiation (IRR) for 30 minutes, as described below. Control samples, i.e. samples without added material were treated in the same manner as the samples

with added materials, during all steps of the experiment. Chinese hamster ovarian (CHO) cells were seeded at a density of 1×10^5 cells mL^{-1} in 6 well plates and allowed to attach for 24 h in D-10 medium (3 mL) at 37 ºC and 5% CO_2. The D-10 medium consists of Dubelcco's Modified Eagle Medium (DMEM) plus 10% equine serum, L-alanyl-L-glutamine, gentamicin, and penicillin/streptomycin. The medium was then replaced by suspensions of prepared materials at specific concentrations (0 μg/mL for CTRL, 10 μg/mL and 25 μg/mL for CCM and 25 μg/mL for CM) in a fresh medium without added serum. Serum was not used in this case in order to increase endocytosis efficiency of the materials. The cells were then protected from light and placed back into the incubator for additional 5 h. After that time the suspensions/solutions were removed, the cells were washed with PBS buffer and fresh aliquots of D-10 medium without materials were added. This procedure was done in order to ensure that only endocytosed material, which cannot be washed out, is responsible for any effect on cell viability. The samples designated as IRR were then immediately subjected to UV irradiation for 30 minutes. That is, 6 well culture plates were placed below Spectroline UV lamp model ENF-240C (115 V, 60 Hz, 0.2 A, measured light intensity = 1.0 mW/cm^2). At the same time DARK samples were kept in the dark, outside of the incubator. After the 30 minutes, all cells were protected again from light and placed back in the incubator for additional 20 h. CHO cells from each well were then harvested by trypsinization, centrifuged, resuspended in fresh D-10 medium (1 mL) and the number of viable cells in each sample was measured by flow cytometry using Guava ViaCount assay (Guava Technologies, Inc.; Hayward, CA).

Results and discussion

The synthesis and full characterization of magnetic mesoporous silica nanoparticles were previously reported.[17] We devised a facile synthetic method for preparing core-shell MMSN by co-condensation of magnetite nanoparticles with silicate precursors in basic solution, in the presence of cetytrimethylammonium bromide as a structure templating agent. The new magnetic analogues of MSN contained Fe_3O_4 nanoparticles in the core and a mesoporous silica framework as the shell of MMSN. When we applied fast addition of silane precursors into the reaction mixture containing surfactant template and well dispersed magnetite nanoparticles in basic conditions, we obtained MMSN with hexagonal pore packing, analogous to our typical MSN material. Final magnetic material was obtained after removal of surfactant by calcination in air, which also oxidized magnetite nanoparticles to maghemite nanoparticles in the core of MMSN. This material was further used for loading anticancer drug camptothecin into the mesopores and capping with 2-Nitro-5-mercaptobenzyl alcohol functionalized cadmium-sulfide nanoparticles (CdS-NMBAl). Ortho-nitrobenzyl moiety is known for several decades as effective photoresponsive protection group.[23] Preparation steps for the final drug loaded MMSN is depicted in Scheme 1. CdS nanoparticles were synthesized by modification of published procedure for synthesis of thioglycerol functionalized CdS nanoparticles.[22] Synthesis was conducted by reacting cadmium-acetate and 2-nitro-5-mercaptobenzyl alcohol in ethanol solution, buffered with sodium-acetate/acetic acid to pH 6.

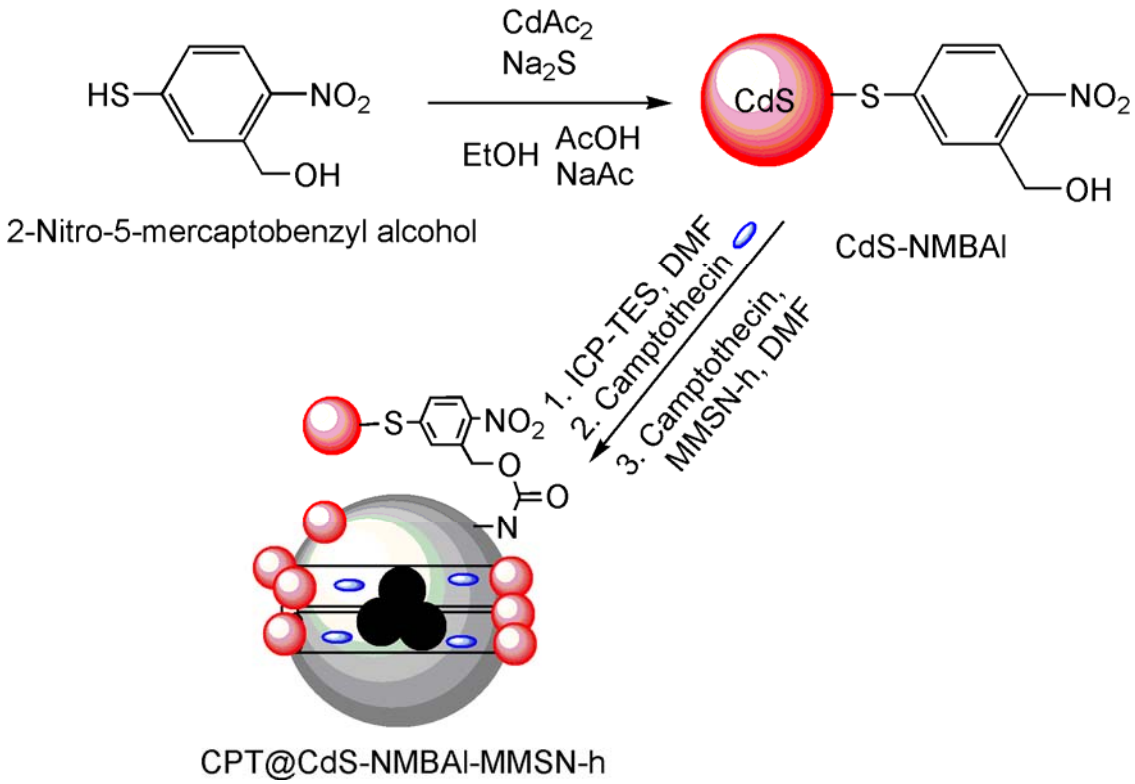

Scheme 1. Preparation of 2-nitro-5-mercaptobenzyl alcohol (NMBAl) functionalized cadmium-sulfide nanoparticles (CdS-NMBAl) and their application for capping the mesopores of MMSN and entrapment of camptothecin. ICP-TES = 3-isocyanatopropyl-triethoxysilane.

Ethanol was evaporated after the reaction and CdS-NMBAl was precipitated by addition of acetone. IR spectrum of CdS-NMBAl is dominated by the presence of acetate ions which precipitated with CdS-NMBAl nanoparticles. Strong carboxylate stretch vibrations are evident at 1575 cm^{-1} and 1417 cm^{-1} and characteristic $\delta(COO^-)$ at 671 cm^{-1} (Figure 1). However, in the spectrum of CdS-NMBAl we still noticed the presence of symmetric stretch of NO_2 group and a doublet arising from benzyl alcohol moiety (Table 1).

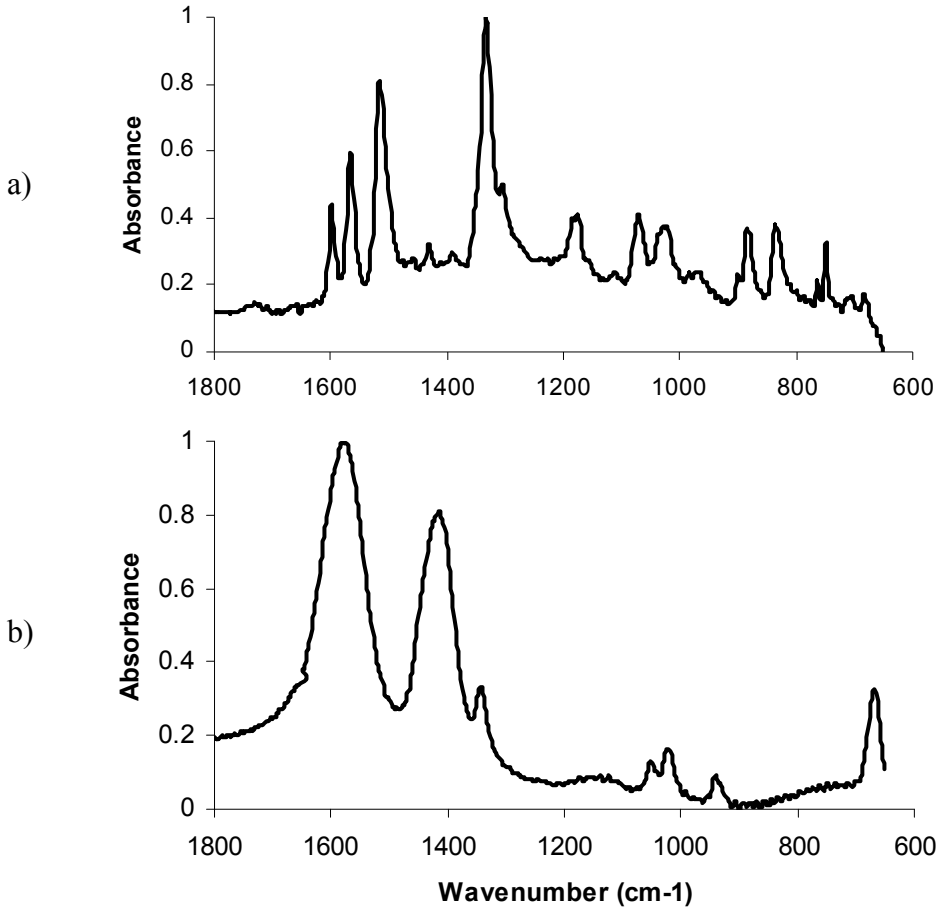

Figure 1. IR spectra of a) NMB-alcohol and b) CdS-NMBAl

Table 1. IR spectra band assignment for NMB-alcohol and CdS-NMBAl

Assignment	ArC-C (cm^{-1})	NO_2 st as (cm^{-1})	NO_2 st sy (cm^{-1})	Ar-CH_2-OH (cm^{-1})	ArC-C (cm^{-1})
NMB-alcohol	1599, 1565	1516	1332	1071, 1022	1599, 1565
CdS-NMBAl	-	-	1344	1052, 1022	-

CdS-NMBAl displayed typical UV-VIS absorbance and fluorescence characteristics of CdS quantum dots (Figure 2). UV-VIS absorbance of CdS-NMBAl in DMF revealed presence of absorption band of CdS nanoparticles with maximum of the band centered at 360

nm and band edge (λe) at 440 nm. Diameter of CdS nanoparticles was calculated to be 3.27 nm which was obtained from band edge value based on Henglein's empirical curve:[24]

$$2R(CdS) = 0.1/(0.1338 - 0.0002345\lambda e) \text{ nm}$$

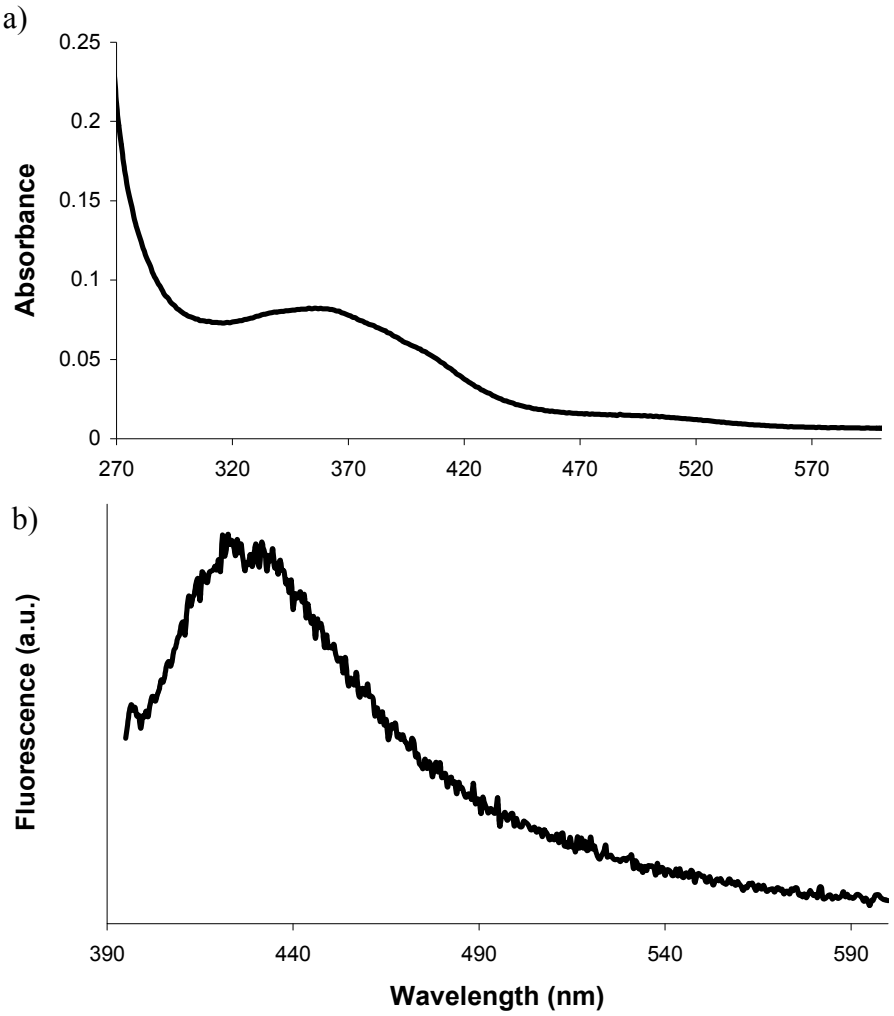

Figure 2. a) UV-VIS and b) fluorescence (exc. 350 nm) spectra of CdS-NMBAl

Loading of the drug and capping of mesopores was done in dry DMF. Camptothecin was first stirred in a suspension of MMSN for 24 h in order to allow for diffusion of the drug into the mesopores. CdS-TNBAl was separately coupled with isocyanatopropyl-TMS to form carbamate linkage and then mixed with CPT before mixing the two solutions and grafting CdS caps on drug filled MMSN. TEM images of the final drug filled material (CPT@CdS-NMBAl-MMSN) are shown on Figure 3.

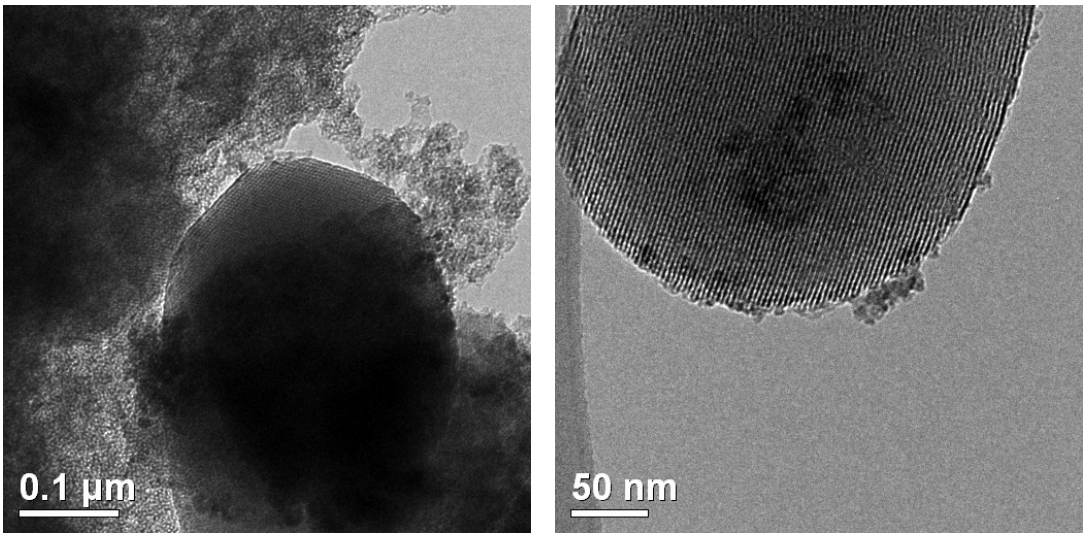

(a) (b)

Figure 3. Transmission electron images (TEM) of CPT@CdS-NMBAl-MMSN; (a) MMSN nanoparticles engulfed by CdS quantum dots and (b) the image showing iron-oxide nanoparticles inside the mesoporous matrix and CdS nanoparticles on the pore entrances.

Figure 3a shows MMSN material engulfed in CdS-NMBAl matrix. It seems that during the capping procedure, which was done at high temperature, *in situ* prepared triethoxysilane functionalized CdS nanoparticles condensed with each other to a certain degree and formed the matrix, in addition to grafting the matrix on MMSN surface. Figure 3b shows a region with smaller amount of CdS caps clearly showing the presence of maghemite nanoparticles inside MMSN, and CdS nanoparticles capping the mesoporous channels.

Nitrogen adsorption/desorption isotherms (Figure 4) revealed that after capping, BET isotherm changed from type IV to type II. Type IV surface is characteristic for mesoporous while type II for microporous materials. BJH analysis confirms these results as the average pore diameter decreases after capping from 2.6 nm to a value below 2 nm, which indicates partial blocking of the mesopores. BET surface area for the material before capping was 859 m^2/g, which changed to 749 m^2/g for CPT@CdS-NMBAl-MMSN, and 688 m^2/g for CdS-NMBAl-MMSN. These values reveal that the encapsulation of the drug in the mesopores was not very efficient. Even though CdS caps clearly influenced the values for BJH average pore diameter, there was still plenty of available room for nitrogen molecules to enter the mesopores and adsorb on available surface area, during the BET analysis.

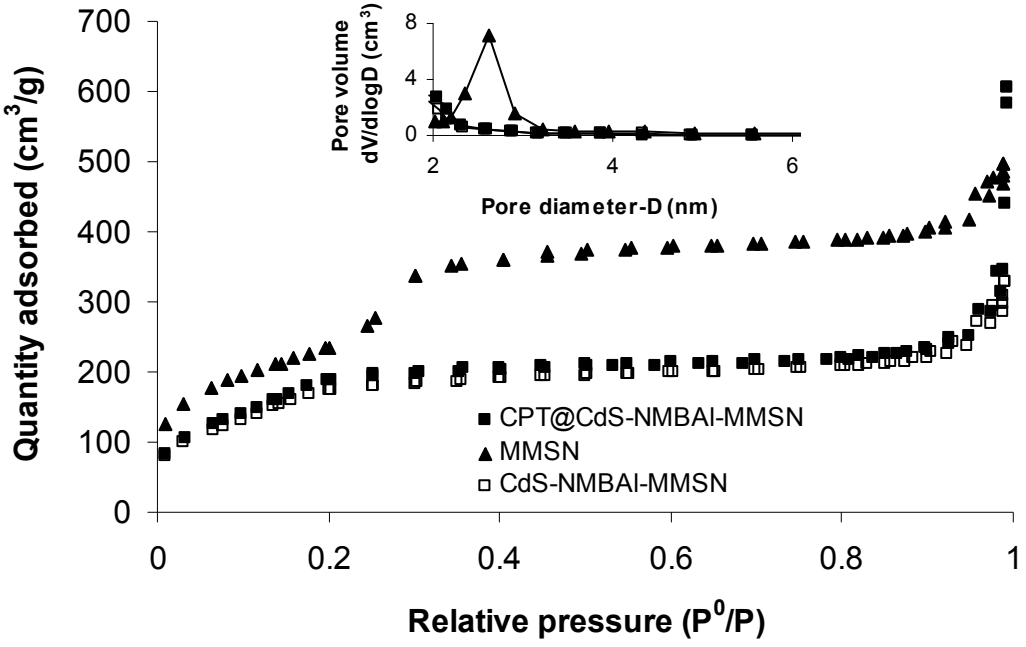

Figure 4. BET nitrogen adsorption/desorption isotherms for MMSN, CPT@CdS-NMBAl-MMSN and CdS-NMBAl-MMSN. Inset shows BJH pore size distributions.

Release of camptothecin was measured in PBS buffer. Since the DDS had magnetic properties we were able to monitor the release of the drug while DDS was fixed to the

internal side wall by the force of external magnetic field. This procedure was used as a simulation of targeting the treatment area by the application of an external magnetic field. We compared the drug release from the DDS that was kept continuously in the dark with the one that was subjected to irradiation for 30 minutes (Figure 5).

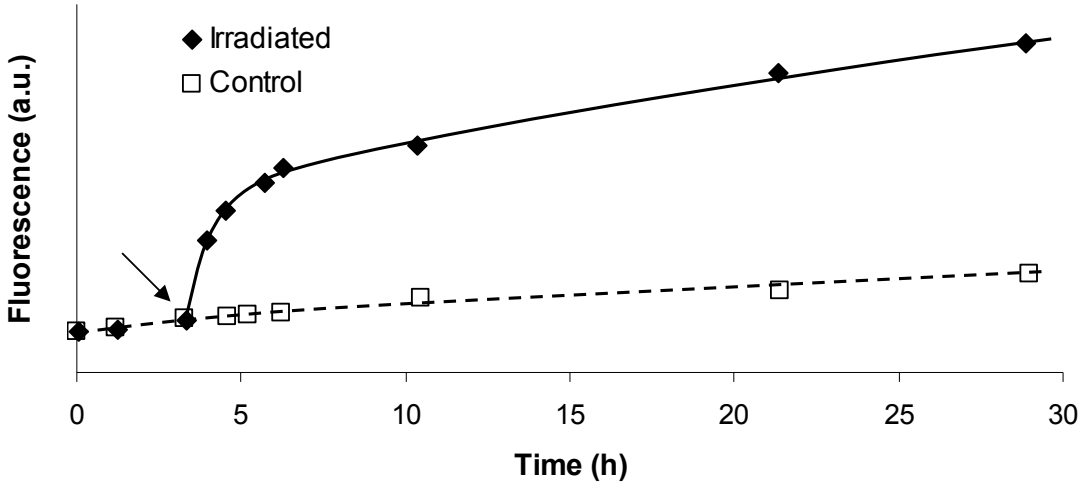

Figure 5. Release of camptothecin from CPT@CdS-NMBAl-MMSN while protected from light at all times (empty squares) and while protected from light at all times except for 30 min period under irradiation with UV light (350 nm) starting with the point marked by arrow (black diamonds).

As evidenced by the drug release kinetics, CPT release was successfully triggered by UV light irradiation. Almost no release of the drug was noticed if DDS was constantly kept in dark. However, upon 30 minutes of UV irradiation, the drug concentration in solution increased, as evidenced by the increase in drug fluorescence. This increase in fluorescence was clearly not due to increased concentration of CdS-NMBAl upon irradiation, because the system that did not contain loaded CPT (CdS-NMBAl-MMSN) did not show this increase in fluorescence after irradiation.

In order to test the applicability of our DDS for drug delivery to cancer cells, we monitored viability of Chinese hamster ovarian (CHO) cells in the presence of CPT@CdS-NMBAl-MMSN (CCM) and CdS-NMBAl-MMSN (CM) material without (Dark) and with

exposure (Irr) to low power UV lamp. The viability of treated cells was then compared to non-treated, control cells (Ctrl). As depicted on Figure 6, there is no influence on cell viability if CHO cells were treated with CPT loaded material, if the culture was kept in dark (Dark-CCM). However, upon exposure to 30 minutes of UV light irradiation number of viable cells in sample Irr-CCM decreased to 84 % of the number of viable cells counted in the culture treated with the same material, but that was kept in dark (Dark-CCM).

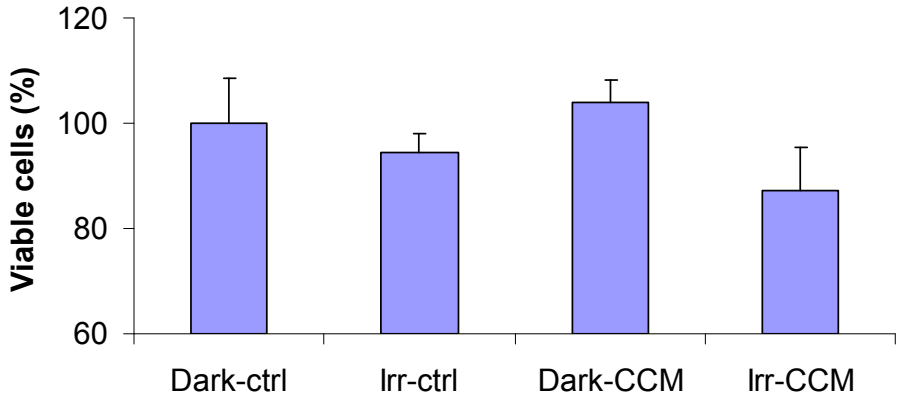

Figure 6. Number of viable CHO cells upon treatment with 10 µg/ml of CCM, while keeping the cell cultures constantly in dark (Dark-CCM); and upon exposure to 30 min irradiation with a low power UV lamp and consequently keeping the culture in dark (Irr-CCM). Viability values are compared to non-treated cells (ctrl) under the same conditions.

Student T test was done by comparison of Dark-CCM and Irr-CCM series and the two-tailed P value equals 0.0370 which means that this difference is considered to be statistically significant by conventional criteria. Even though the error bars for Dark-ctrl and Irr-CCM overlap for this experiment, if the treatment concentration was increased to 25 µg/ml, clear distinction between the two samples could be established (Figure 7).

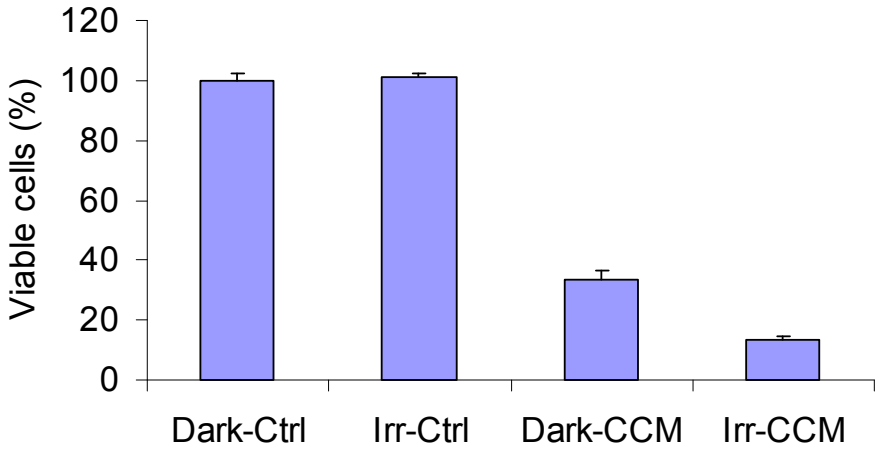

Figure 7. Number of viable CHO cells upon treatment with 25 μg/ml of CCM. Experiment conditions and Figure legend is the same as for Figure 6.

However, under these conditions sample Dark-CCM also showed the influence on CHO cell viability. This decrease in cell viability upon treatment with CPT@CdS-NMBAl-MMSN while keeping the cell cultures in dark can be explained by the well known cytotoxicity of CdS nanoparticles. Still, exposure to UV irradiation of CCM sample (Irr-CCM) clearly led to increase in toxicity. In this case, the cell cultures had 41 % less viable cells then the viable cells found in the sample Dark-CCM. This value is more then double lower then 84 %, which was determined in the treatment with 10 μg/ml of CCM, which agrees well with more then doubling the concentration of the DDS (from 10 to 25 μg/ml), which led to more then doubling released drug concentration.

In order to prove that it is not only CdS nanoparticles that are responsible for killing the cells before and after irradiation, we tested the citotoxicity of the magnetic material with attached CdS caps but without loaded material (CdS-NMBAl-MMSN = CM), under the same experimental conditions (Figure 8). As can be seen, there is no increase in toxicity of CdS nanoparticles upon exposure of CdS-NMBAl-MMSN to UV light (Irr-CM). In addition, from the same figure we can conclude that CdS nanoparticles are indeed responsible for the low

viability measured in sample Dark-CCM and not conceivable leaking of the anticancer drug from the DDS in the applied conditions, because the same viability values were found in the sample Dark-CM.

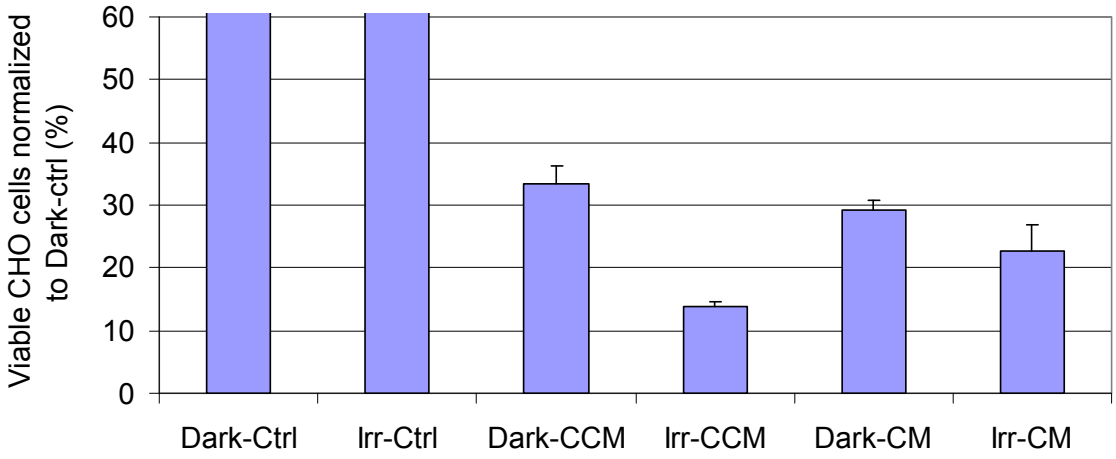

Figure 8. Comparison of cytotoxicity of treatments with 25 µg/ml of CPT loaded, CdS-NMBAl capped MMSN (CCM) and empty CdS-NMBAl capped MMSN (CM) when subjected to 30 minutes of UV irradiation (IRR) or kept in dark (DARK). Viability values are normalized to Dark-ctrl sample.

The two-tailed P value for Irr-CCM and Irr-CM samples equals 0.0202, which means that this difference in viability is considered to be statistically significant by conventional criteria. Hence, the mesopore-loaded drug and CdS nanocaps are exhibiting cooperative anticancer effect for this DDS on CHO cells. We believe that this strategy can be used to improve the antitumor efficacy of cytotoxic drugs because: a) DDS is magnetic which allows targeting of the cancer tissue with externally applied magnetic field and b) capping moieties can act in cooperation with loaded drugs to improve the toxic potency of DDS. Since the drug delivery system is magnetic, we believe that it may be possible to target the cancer tissue *in vivo* rapidly enough so that CdS nanocaps are not inducing much damage to healthy tissue in dark. Light induced drug delivery would then further increase the selectivity of a treatment. Finally, magnetic analogues of mesoporous silica nanoparticles were shown

already as good contrast agents, which may open the possibilities for *in situ* monitoring of anticancer treatment.

Conclusions

We prepared magnetically active drug delivery system which is capable of delivering its cytotoxic cargo upon triggering the drug release with UV light. Magnetite nanoparticles-incorporated mesoporous silica nanoparticles were loaded with anticancer drug camptothecin and mesopore entrances were capped with CdS quantum dots through photocleavable o-nitrobenzyl based carbamate linkage. Camptothecin release was successfully triggered with UV light irradiation while location of drug delivery system was controlled with externally applied magnetic field. Cooperative anticancer effect of capping CdS nanoparticles and loaded camptothecin was observed upon treatment of Chinese hamster ovarian cells *in vitro* with CPT@CdS-TNBAl-MMSN at 25 μg/ml concentration**.**

References

[1] G. B. Sukhorukov, A. L. Rogach, B. Zebli, T. Liedl, A. G. Skirtach, K. Kohler, A. A. Antipov, N. Gaponik, A. S. Susha, M. Winterhalter, W. J. Parak, *Small* 2005, *1*, 194.

[2] A. N. Koo, H. J. Lee, S. E. Kim, J. H. Chang, C. Park, C. Kim, J. H. Park, S. C. Lee, *Chem Commun (Camb)* **2008**, 6570.

[3] C. Alexiou, W. Arnold, R. J. Klein, F. G. Parak, P. Hulin, C. Bergemann, W. Erhardt, S. Wagenpfeil, A. S. Lubbe, *Cancer Res.* **2000**, *60*, 6641.

[4] W. Arap, R. Pasqualini, E. Ruoslahti, *Science* **1998**, *279*, 377.

[5] K. Greish, *J. Drug Target.* **2007**, *15*, 457.

[6] J. M. Rosenholm, A. Meinander, E. Peuhu, R. Niemi, J. E. Eriksson, C. Sahlgren, M. Linden, *ACS Nano* **2009**, *3*, 197.

[7] R. Jurgons, C. Seliger, A. Hilpert, L. Trahms, S. Odenbach, C. Alexiou, *J. Phys.: Condens. Matter* **2006**, *18*, S2893.

[8] N. K. Mal, M. Fujiwara, Y. Tanaka, *Nature* 2003, *421*, 350.

[9] J. L. Vivero-Escoto, I. I. Slowing, C.-W. Wu, V. S. Y. Lin, *J. Am. Chem. Soc.* **2009**, *131*, 3462.

[10] C.-Y. Lai, B. G. Trewyn, D. M. Jeftinija, K. Jeftinija, S. Xu, S. Jeftinija, V. S. Y. Lin, *J. Am. Chem. Soc.* **2003**, *125*, 4451.

[11] S. Giri, B. G. Trewyn, M. P. Stellmaker, V. S. Y. Lin, *Angew. Chem., Int. Ed.* **2005**, *44*, 5038.
[12] Y. Zhao, B. G. Trewyn, Slowing, II, V. S. Lin, *J. Am. Chem. Soc.* **2009**, *131*, 8398.
[13] I. Slowing, B. G. Trewyn, V. S. Y. Lin, *J. Am. Chem. Soc.* **2006**, *128*, 14792.
[14] S. Huh, H.-T. Chen, J. W. Wiench, M. Pruski, V. S. Y. Lin, *Angew. Chem., Int. Ed.* **2005**, *44*, 1826.
[15] D. R. Radu, C.-Y. Lai, J. W. Wiench, M. Pruski, V. S. Y. Lin, *J. Am. Chem. Soc.* **2004**, *126*, 1640.
[16] S. Oh, T. Kang, H. Kim, J. Moon, S. Hong, J. Yi, *J. Membr. Sci.* **2007**, *301*, 118.
[17] N. Z. Knezevic, I. I. Slowing, B. G. Trewyn, V. S.-Y. Lin, *J. Controlled Release* **2009**, *Submitted*.
[18] R. P. Hertzberg, M. J. Caranfa, K. G. Holden, D. R. Jakas, G. Gallagher, M. R. Mattern, S. M. Mong, J. O. Bartus, R. K. Johnson, W. D. Kingsbury, *J. Med. Chem.* **1989**, *32*, 715.
[19] N. Masuda, M. Fukuoka, Y. Kusunoki, K. Matsui, N. Takifuji, S. Kudoh, S. Negoro, M. Nishioka, K. Nakagawa, M. Takada, *J. Clin. Oncol.* **1992**, *10*, 1225.
[20] L. Vayssieres, C. Chaneac, E. Tronc, J. P. Jolivet, *J. Colloid Interface Sci.* **1998**, *205*, 205.
[21] M. C. Venuti, G. H. Jones, R. Alvarez, J. J. Bruno, *J. Med. Chem.* **1987**, *30*, 303.
[22] S. Jamali, E. S. I. Zad, S. F. Shayesteh, *Synthesis and Reactivity in Inorganic Metal-Organic and Nano-Metal Chemistry* **2007**, *37*, 381.
[23] Patchorn.A, B. Amit, R. B. Woodward, *J. Am. Chem. Soc.* **1970**, *92*, 6333.
[24] A. Henglein, *Chem. Rev.* **1989**, *89*, 1861.

CHAPTER 5. VISIBLE LIGHT AND LIGAND SUBSTITUTION MULTIPLE STIMULI RESPONSIVE SYSTEM FOR DRUG DELIVERY FROM $Ru(bpy)_2(PPh_3)$-CAPPED MESOPOROUS SILICA NANOPARTICLES

Manuscript in preparation for publication

Nikola Ž. Knežević, Brian G. Trewyn, Victor S.-Y. Lin*

Department of chemistry, Iowa State University, Ames, Iowa, 50011

Abstract

We devised a functional supramolecular assembly with multiple-stimuli responsive drug release capability. The dye sulforhodamine 101 was used as a model drug and it was entrapped inside the mesopores of mercaptopropyl-functionalized mesoporous silica nanoparticles (MP-MSN) by the MSN-propylmercapto-coordinated $Ru(bpy)_2(PPh)_3$-moiety (bpy = 2,2'-bipyridine, PPh_3 = triphenylphosphine). Upon irradiation with visible light the Ru-S coordination bond is cleaved which induces release of the mesopore-loaded dye molecules. The release of the cargo molecules was also responsive to addition of biologically relevant ligands, nitrogen-monoxide, histidine and imidazole. Release of both the capping moiety and entrapped dye was monitored in PBS solution with UV-VIS and fluorescence spectroscopy.

Introduction

Stimuli responsive drug delivery systems (DDSs) are gaining interest of the research community in recent years.[1-3] The main goal for the research field is to safely deliver drugs to specific treatment area.[4-6] This goal is established in order to overcome problems with

adverse effects of cytotoxic drugs. Typically, these DDSs are nanoscopic macromolecular assemblies of drugs and DDS structure-forming molecules. Mesoporous silica nanoparticles (MSN) in particular are attractive scaffolds for construction of such nanodevices for drug delivery.[7-9] Drugs can be effectively loaded inside the mesoporous framework and entrapped by the addition of various mesopore capping agents. Cargo molecules are then released only upon exposure to stimuli which are able to remove capping moieties. A variety of reports on this topic can be found in the literature. Studies from our research group have demonstrated effective application of CdS,[10] Fe_3O_4,[11] and gold nanoparticles,[12] as well as PAMAM dendrimers and insulin as capping moieties.[13,14] Other authors reported the use of rotaxanes and other organic molecules and macromolecules for this purpose.[15,16] Triggering of the drug release was achieved by addition of various redox agents, enzymes, anions, by UV light irradiation, change in temperature or pH value.

Ideally, a functional stimulus responsive DDS would have no pre-stimulus toxicity. This would require application of nontoxic DDS framework as well as zero drug release before the triggering event. Additionally, it would be highly beneficial if DDS is responsive to externally applied stimulus, which could effectively target the treatment area. We reported previously application of UV light irradiation as an external stimulus for triggering drug release from MSN carrier.[12] However, triggering the release with visible light would be more desirable because irradiation with UV light can lead to photodamage of the tissue and moreover, light scattering decreases with increasing irradiation wavelength.[17] Thus, visible light would penetrate further into the tissue and would be more applicable for *in vivo* triggering of drug release.

Recent report has shown that γ-aminobutyric acid (GABA) can be effectively released from a coordination compound $[Ru(bpy)_2(PPh_3)(GABA)]Cl$ by visible light induced cleavage of Ru-GABA coordination bond.[18] Herein, we report on an application of similar principle to deliver cargo molecules from a mesoporous silica nanoparticle-based assembly

upon irradiation with visible light. Sulforhodamine 101 (Sr101) molecules were loaded inside the mesopores of mercaptopropyl-functionalized mesoporous silica nanoparticles (MP-MSN). The dye molecules were then entrapped inside the mesoporous space by addition of $[Ru(bpy)_2(PPh_3)Cl]Cl$ which forms coordination bonds with mercaptopropyl moieties from the silica surface and prevents the cargo molecules to diffuse out into the bulk solution (Scheme 1). Upon irradiation with visible light the release of both the capping moieties and cargo Sr101 was detected by UV-VIS and fluorescence spectroscopy.

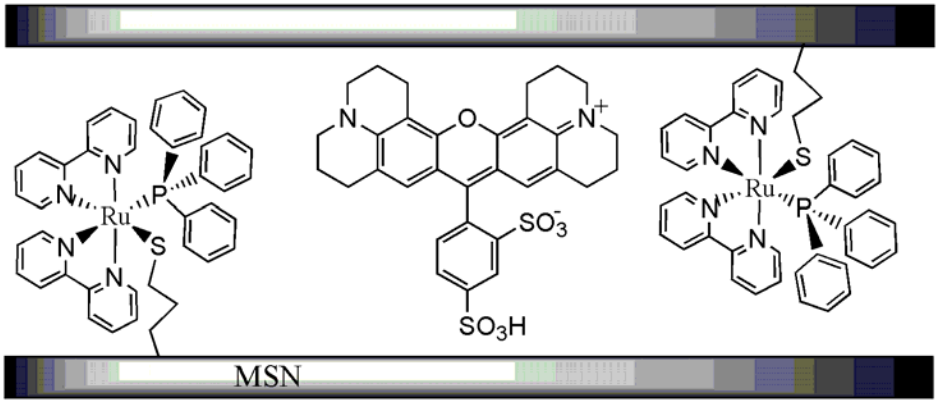

Figure 1 Mesopore-encapsulation of sulforhodamine 101 by $[Ru(bpy)_2(PPh_3)$-moieties S-coordinated to mercaptopropyl-functionalized MSN

We also monitored response of the DDS to the presence of nitrogen-monoxide, histidine and imidazole. These physiological species are known for their strong metal coordination capability, which can be utilized for substitution of Ru-coordinated MP-MSN and thus for the release of the loaded dye and the as synthesized $[Ru(bpy)_2(PPh_3)L]^{2+}$ ions (L = incoming ligand).

Experimental procedure

Reagents and solvents were commercially available and were used as received. $[Ru(bpy)_2(PPh_3)Cl]Cl$ was synthesized according to the literature.[18]

Instrumental Methods, Conditions and Parameters for Structural Characterization

Powder XRD diffraction data were collected on a Scintag XRD 2000 X-ray diffractometer using Cu (Kα) radiation. Nitrogen adsorption and desorption isotherms, surface areas, and median pore diameters were measured using a Micromeritics Tristar 3000 surface area and porosity analyzer. Sample preparation included degassing at 100 °C for 5 h. Specific surface areas and pore size distributions were calculated using the Brunauer-Emmett-Teller (BET) and Barrett-Joyner-Halenda (BJH) method, respectively. Particle morphology of the material was determined by scanning electron microscopy (SEM) using a JEOL 840A scanning electron microscope. Fluorescence measurements were performed on Horiba group Fluoromax-2 fluorometer.

Synthesis of mercaptopropyl-functionalized MSN material (MP-MSN)

n-Cetyltrimethylammoniumbromide (CTAB, 1.00 g, 2.74 x 10^{-3} mol) was first dissolved in 480 mL of Nanopure water. NaOH(aq) (2.00 M, 3.50 mL) was added to CTAB solution, followed by adjusting the solution temperature to 353 K. TEOS (5.00 mL, 2.57 x 10^{-2} mol) was first introduced dropwise to the surfactant solution, followed by dropwise addition of 3-mercaptopropyltrimethoxysilane (MP-TMS) (0.97 mL, 5.13 x 10^{-3} mol). The mixture was allowed to stir for 2 h to give rise to a white precipitate (as synthesized MP-MSN). The solid product was filtered, washed with copious amount of deionized water and methanol, and dried for 12 h under high vacuum and 353 K in order to stabilize the mesoporous structure. Final mercaptopropyl-MSN material was obtained upon removal of

the CTAB surfactant template by stirring in a solution of conc. HCl in methanol (1%, v:v) for 6 h at 60ºC . Material was then additionally washed with copious amount of deionized water and methanol, and it was again placed under high vacuum at 353 K to remove the remaining solvent from the mesopores.

Loading of sulforhodamine 101 into the mesopores of MPMSN and capping with $[Ru(bpy)_2(PPh_3)Cl]Cl$

MP-MSN (100 mg) was added to an aqueous solution (3 ml) of sulforhodamine 101 (1 mg/ml) and the suspension was stirred for 24 h at RT. A separate solution (2 ml) of sulforhodamine 101 (1 mg/ml) was prepared containing $[Ru(bpy)_2(PPh_3)Cl]Cl$ (100 mg) and the solution was degassed with Ar prior to heating at 80 ºC for 1 h. After this time the solution containing $[Ru(bpy)_2(PPh_3)Cl]Cl$ and dye molecules was added to the suspension containing MP-MSN and the dye, which was previously degassed with Ar. Combined solution was protected from light and was heated to 80 ºC for 24 h under argon. As-synthesized material (SR101@[Ru]-MPMSN) was filtered, washed with copious amounts of PBS buffer (pH 7.4, I = 154 M), water and methanol and finally dried in lyophilizer. The filtrate was collected and the loading of the dye was determined from the difference in UV-VIS absorption of the filtrate in PBS solution vs. starting concentration.

Release kinetics measurements

Suspensions of the dye loaded material (1 mg/ml) were prepared in PBS solution and the drug release was measured for sulforhodamine 101 by fluorescence emission at 595 nm (exc. 568 nm) and by UV-VIS spectroscopy (maximum at 568 nm) and for the release of capping ruthenium complex by measuring UV-VIS absorbance at 288 nm. After initial stirring for a prolonged time while protected from light, one of the suspensions was subjected to visible light irradiation with a photoreactor equipped with 3 serially connected LEDs

(Luxeon III Star LED - Royal Blue Lambertian, 340 mW, 700mA, emission maximum at 455 nm, I = 1500 lux). Other suspensions of the same concentration were used for testing the influence of ligand substitution on dye release or were not subjected to any stimuli and were stirred in dark (control samples). For ligand induced dye release, calculated amount of solid MAHMA NONOate (Aldrich), used as a source of nitrogen-monoxide ($t_{1/2}$ = 3 min), histidine or imidazole were added into the stirred suspension of Sr101@[Ru]-MP-MSN after 20 h of initial stirring in dark. The concentration of ligands was first set to 20 mM and then after the release of the dye reached plateau, the concentration of ligands was increased to 50 mM.

Synthesis of $[Ru(bpy)_2(PPh_3)MPA]PF_6$

Synthetic procedure was analogous to the published procedure for preparation of $[Ru(bpy)_2(PPh_3)GABA]PF_6$, (GABA = γ-aminobutyric acid).[18] Namely, $[Ru(bpy)_2PPh_3Cl]Cl$ (110 mg, 147 mmol) was dissolved in water (10 mL). The mixture was heated at 80 ºC for half an hour after which 3-mercaptopropionic acid (MPA) (469 mg, 4.42 mmol) and aqueous NaOH (4.4 mL, 1m) were added. Heating was continued for 3 h and the final complex was precipitated with KPF_6 (0.8 mL, 1m) in ice and centrifuged. The product was washed twice with water (3 ml) and dried.

Results and discussion

Preparation of the light responsive nanocarrier initially involved synthesis of mercaptopropyl functionalized MSN by our well established co-condensation procedure.[10] This method has been shown to yield the material with most of the organic functional groups distributed along the internal surface of the mesopores. After removal of the templating surfactant (CTAB) by washing with a solution of HCl in methanol, the entire volume of the

mesopores was available for loading of the dye molecules, while mercaptopropyl groups were available for reaction with capping moieties (Figure 2).

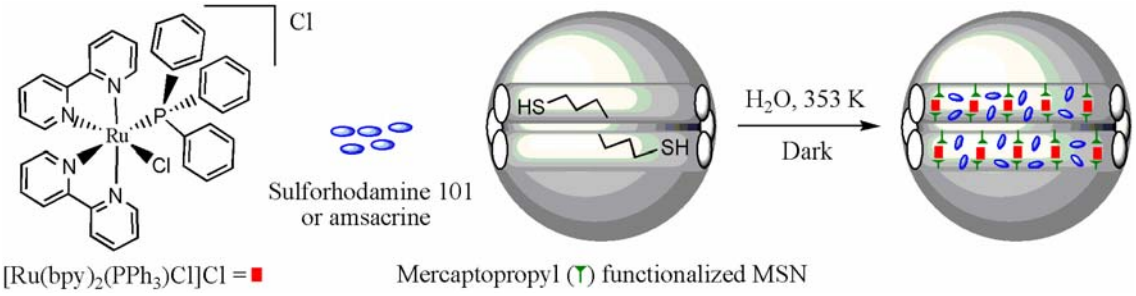

Figure 2. Loading of Sr101 into the mesopores of MP-MSN and capping with [Ru(bpy)$_2$(PPh$_3$)Cl]Cl

Coordination compound [Ru(bpy)$_2$(PPh$_3$)Cl]Cl was used as a capping precursor for this DDS. At an elevated temperature in a water solution, this complex undergoes substitution of its chloro ligand by water molecules, which are then susceptible to substitution with other incoming ligands. In our system the incoming ligands are mercaptopropyl moieties from the internal surface of the mesopores. Coordination of ligands containing sulfur donor atoms to ruthenium(II)-bipyridyl complexes have been reported.[19] Analogous complex ion $[Ru(bpy)_3]^{2+}$ was also applied as a dye for loading into the mesopores of MSN-based DDS.[20] However, since the size of $[Ru(bpy)_3]^{2+}$ ion is around 1.5 nm,[21] we believed that the analogous complex can be used as an effective capping moiety as well. Since the complex ion, [Ru(bpy)$_2$(PPh$_3$)GABA]Cl, recently showed the capability to release coordinated γ-aminobutyric acid (GABA) upon irradiation with visible light, we wanted to test the same moiety as a visible light responsive cap, which would be released from coordination to mercaptopropyl functionalized MSN. The dye sulforhodamine 101 (Sr101) was chosen for loading into the mesopores because its absorption band does not overlap with the absorption bands of the capping ruthenium complex, which simplifies the release kinetics study. Additionally, Sr101 molecule has weak donor atoms and would not interfere with the capping process.

Nitrogen adsorption/desorption isotherms and BJH data of the materials before and after capping revealed that $Ru(bpy)_2(PPh_3)$- moiety ([Ru]) successfully capped the mesopores since it induced a decrease in BET surface area and average pore diameter in the materials that contained loaded Sr101 (Sr101@[Ru]-MP-MSN) or even after capping the empty MP-MSN ([Ru]-MP-MSN) (Figure 2, Table 1).

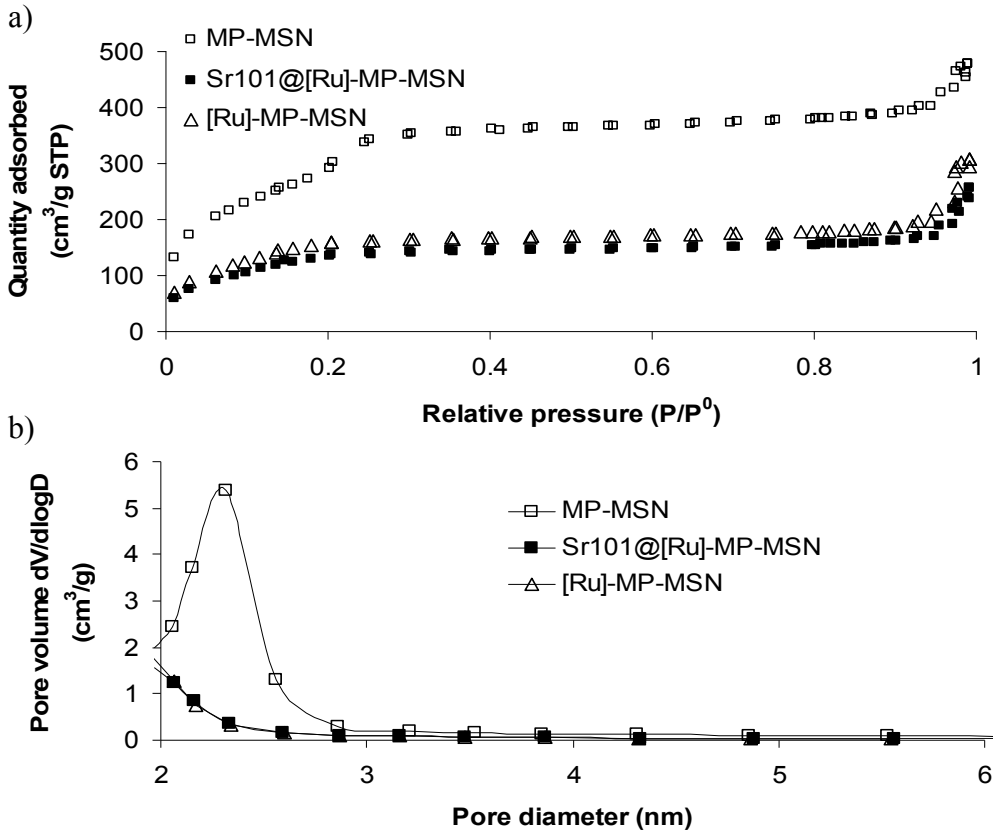

Figure 3. a) BET nitrogen adsorption/desorption isotherms and b) BJH average pore diameters for MP-MSN, Sr101@[Ru]-MP-MSN and [Ru]-MP-MSN

Table 1. BJH data for MP-MSN, Sr101@[Ru]-MP-MSN and [Ru]-MP-MSN

	MP-MSN	[Ru]-MP-MSN	Sr101@ [Ru]-MP-MSN
BET Surface area (m^2/g)	1082	610	522
BJH pore diameter (nm)	2.3	≤2	≤2

Scanning electron micrograph (SEM) of the material revealed spherical nanoparticles that did not change after the loading of cargo molecules and capping with [Ru] (Figure 4a). Low angle powder X-ray diffraction of MP-MSN showed typical diffraction pattern of hexagonally packed mesopores (Figure 4b). After the loading and capping, the XRD pattern changes due to disruption of symmetry. Energy dispersive spectroscopy (EDS) of the material revealed the presence of ruthenium in the amounts of 1.9 ± 0.4 wt% for Sr101@[Ru]-MP-MSN. Loading of the dye was determined as 71.1 μmol/g of MP-MSN.

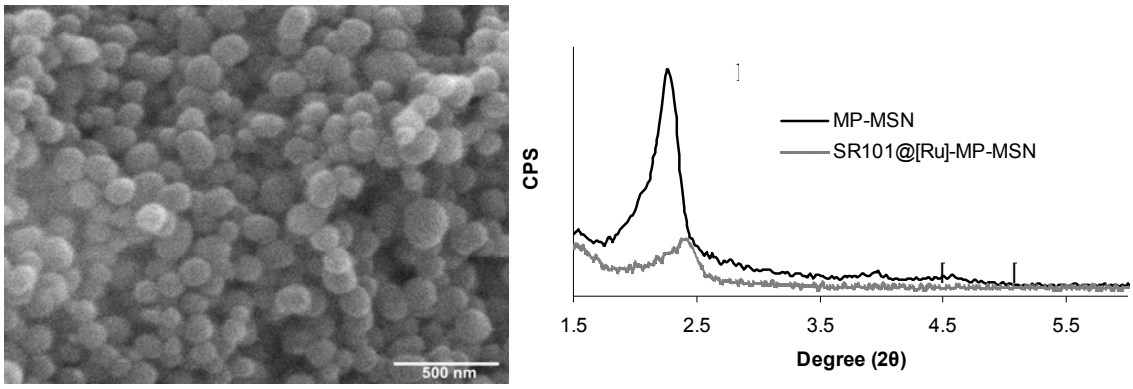

(a) (b)

Figure 4. Scanning electron micrograph (SEM) of Sr101@[Ru]-MP-MSN (a) and low angle X-ray diffractograms of MP-MSN and Sr101@[Ru]-MP-MSN (b)

In order to measure the release of cargo molecules, 1 mg/ml suspensions of the material in PBS buffer (10 mM, pH 7.4) were prepared and the release kinetics were measured by changes in UV-VIS absorbance at 288 nm for released [Ru] and at 568 nm for released Sr101 as well as the change in fluorescence at 595 nm (exc. 568 nm) for Sr101. Suspensions were centrifuged at designated times and only the quantity of species in PBS solutions was measured. Figure 5a shows the comparison of UV-VIS spectra of the supernatants obtained from suspension that was kept in dark for 44 h and the suspension that was subjected to irradiation for 22 h after 22 h of stirring in dark.

It is evident that irradiation with visible light (455 nm) successfully releases capping [Ru] moiety and loaded Sr101 dye. Bands at 288 nm and 450 nm are absorptions of [Ru] moiety assigned to intraligand and metal to ligand charge transfer (MLCT) transitions respectively. Bands centered at 530 nm and 567 nm are absorptions of sulforhodamine 101. However, these bands are noticeably blue-shifted when compared to the typical bands of the dye in PBS solution which appear around 545 nm and 586 nm respectively. This hipsochromic shift of the UV-VIS bands of Sr101 was already reported to occur in the case of adsorption on mesoporous silicate materials with 2.2 nm pore size.[22]

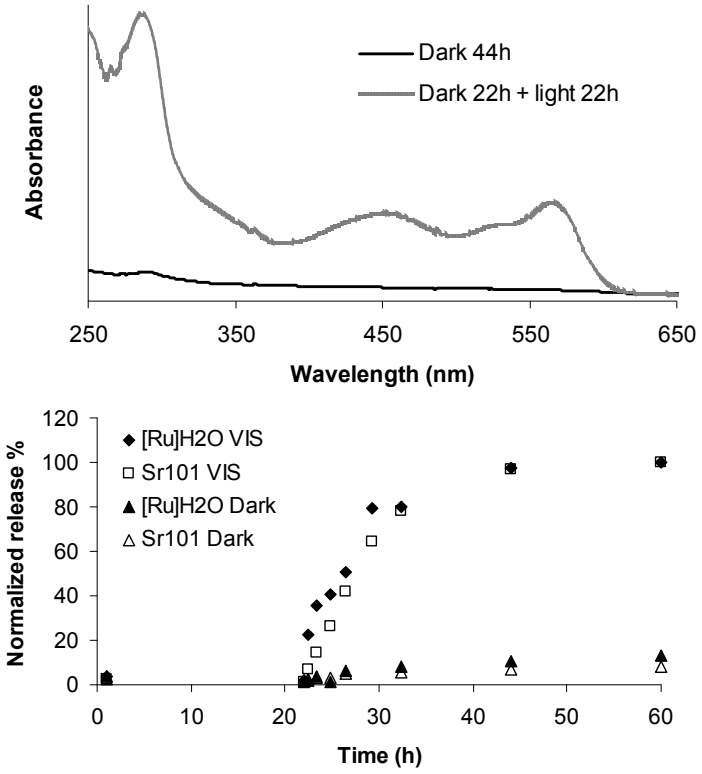

Figure 5. a) Comparison of UV-VIS spectra of the supernatants obtained from the suspension of Sr101@[Ru]-MP-MSN in PBS (10 mM, pH 7.4) that was stirred in dark for 44 h and the suspension that was subjected to irradiation for 22 h after 22 h of stirring in dark. b) Release kinetics of $[Ru(bpy)_2(PPh_3)(H_2O)]^{2+}$ ($[Ru]H_2O$) and sulforhodamine 101 (Sr101) from the suspension of Sr101@[Ru]-MP-MSN in PBS while suspension was protected from light at all times (Dark) and for the suspension that was subjected to irradiation after 22 h of stirring in dark (VIS). Absorbance of $[Ru]H_2O$ was measured at 288 nm and absorbance of Sr101 was measured at 568 nm. Results for released $[Ru]H_2O$ are normalized to the total released amount of $[Ru]H_2O$ for "$[Ru]H_2O$ VIS" sample and released amount of Sr101 was normalized to total released amount of Sr101 for "Sr101 VIS" sample.

The authors explained the effect as a consequence of a change in resonance structure of the molecule, which in turn yields a change from a planar molecule to a pyramidal shape in response to concave silica surface inside the mesopores. The change in dye absorbance is not observed if silicate materials with larger pores were used, which reveals the necessity of a suitable concave curvature. Even though this behavior was reported only for Sr101 while it was adsorbed on MSN surface; herein we observed that the dye was also released into the solution in the same conformation. The result directly confirms the premise that Sr101 was released from the depth of mesoporous space and not just from the external silica surface. We further tested if only $[Ru(bpy)_2(PPh_3)Cl]Cl$ would have an influence on the position of absorption bands of Sr101. No band shifting was observed after adding only the ruthenium complex to PBS solution of Sr101 even after prolonged stirring, heating or exposure to light irradiation. Only after addition of MP-MSN into the same solution we observed the hiposchromic shifting of the absorption bands of Sr101, after stirring over night (Figure S1).

Normalized release kinetics of the capping moiety and the cargo dye are represented on Figure 5b. We can notice that almost zero release was observed with suspensions that were kept in the dark. We employed irradiation on the suspensions with visible light (455 nm) after 22 hours of stirring in the dark and the release of $[Ru(bpy)_2(PPh_3)(H_2O)]$ ($[Ru]H_2O$) and loaded Sr101 was clearly evident. By comparison of the normalized release curves for $[Ru]H_2O$ and Sr101 we observed that the release kinetics of the "cap" and the "cargo" molecules are identical. We believe that this behavior is a consequence of having both [Ru] and Sr101 inside the mesopores, and each release of the cap is followed by immediate release of the cargo molecules (Figure 6).

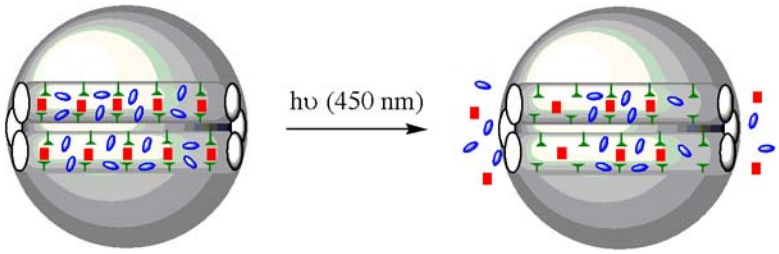

Figure 6. Schematic representation of visible light induced release of [Ru] caps (■) and Sr101 (⬮) as cargo molecules from mercaptopropyl (⊤) functionalized MSN

In order to prove that cleavage of thiol coordinated $Ru(bpy)_2(PPh_3)$-moiety is responsible for the visible light induced dye release, we synthesized analogous coordination compound $[Ru(bpy)_2(PPh_3)MPA]PF_6$ (MPA = 3-mercaptopropionic acid). UV-VIS absorbance of the new ruthenium complex showed the presence of MLCT band centered at 396 nm. After 30 minutes of irradiation of PBS solution of this complex with visible light, the MLCT band shifted to around 430 nm (Figure S2). This result indicates that $[Ru(bpy)_2(PPh_3)H_2O]^{2+}$ ion was formed due to expulsion of MPA ligand from the coordination sphere.

To test the influence of different ligands on the release of the species, we monitored the fluorescence of the PBS supernatants (pH 7.4) after addition of MAHMA NONOate, imidazole and histidine (Figure 7). MAHMA NONOate is a known NO donor with a half life of 3 minutes at pH 7.4. As can be seen, the dye release is substantially less responsive to ligand induced release when compared to visible light irradiation. Even the most effective of the three tested ligands, nitrogen-monoxide, released only about 20 % of the total amount of the dye that was released by irradiation. This discrepancy between irradiation induced and ligand induced dye release can be explained by the need of achieving equilibrium for the ligand substitution reaction. That is, in order for a substitution reaction to take place, the rate of the reaction of capping [Ru] with the incoming ligand (L) must be faster then the

regeneration of [Ru]-mercaptopropyl-MSN bond. Since [Ru] moiety is already inside the mesopores which contains mercaptopropyl moieties along its walls, regeneration of [Ru]-MP-MSN is favored. The probability of substitution reaction decreases further if [Ru] is farther inside the mesopores, which explains why the release of the dye stops soon after the initial release.

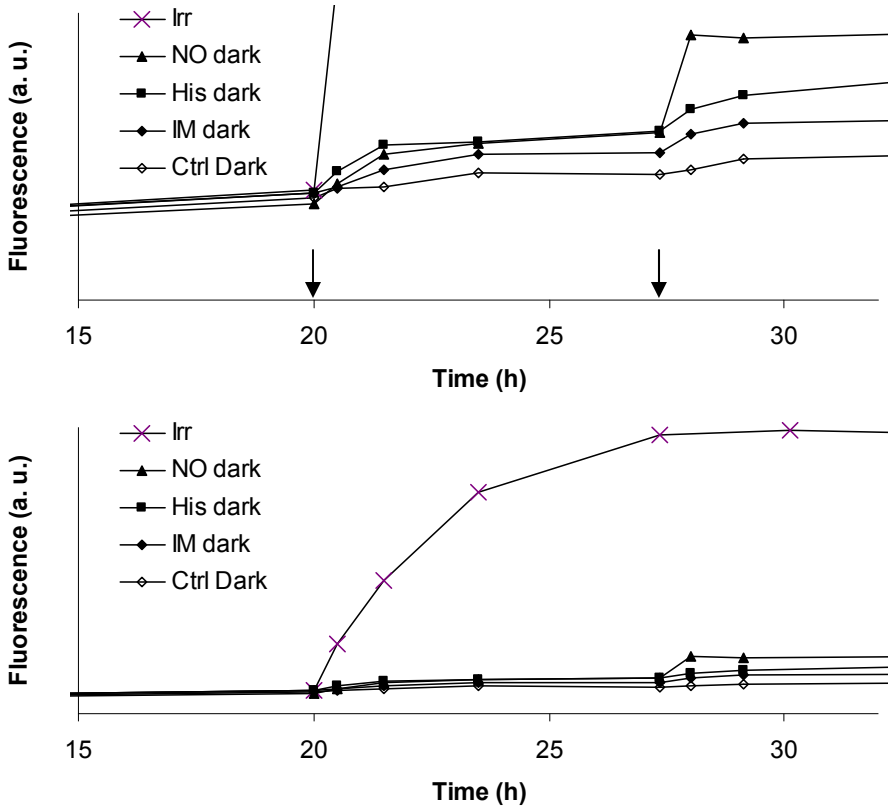

Figure 7. Comparison of the release curves of Sr101 triggered by visible light irradiation (Irr), nitrogen-monoxide in dark (NO dark), histidine in dark (His dark), imidazole in dark (IM dark) and release from a control sample, with no stimulus applied (Ctrl). Suspensions were initially stirred in dark for 20 h after which continuous irradiation was applied (for Irr sample) or the samples were treated with 20 mM ligand concentration (for NO dark, His dark and IM dark samples). After additional 7.5 h the ligand concentration was increased to 50 mM. Top graph shows a zoom in on ligand induced dye release portion. Bottom graph includes visible light induced release along with ligand induced release.

The release of the dye was successfully increased by increasing the ligand concentration from 20 mM to 50 mM, due to increased reaction probability. Strictly based on

comparison of stability constants,[23] substitution with histidine was expected to be the most efficient. However, after increasing concentration of the ligands to 50 mM it is evident that substitution by NO was the most successful. This result can be explained by the small diameter of NO molecules which allows the presence of more NO molecules inside the mesopores, when compared to histidine or imidazole, and hence probability of substitution increases.

The above results suggest that the employed cargo delivery system could be useful for a range of potential applications. Various stimuli responsive nanocarriers can be devised with the same basic triggering principle in order to fit the desired application. In addition to drug delivery either by externally applied light irradiation or by internal ligand induced triggering, we envision that the triggering principle can be useful for sensing of NO molecules and other relevant ligands in the environment or in biological systems.

Conclusions

We report on mesoporous silica nanoparticle-based supramolecular assembly for visible light and ligand substitution responsive release of cargo molecules. Sulforhodamine 101 was loaded inside the mesopores of mercaptopropyl-functionalized MSN and it was entrapped by the presence of $Ru(bpy)_2(PPh_3)$- moieties, which were coordinated to mercaptopropyl functional groups. Upon irradiation with visible light Ru-S coordination bond is cleaved which triggers the release of capping species and loaded dye. Release of the cargo molecules was also shown to be responsive to ligand substitution by nitrogen monoxide, imidazole and histidine. We believe that this multiple-stimuli responsive triggering principle can be effectively applied for the construction of functional nanoassemblies for applications in drug delivery and sensing.

References

(1) Bawa, P.; Pillay, V.; Choonara, Y. E.; du Toit, L. C. *Biomed. Mater.* **2009**, 4, 22001.
(2) Fong, W. K.; Hanley, T.; Boyd, B. J. *J. Controlled Release* **2009**, 135, 218-26.
(3) Klaikherd, A.; Nagamani, C.; Thayumanavan, S. *J. Am. Chem. Soc.* **2009**, 131, 4830-8.
(4) Sukhorukov, G. B.; Rogach, A. L.; Zebli, B.; Liedl, T.; Skirtach, A. G.; Kohler, K.; Antipov, A. A.; Gaponik, N.; Susha, A. S.; Winterhalter, M.; Parak, W. J. *Small* **2005**, 1, 194-200.
(5) Alexiou, C.; Arnold, W.; Klein, R. J.; Parak, F. G.; Hulin, P.; Bergemann, C.; Erhardt, W.; Wagenpfeil, S.; Lubbe, A. S. *Cancer Res.* **2000**, 60, 6641-8.
(6) Arap, W.; Pasqualini, R.; Ruoslahti, E. *Science* **1998**, 279, 377-80.
(7) Vallet-Regi, M.; Balas, F.; Arcos, D. *Angew. Chem., Int. Ed.* **2007**, 46, 7548-7558.
(8) Trewyn, B. G.; Giri, S.; Slowing, I. I.; Lin, V. S. Y. *Chem. Commun. (Cambridge, U. K.)* **2007**, 3236-3245.
(9) Angelos, S.; Liong, M.; Choi, E.; Zink, J. I. *Chem. Eng. J. (Amsterdam, Neth.)* **2008**, 137, 4-13.
(10) Lai, C.-Y.; Trewyn, B. G.; Jeftinija, D. M.; Jeftinija, K.; Xu, S.; Jeftinija, S.; Lin, V. S. Y. *J. Am. Chem. Soc.* **2003**, 125, 4451-4459.
(11) Giri, S.; Trewyn, B. G.; Stellmaker, M. P.; Lin, V. S. Y. *Angew. Chem., Int. Ed.* **2005**, 44, 5038-5044.
(12) Vivero-Escoto, J. L.; Slowing, I. I.; Wu, C.-W.; Lin, V. S. Y. *J. Am. Chem. Soc.* **2009**, 131, 3462-3463.
(13) Radu, D. R.; Lai, C.-Y.; Jeftinija, K.; Rowe, E. W.; Jeftinija, S.; Lin, V. S. Y. *J. Am. Chem. Soc.* **2004**, 126, 13216-13217.
(14) Zhao, Y.; Trewyn, B. G.; Slowing, II; Lin, V. S. *J. Am. Chem. Soc.* **2009**, 131, 8398-400.
(15) Nguyen, T. D.; Liu, Y.; Saha, S.; Leung, K. C. F.; Stoddart, J. F.; Zink, J. I. *J. Am. Chem. Soc.* **2007**, 129, 626-634.
(16) Mal, N. K.; Fujiwara, M.; Tanaka, Y. *Nature* **2003**, 421, 350-3.
(17) Svaasand, L. O.; Ellingsen, R. *Photochem. Photobiol.* **1983**, 38, 293-9.
(18) Zayat, L.; Noval, M. G.; Campi, J.; Calero, C. I.; Calvo, D. J.; Etchenique, R. *ChemBioChem* **2007**, 8, 2035-8.
(19) Greaney, M. A.; Coyle, C. L.; Harmer, M. A.; Jordan, A.; Stiefel, E. I. *Inorg. Chem.* **1989**, 28, 912-920.
(20) Aznar, E.; Coll, C.; Marcos, M. D.; Martinez-Manez, R.; Sancenon, M.; Soto, J.; Amoros, P.; Cano, J.; Ruiz, E. *Eur. J. Chem.* **2009**, 15, 6877-6888.
(21) Zanarini, S.; Rampazzo, E.; Della Ciana, L.; Marcaccio, M.; Marzocchi, E.; Montalti, M.; Paolucci, F.; Prodi, L. *J. Am. Chem. Soc.* **2009**, 131, 2260-2267.
(22) Ferreira, L. F. V.; Lemos, M. J.; Reis, M. J.; do Rego, A. M. B. *Langmuir* **2000**, 16, 5673-5680.
(23) Martell, A. E.; Sillen, L. G. *Chem. Soc. (London), Spec. Publ.* **1964**, 17, 754.

Appendix

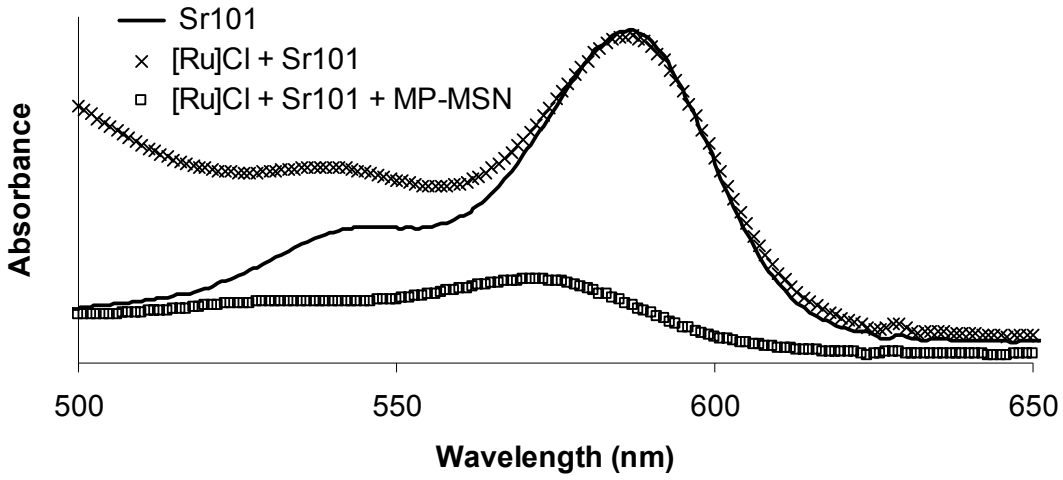

Figure S1. Comparison of UV-VIS spectra of Sr101 before and after addition of $[Ru(bpy)_2(PPh_3)Cl]Cl$ ([Ru]Cl) and MP-MSN

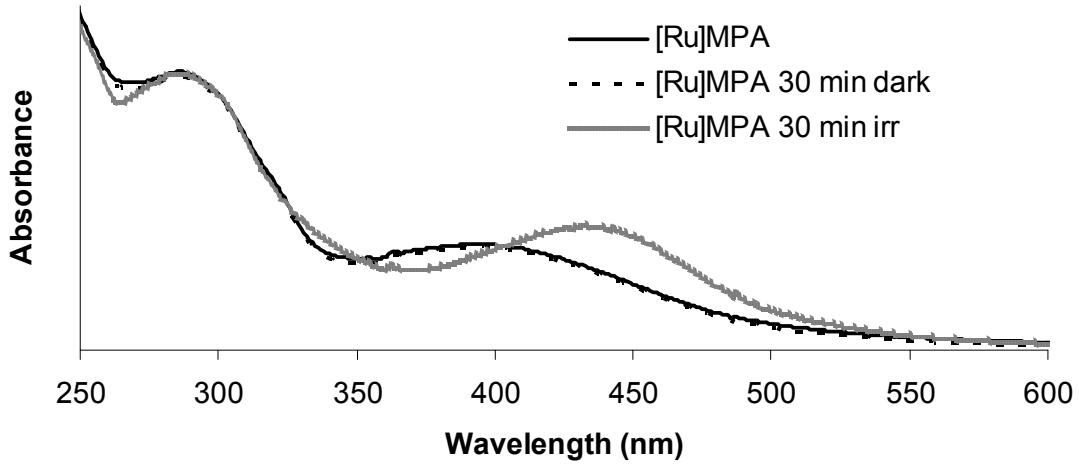

Figure S2. UV-VIS spectra of $[Ru(bpy)_2(PPh_3)MPA]PF_6$ ([Ru]MPA) before and after 30 minutes of irradiation and 30 minutes of stirring in dark

CHAPTER 6. GENERAL CONCLUSIONS

In this dissertation, I presented my research accomplishments for the past 6 years of my graduate studies, in chronological order. From the beginning of my research work I concentrated my efforts on the construction and development of functional various stimuli-responsive supramolecular assemblies for applications in drug delivery.

The development of functional supramolecular assemblies is of considerable importance in the scientific community in recent years. From a theoretical standpoint, studies on organization of individual molecules into more complex structures are still in demand. Broad spectrum of possibilities for applications of these complex assemblies further increases the interest in such structures. Several examples for application of supramolecular systems containing mesoporous silica nanoparticles are described within this dissertation.

We first described functional UV light responsive doxorubicin delivery system. The anticancer drug is positively charged at physiological conditions and it was adsorbed on organically modified surface of MSN. The drug delivery principle was based on charge repulsion between UV light-generated positively charged moieties on MSN surface and doxorubicin molecules. Increase in the released drug amount was also observed with increase in acidity.

We also developed magnetic analogues of mesoporous silica nanoparticles. A series of new materials was obtained with radial and hexagonal packing of the mesopores, containing magnetic nanoparticles inside the core of mesoporous silicate framework. Loading and delivery capabilities of 9-aminoacridine (9AA) and camptothecin (CPT) from magnetic mesoporous silica nanoparticles (MMSN) were shown to depend on porous structure and presence of phenylethyl moiety inside the mesopores. Characterization of the

magnetic drug delivery systems and *in* vitro viability studies on Chinese hamster ovarian (CHO) cells were also presented.

Magnetic mesoporous silica nanoparticles wee further applied for the construction of functional supramolecular assembly for UV light sensitive drug delivery. Anticancer drug camptothecin was loaded inside the mesopores of the magnetic material and it was entrapped by functionalized cadmium-sulfide nanoparticles though a photolabile MSN-bonded linker. Release of the drug was triggered upon irradiation with UV light. Cooperative cytotoxic activity of capping CdS nanoparticles and loaded drug was observed upon the treatment of CHO cells and exposure to low power UV irradiation

Finally, we described the construction and characterization of a mesoporous silica nanoparticle-based nanocarrier which was capable of delivering the mesopore-loaded molecules upon irradiation with visible light or upon the treatment with nitrogen-monoxide, histidine or imidazole. Sulforhodamine 101 was used as a cargo molecule and it was entrapped inside the mercaptopropyl functionalized mesopores of MSN by mercapto-coordinated $Ru(bpy)_2(PPh_3)$-moieties (bpy = 2,2'-bipyridine, PPh_3 = triphenylphosphine). Upon exposure to aforementioned ligands or to visible light, the Ru-S coordination bond was cleaved and the cargo molecules were released into the bulk PBS solution.

ACKNOWLEDGMENTS

I would like to express my sincere gratitude to several people that helped me along the course of this work.

First and foremost, I thank my advisor, Dr. Victor Shang-Yi Lin, for all the helpful suggestions, support and guidance over the years of graduate studies.

I am also grateful to all POS committee members, Dr. Keith Woo, Dr. Srdija Jeftinija, Dr. Aaron Sadow and Dr. Marek Pruski for their helpful suggestions during the work on this thesis.

I would like to thank Dr. Brian G. Trewyn and Dr. Igor I. Slowing for the help with some of the experimental work and helpful discussions. To all other past and present members of Lin research group, thank you, it has been a delight working with you.

Finally, I am grateful to my family for all the emotional and financial support over the years of my education.